AUTOMATIC CLASSIFICATION OF DIGITAL COMMUNICATION SIGNAL MODULATIONS

A thesis submitted for the degree of Doctor of Philosophy

by

ZHECHEN ZHU

Department of Electronic and Computer Engineering Brunel University London October 2014

Abstract

Automatic modulation classification detects the modulation type of received communication signals. It has important applications in military scenarios to facilitate jamming, intelligence, surveillance, and threat analysis. The renewed interest from civilian scenes has been fuelled by the development of intelligent communications systems such as cognitive radio and software defined radio. More specifically, it is complementary to adaptive modulation and coding where a modulation can be deployed from a set of candidates according to the channel condition and system specification for improved spectrum efficiency and link reliability. In this research, we started by improving some existing methods for higher classification accuracy but lower complexity. Machine learning techniques such as k-nearest neighbour and support vector machine have been adopted for simplified decision making using known features. Logistic regression, genetic algorithm and genetic programming have been incorporated for improved classification performance through feature selection and combination. We have also developed a new distribution test based classifier which is tailored for modulation classification with the inspiration from Kolmogorov-Smirnov test. The proposed classifier is shown to have improved accuracy and robustness over the standard distribution test. For blind classification in imperfect channels, we developed the combination of minimum distance centroid estimator and non-parametric likelihood function for blind modulation classification without the prior knowledge on channel noise. The centroid estimator provides joint estimation of channel gain and carrier phase offset where both can be compensated in the following non-parametric likelihood function. The non-parametric likelihood function, in the meantime, provide likelihood evaluation without a specifically assumed noise model. The combination has shown to have higher robustness when different noise types are considered. To push modulation classification techniques into a more timely setting, we also developed the principle for blind classification in MIMO systems. The classification is achieved through expectation maximization channel estimation and likelihood based classification. Early results have shown bright prospect for the method while more work is needed to further optimize the method and to provide a more thorough validation.

Contents

List of Figures

List of Tables

List of Symbols

α	channel gain
$\boldsymbol{\omega}$	additive noise
$\boldsymbol{r}$	received signal
$\boldsymbol{s}$	transmitted signal
$\mathbb{I}$	indicator function
$\mathcal{F}$	fitness functions
$\mathcal{H}$	Modulation Hypothesis
$\mathcal{M}$	modulation
$\mathfrak{M}$	modulation pool
Σ	covariance matrix
θ_o	phase offset
A	modulation alphabet
H	channel coefficient
I	number of modulation candidates
M	modulation order/alphabet size/number of symbol states

N	number of sample/signal length
P_{cc}	Classification accuracy

Acronyms

AMC Automatic Modulation Classification

ANN Artificial Neural Network

ALRT Average Likelihood Ratio Test

CDF Cumulative Distribution Function

CSI Channel State Information

EA Electronic Attack

ECDF Empirical Cumulative Distribution Function

ECM Expectation Conditional Maximization

EM Expectation Maximization

EP Electronic Protect

ES Electronic Support

EW Electronic Warfare

GA Genetic Algorithm

GLRT General Likelihood Ratio Test

GMM Gaussian Mixture Model

GoF Goodness of Fit

GP Genetic Programming

HLRT Hybrid Likelihood Ratio Test

HOS High Order Statistics

ICA Independent Component Analysis

KS test Kolmogorov-Smirnov test

KNN K-nearest Neighbour

LA Link Adaptation

LB Likelihood Based

LR Logistic Regression

MDCE Minimum Distance Centroid Estimator

MIMO Multiple-input Multiple-output

ML Machine Learning

NPLF Non-parametric Likelihood Function

ODST Optimized Distribution Sampling Test

PDF Probability Density Function

SISO Single-input Single-output

SM Spatial Multiplexing

STC Space-time Coding

SVM Support Vector Machine

Acknowledgments

First and foremost, I would like to thank my parents for their endless and unconditional support. Equally, if not more, I am grateful for the guidance provided by my primary supervisor Prof. Asoke K. Nandi. Without his patient supervision, none of my research outcomes would be possible. Same acknowledgement should be given to Dr. Hongying Meng and Dr. Waleed Al-Nauimy as my secondary supervisors.

In the meantime, I owe much to my colleagues who have provided me companionship, motivation, and inspiration. Especially to Dr. Muhammad Waqar Aslam, whom I have extended and fruitful collaboration with. My gratitude also goes to Dr. Elsayed E. Azzouz and Dr. M. L. Dennis Wong whose work has greatly inspired my research.

I would also like to acknowledge the financial support from th School of Engineering and Design Brunel University London, th Faculty of Engineering University of Liverpool, and the University of Liverpool Graduate Association (Hong Kong). The funding has helped me focus on my research and made it possible for me to attend conferences which has much benefited my work.

Last but not least, I would like to thank the researchers who have reviewed and provided valuable feedback on my work. It is with your help that I am able to gauge the quality of my work and make progress to improve.

Copyright

This thesis is dedicated to my parents Qiaonan Zhu and Xiaoyan Zhu.

Chapter 1

Introduction

1.1 Motivation

1.1.1 Military applications

Automatic Modulation Classification (AMC) was first motivated by its application in military scenarios where electronic warfare, surveillance and threat analysis requires the recognition of signal modulations in order to identify adversary transmitting units, to prepare jamming signals and to recover the intercepted signal. The term automatic is used as opposed to the initial implementation of manual modulation classification where signals are processed by engineers with the aid of signal observation and processing equipment. Most modulation classifiers developed in the past 20 years are implemented through electronic processors.

There are three components in Electronic Warfare (EW) namely Electronic Support (ES), Electronic Attack (EA), and Electronic Protect (EP) (Poisel, 2008). For ES, the goal is to gather information from radio frequency emissions. This is often where AMC is employed after the signal detection is successfully achieved. The resulting modulation information could have several uses extending into all the components in EW. An illustration of how a modulation classifier is incorporated in the military EW systems is given in Figure 1.1.

To further the process of ES, the modulation information can be used for demodulating the intercepted signal in order to recover the transmitted message among adversary

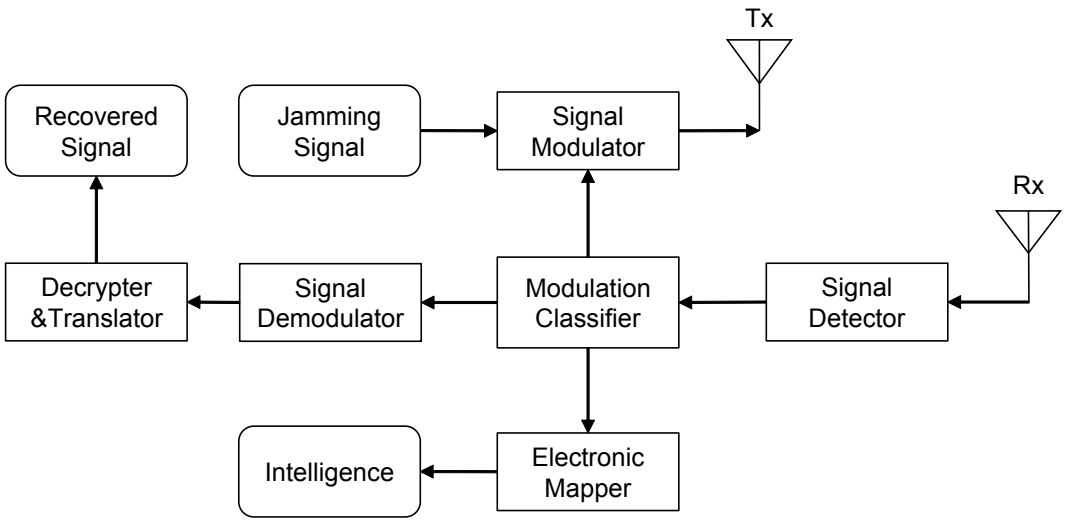

Figure 1.1: Application of AMC in military electronic warfare systems.

units. This is, of course, completed with the aid of signal decryption and translation. Meanwhile, the modulation information alone can also provide vital information to the electronic mapping system where it could be used to identify the adversary units and their possible locations.

In EA, jamming is the primary measure to prevent the communication between adversary units. There are many jamming techniques. However, the most common one relies on deploying jammers in the communication channel between adversary units and transmitting noise signals or made up signals using the matching modulation type. To override the adversary communication, the jamming signal must occupy the same frequency band as the adversary signal. This information is available from the signal detector. The power of the jamming signal must be significantly higher which is achieved using an amplifier before transmitting the jamming signal. More importantly, the jamming signal must be modulated using the modulation scheme detected by the modulation classifier. It is necessary because information can be conveyed in the carrier signal in different ways. To maximized the interference, matching modulation is required to alter the signal component where the adversary message is embedded.

In EP, the objective is to protect the friendly communication from adversary EA mea-

sures. As mentioned above, jammers transmit higher power signals to override adversary communication in the same frequency band. The key is to have the same signal modulation. An effective strategy to prevent friend communication being jammed is to have awareness of the EA effort from adversary jammers and to dodge the jamming effort. More specifically, the friendly transmitter could monitor the jamming signals modulation and switch the friendly unit to a different modulation scheme to avoid jamming.

During the 1980s and 1990s, there were considerable numbers of researchers in the field of signal processing and communications who dedicated their works to the problem of automatic modulation classification. It leads to the publication of the first well received book on the subject by Azzouz and Nandi in 1996 (Azzouz and Nandi, 1996a). The interest in AMC for military purposes is sustained till this very day.

1.1.2 Civilian applications

The beginning of 21st century sees a large number of innovations in communications technology. Among them are a few that have made essential contributions to the staggering increase of transmission throughput in various communication systems. Link Adaptation (LA), also known as adaptive modulation and coding, creates an adaptive modulation scheme where a pool of multiple modulations are employed by the same system (Goldsmith and Chua, 1998). It enables the optimizing of the transmission reliability and data rate through the adaptive selection of modulation schemes according to channel conditions. While the transmitter has the freedom to choose how the signals are modulated, the receiver must have the knowledge of the modulation type to demodulate the signal so that the transmission could be successful. An easy way to achieve this is to include the modulation information in each signal frame so that the receivers would be notified about the change in modulation scheme and react accordingly. However, this strategy affects the spectrum efficiency due to the extra modulation information in each signal frame. In the current situation where wireless spectrum is extremely limited and valuable, the aforementioned strategy is simply not efficient enough. For this reason, AMC becomes an attractive solution to the problem.

As demonstrated in Figure 1.2, the signal modulator in the LA transmitter is replaced

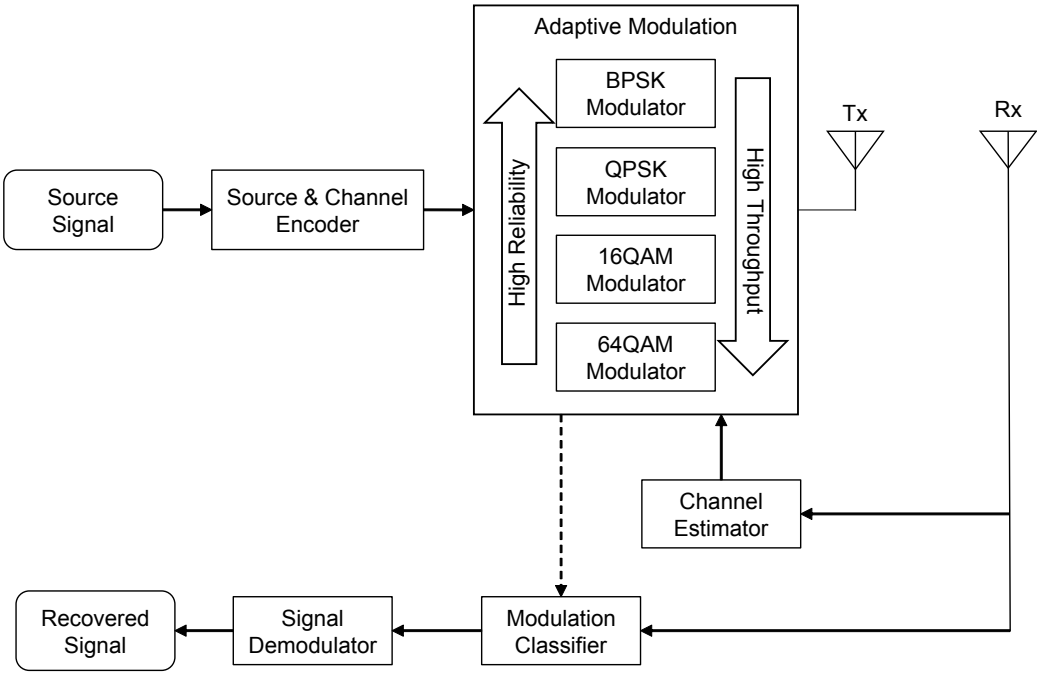

Figure 1.2: Application of AMC in civilian link adaptation systems.

by an adaptive modulation unit. The role of adaptive modulator is to select the modulation from a pre-defined candidate pool and to complete the modulation process. The selection of modulation from the candidate pool is determined by the system specification and channel conditions. The lower order and more robust modulations such as BPSK and QPSK are often selected when the channel is noisy and complex, given that the system requires high link reliability. The higher order and more efficient modulations such as 16-QAM and 64-QAM are often selected to satisfy the demand for high speed transmission in clear channels. The only communication between adaptive modulation module and the receiver is completed at system initialization where the information of modulation candidate pool is notified to the receiver. During normal transmission, the adaptive modulator embeds no extra information in the communication stream. At the receiving end of the LA system, channel estimation is performed prior to other tasks. If the channel is static, the estimation is only performed at the initial stage. If the channel is time variant, the channel state information Channel State Information (CSI) could be estimated regularly throughout the transmission. The estimated

CSI and other information would then be feedback to the transmitter where the CSI will be used for the selection of modulation schemes. More importantly, the CSI is required to assist the modulation classifier. Depending on the AMC algorithm, different channel parameters are needed to complete modulation classification. Normally the accuracy of channel estimation has a significant impact on the performance of the modulation classifier. The resulting modulation classification decision is then fed to the reconfigurable signal demodulator for appropriate demodulation. If the modulation classification is accurate, the correct demodulation method would capture the message and complete the successful transmission. If the modulation classification is incorrect, the entire transmission fails as the message cannot be recovered from the demodulator. It is not difficult to see the importance of AMC in LA systems.

Thanks to the development in microprocessors, receivers nowadays are much more able in terms of their computational power. Thus, the signal processing required by AMC algorithms becomes feasible. By automatically identifying the modulation type of the received signal, the receiver does not need to be notified about the modulation type and the demodulation can still be successfully achieved. In the end, the spectrum efficiency is improved as no modulation information is needed in the transmitted signal frame. AMC has become an integral part of the intelligent radio systems including cognitive radio and software defined radio.

1.2 Problem statement

Assuming there is a finite set of modulation candidates, the modulation pool $\mathfrak{M}$ consists of I number of candidate modulations with $\mathcal{M}(i)$ being the ith modulation candidate. The transmitted signal $\boldsymbol{s}$ consisting of N samples is modulated using $\mathcal{M}$ which is unknown to the receiver. For each digital modulation scheme, the transmitted signal samples are mapped from a unique set of symbol alphabet dictated by the modulation scheme. The received signal $\boldsymbol{r} = H\boldsymbol{s} + \boldsymbol{\omega}$ is the main or sometime sole subject for analysis where H is associated with different channel effects and $\boldsymbol{\omega}$ is the additive noise. The task of AMC is to find

the modulation candidate from the modulation pool which matches the actual modulation scheme used for the signal transmission. The criteria for a good modulation classifier are based on four aspects.

First, a modulation classifier should be able to classify as many modulation types as possible. Such a trait makes a modulation classifier easily applicable to different applications without needing any modification to accommodate extra modulations. Second, a modulation classifier should provide high classification accuracy. The high classification accuracy is relative to different noise levels. Third, the modulation classifier should be robust for many different channel conditions. The robustness can be provided by either the built in channel estimation and compensation mechanism or the natural resilience of the modulation classifier against channel conditions. Fourth, the modulation classifier should be computationally efficient. In many applications, there is a strict limitation on computation power which may be unsuitable for over complicated algorithms. Meanwhile, some applications may require fast decision making which demands the classification to be completed in real time. Only a modulation classifier with high computational efficiency could meet this requirement. After all, a simple and fast modulation classifier algorithm is always appreciated.

In practice, there is no one classifier that is perfect in all aspects. Therefore, the goal of this research is to develop different AMC strategies that excel in certain aspects with reasonable compromise in other departments. The significance of these different AMC strategies is accentuated by the wide variety of applications which demand a unique set of attributes from the classifier.

1.3 Summary of contributions

As of this stage, I believe that the following contributions to the field has been achieved through this project:

- Machine Learning (ML) algorithms are introduced to feature based modulation classification strategy. The machine learning based classifiers incorporate logistic regression, genetic algorithm, or genetic programming as feature selection/combination methods

and k-nearest neighbour or support vector machine as classifiers. The machine learning based classifiers are proven to be more intuitive in their implementation and more accurate than the traditional feature based classifiers. (Chapter 3)

- Empirical cumulative distribution of modulation signals are studied to suggest distribution test based modulation classifiers as well as distribution statistics that can be used as features. The distribution based modulation classification approaches have very low computational complexity while preserving high classification accuracy when limited number of signal samples are available for analysis.(Chapter 4)

- Thus far, noise models are always assumed when constructing a modulation classifier. In this research, the blind modulation classifier which operates without an assumed noise model is developed using a centroid estimator and a Non-parametric Likelihood Function (NPLF). The combination provides improved robustness in fading channels as well as superior classification performance with impulsive noises. (Chapter 5)

- The combination of expectation maximization (EM) estimator and maximum likelihood classifier is extended to the Multiple-input Multiple-output (MIMO) systems. Oppose to Independent Component Analysis (ICA) enabled MIMO modulation classifier, the EM and ML combination doesn't require the knowledge of noise power or extra calculation for phase offset correction. (Chapter 6)

1.4 Thesis organization

This thesis begins with a brief introduction to the subject, some basic theories, and a literature review. The following contents include different modulation classifiers developed in this research presented in chronological order. The thesis is concluded with a review of the developed classifiers and suggestions for further research direction. The summary of each chapter is given below.

Chapter 1 provides the historical background of AMC as well as its important applications in military and modern civilian communication systems. The contribution of this

research is highlighted with complimentary list of publications.

Chapter 2 provides the modelling of communication systems and different communication channels that are used for the development of modulation classifiers. The scope of the research and assumptions made are described. A literature review is included to provide an understanding of the development progress of AMC at the current stage. Three of the state-of-the-art algorithms are described in details as they are used in performance benchmarking versus the newly developed algorithms in this research.

Chapter 3 lists several machine learning techniques that have been introduced to AMC (Zhu et al., 2011, 2013c, 2014; Aslam et al., 2012). K-nearest neighbour and support vector machine are suggested as classifiers based on high order statistics features. Feature selection and combination are practised using logistic regression, genetic algorithm, and genetic programming. The combination of these classifiers and feature enhancement methods are also discussed to provide a complete solution to AMC. For each algorithm, its implementation is described in details. The advantages and disadvantages of each algorithm are listed with numerical results to support the observation.

Chapter 4 explores the AMC algorithms based on signal distributions (Zhu et al., 2013c, 2014). The optimized distribution sampling test is suggested as an improved version of the Kolmogorov-Smirnov test. The strategies of optimizing the sampling locations and the distribution test as classifier are described in detail. The additional use of sample distribution statistics as features is explored for AMC accompanied with ML classifiers. The numerical results from computer aided simulations are provided to validate the proposed methods.

Chapter 5 describes the new AMC solution which does not require known noise model (Zhu et al., 2013b; Zhu and Nandi, 2014a). The preliminary step of centroid estimation can be achieved through two iterative algorithms. The likelihood based modulation classification is realized by a non-parametric likelihood function. The theoretical analysis is given for the validation of the centroid estimator and the optimization of the NPLF classifier. Numerical results are given to illustrate the superior performance of this classifier in complex channels.

Chapter 6 gives the blind modulation classification solution for MIMO systems (Zhu and Nandi, 2014b). The joint estimation of channel matrix and noise variance is achieved with

expectation maximization in the context of MIMO channels. The expectation/conditional maximization update functions for the channel parameters are derived. The classification is completed with a ML classifier and updated likelihood functions for MIMO signals. The simulated classification performance is given for several selected modulations.

Chapter 7 reviews the new classifiers developed in this research and concludes their advantages and disadvantages. The remaining challenges and new directions for the subject is also listed in this chapter.

1.5 List of publications

Journal Papers

- Zhu, Z., and Nandi, A. K. (2014). Blind Digital Modulation Classification using Minimum Distance Centroid Estimator and Non-parametric Likelihood Function. IEEE Transactions on Wireless Communications, 13(8) 4483-4494.

- Zhu, Z., Aslam, M. W., and Nandi, A. K. (2014). Genetic Algorithm Optimized Distribution Sampling Test for M-QAM Modulation Classification. Signal Processing, 94, 264-277.

- Aslam, M. W., Zhu, Z., and Nandi, A. K. (2013). Feature generation using genetic programming with comparative partner selection for diabetes classification. Expert Systems with Applications, 40(13), 5402-5412.

- Aslam, M. W., Zhu, Z., and Nandi, A. K. (2012). Automatic Modulation Classification Using Combination of Genetic Programming and KNN. IEEE Transactions on Wireless Communications, 11(8), 2742-2750.

Conference papers

- Zhu, Z., and Nandi, A. K. (2014). Blind Modulation Classification for MIMO Systems using Expectation Maximization. In Military Communications Conference (pp. 1-6).

- Zhu, Z., Nandi, A. K., and Aslam, M. W. (2013). Approximate Centroid Estimation with Constellation Grid Segmentation for Blind M-QAM Classification. In Military Communications Conference (pp. 46-51).

- Zhu, Z., Aslam, M. W., and Nandi, A. K. (2013). Adapted Geometric Semantic Genetic Programming for Diabetes and Breast Cancer Classification. In IEEE International Workshop on Machine Learning for Signal Processing (pp. 1-5).

- Aslam, M. W., Zhu, Z., and Nandi, A. K. (2013). Improved Comparative Partner Selection with Brood Recombination for Genetic Programming. In IEEE International Workshop on Machine Learning for Signal Processing (pp. 1-5).

- Zhu, Z., Nandi, A. K., and Aslam, M. W. (2013). Robustness Enhancement of Distribution Based Binary Discriminative Features for Modulation Classification. In IEEE International Workshop on Machine Learning for Signal Processing (pp. 1-6).

- Zhu, Z., Aslam, M. W., and Nandi, A. K. (2011). Support Vector Machine Assisted Genetic Programming for MQAM Classification. In International Symposium on Signals, Circuits and Systems (pp. 1-6).

- Aslam, M. W., Zhu, Z., and Nandi, A. K. (2011). Robust QAM Classification Using Genetic Programming and Fisher Criterion. In European Signal Processing Conference (pp. 995-999).

- Zhu, Z., Aslam, M. W., and Nandi, A. K. (2010). Augmented Genetic Programming for Automatic Digital Modulation Classification. In IEEE International Workshop on Machine Learning for Signal Processing (pp. 391-396).

- Aslam, M. W., Zhu, Z., and Nandi, A. K. (2010). Automatic Digital Modulation Classification Using Genetic Programming with K-Nearest Neighbor. In Military Communications Conference (pp. 1731-1736).

Chapter 2

Signal Model and Existing Methods

2.1 Introduction

Signal models are the starting point of every meaningful modulation classification strategy. Algorithms such as likelihood based, distribution test based and feature based classifiers all require an established signal model to derive the corresponding rules for classification decision making. While some unsupervised machine learning algorithms could function without a reference signal model, the optimization of such algorithms still relies on the knowledge of a known signal model. Meanwhile, as the validation of modulation classifiers is often realized by computer-aided simulation, accurate signal modelling provides meaningful scenarios for evaluating the performance of various modulation classifiers. The objective of this chapter is to establish some unified signal models for different modulation classifiers listed in Chapter 3 to Chapter 6. Through the process, the accuracy of the models will be the first priority. That, however, is with a fine balance of simplicity in the models to enable theoretical analysis and to provide computational efficient implementations. Signal models are presented in three different channels namely AWGN channel, fading channel, and non-Gaussian channel.

To establish an understanding of the current AMC development status, a literature review of some the key existing methods is also included in this chapter. Three major categories of classifiers are visited including likelihood based classifiers, distribution test based classifiers and feature based classifiers. For some classifiers that are used in the performance

benchmarking, their implementation is describe in details.

2.2 Signal model in AWGN channels

Additive white Gaussian noise is one of the most widely used noise models in many signal processing problems. It is of much relevance to the transmission of signals in both wired and wireless communication media where wideband Gaussian noise is produced by thermal vibration in conductors and radiation from various sources. The popularity of additive white Gaussian noise is evidential in most published literature on modulation classification where the noise (model) is considered the fundamental limitation to accurate modulation classification.

Additive white Gaussian noise is characterized with constant spectral density and a Gaussian amplitude distribution of zero mean. Giving the additive noise a complex representation $\omega = I(\omega) + jQ(\omega)$, the complex Probability Density Function (PDF) of the complex noise can be found as

$$f_\omega(x) = \frac{1}{2\pi\sqrt{|\Sigma|}} e^{-\frac{|x|^2}{2\sqrt{|\Sigma|}}} \tag{2.1}$$

where Σ is the covariance matrix of the complex noise, $|\Sigma|$ is the determinant of Σ, $|x|$is the Euclidean norm of the complex noise and the noise mean is zero. Since many algorithms are interested in the in-phase and quadrature segments of the signal, it is important to derive the corresponding PDF of the in-phase and quadrature segments of the additive noise. Fortunately, when AWGN noises are projected onto any orthonormal segments the resulting projection has independent and identical Gaussian distribution (Gallager, 2008). The resulting covariance matrix can be found as

$$\Sigma = \begin{bmatrix} \sigma_I^2 & \rho\sigma_I\sigma_Q \\ \rho\sigma_I\sigma_Q & \sigma_Q^2 \end{bmatrix} = \begin{bmatrix} \sigma^2 & 0 \\ 0 & \sigma^2 \end{bmatrix} \tag{2.2}$$

where variance for the in-phase segment σ_I^2 and the quadrature segment σ_Q^2 and are replaced with a shared identical variance σ^2, and the correlation between two segments is zero. Thus,

the desired PDFs of each segment can be easily derived as

$$f_{I(\omega)}(x) = f_{Q(\omega)}(x) = \frac{1}{\sigma\sqrt{2\pi}} e^{-\frac{|x|^2}{2\sigma^2}} \tag{2.3}$$

As suggested by the term "additive", the AWGN noise is added to the transmitted signal giving the signal model in AWGN channel.

$$r(t) = s(t) + \omega(t). \tag{2.4}$$

Assuming the signal modulation $\mathcal{M}$ has an alphabet A of M symbols and the symbol A_m having the equal probability to be transmitted, with overall distribution being considered as M number of AWGN noise distributions shifted to different modulation symbols, the complex PDF of the received signal is given by

$$f_r(x) = \sum_{m=1}^{M} \frac{1}{M} f_\omega(x|A_m, \Sigma) = \sum_{m=1}^{M} \frac{1}{M} \frac{1}{2\pi\sqrt{|\Sigma|}} e^{-\frac{|x-A_m|^2}{2\sqrt{|\Sigma|}}} \tag{2.5}$$

where $1/M$ is the probability of A_m being transmitted.

Following the same logic of the derivation of the complex PDF, the distribution of received signals on their in-phase and quadrature segments can be found by replacing the variance by half of the noise variance and the mean of the noise distribution with in-phase and quadrature segments of the modulation symbols.

$$f_{I(r)}(x) = \sum_{m=1}^{M} \frac{1}{M} f_{I(\omega)}(x|A_m, \sigma) = \sum_{m=1}^{M} \frac{1}{M} \frac{1}{\sigma\sqrt{2\pi}} e^{-\frac{|x-I(A_m)|^2}{2\sigma^2}} \tag{2.6}$$

2.3 Signal model in fading channels

The fading channel is largely concerned with wireless communication, where signals are received as delayed and attenuated copies after being absorbed, reflected and diffracted by different objects. Fading, especially deep fading, drastically changes the property of the transmitted signal and imposes a tough challenge on the robustness of a modulation classifier. Though early literature on modulation classifier focuses on the validation of algorithms in AWGN channel, the current standard requires the robustness in fading channel as an important attribute In this chapter, a unified model of a fading channel is presented with

flexible representation of different fading scenarios. It is worth noting that AWGN noise will also be considered in the fading channel as to approach a more realistic real world channel condition.

Instead of modelling each fading type, we characterize the joint effect of them into three categories: attenuation, phase offset, and frequency offset. Depending on the nature of the fading channel, two types of fading scenarios are generally considered for signal phase offset: slow fading and fast fading. Slow fading are normally caused by shadowing (or shadow fading) when the signal is obscured by large object from a line of sight communication (Goldsmith, 2005). As the coherent time of the shadow fading channel is significantly longer than the signal period, the effect of attenuation and phase offset remains constant. Therefore, a constant channel gain α and phase offset θ_o can be used to model the received signal after slow fading.

$$r(t) = \alpha e^{j\theta_o} s(t) + \omega(t) \tag{2.7}$$

Fast fading, caused by multipath fading where signals are reflected by objects in the radio channel of different properties, imposes a much different effect on the transmitted signal. As the coherent channel time in a fast fading channel is considered small. The effects of attenuation and phase offset vary with time. In this research, we assume that both the attenuation and phase offset are random processes with Gaussian distributions. The attenuation is given by

$$\alpha(t) \sim \mathcal{N}(\alpha, \sigma_\alpha) \tag{2.8}$$

where $\alpha(t)$ is the channel gain at time t, α is the mean attenuation, and σ_α is the variance of the channel gain. The phase offset is given by

$$\theta_o(t) \sim \mathcal{N}(\theta_o, \sigma_{\theta_o}) \tag{2.9}$$

where $\theta_o(t)$ is the channel gain at time t, θ_o is the mean attenuation, and σ_{θ_o} is the variance of the channel gain. Both expressions give a combined effect of slow and fast fading. When α and θ_o are both zero, the fading consist of only fast attenuation and fast phase offset. When σ_α and σ_{θ_o} are both zero, the model reverts back to the case of slow fading. The resulting

channel model becomes

$$r(t) = \alpha(t)e^{j\theta_o(t)}s(t) + \omega(t). \tag{2.10}$$

Apart from the channel attenuation and phase offset, frequency offset is another important effect in a fading channel that is worth investigating. The shift in frequency of received signal is mostly cause by moving antennas in mobile communication devices. Given the carrier frequency of a modulated signal as f_c, when the antenna is moving at a speed of v the resulting frequency offset caused by Doppler shift can be found as $f_c v/c$ where c is the speed of travelling light in the channel medium (Gallager, 2008). As we are only interested in the amount of frequency offset, the expression is simplified by denoting the frequency offset set as f_o and the resulting signal model with frequency offset set given by

$$r(t) = e^{j2\pi t f_o}s(t) + \omega(t) \tag{2.11}$$

Combining the attenuation, phase offset, and frequency offset, we can derive a signal model of fading channel of all mentions effects.

$$r(t) = \alpha(t)e^{j(2\pi t f_o + \theta_o(t))}s(t) + \omega(t) \tag{2.12}$$

2.4 Signal model in non-Gaussian channels

Non-Gaussian noises are often used to model impulsive noises which are a step further to model the noises in a real radio communication channel. Impulsive noise, unlike Gaussian noise, has heavy-tailed probability density function meaning higher probability for high power noise components. Such noises are often the result of incidental electromagnetic radiation from man-made sources. While not featured in most modulation classification literature, impulsive noises have received increasing amount of attention in recent years. Despite the complexity in the modelling of impulsive noise, it is worth the effort to try and accommodate the signal model for a more practical approximation of the real world radio channels. In this chapter, two non-Gaussian noise models will be presented for modelling the impulsive noise. However, such noises will be considered solely without extra AWGN noise or fading effects.

In this section, we start with Middleton's class A non-Gaussian noise model as a complex but accurate modelling of impulsive noises. In addition, the Gaussian mixture model is established for the analytical convenience in some of the complex modulation classification algorithms. The subject of non-Gaussian noise in AMC has been studied by Chavali and Silva extensively (Chavali and da Silva, 2011, 2013).

Middleton proposed a series of noise models (Middleton, 1999) to approximate the impulsive noise generated by different natural and man-made electromagnetic activities in physical environments. These models have become popular in many fields, including wireless communication, thanks to the canonical nature of the model which is invariant of the noise sauce, noise waveform, and propagation environments. The versatility of the model is enhanced by the model parameters which provide possibility to specify the source distribution, propagation properties, and bean patterns. The class A model is defined for the non-Gaussian noises with bandwidth narrower than the receiver bandwidth, while the class B model is defined for the non-Gaussian noises with wider spectrum than the receiver. In the meantime, the class C model provides a combination of the class A and class B model. The PDF of the class A noise is derived as

$$f_{\omega}(x) = e^{-A_A} \sum_{k=0}^{\infty} \frac{A_A^k}{k!\sqrt{4\pi\sigma_{kA}^2}} e^{-\frac{x^2}{4\pi\sigma_{kA}^2}} \tag{2.13}$$

where A_A is the overlap index which defines the number of noise emissions per second times the mean duration of the typical emission (Middleton, 1999). The variance of the kth emission element is given by

$$2\sigma_{kA}^2 = \frac{\frac{k}{A_A} + \Gamma_A}{1 + \Gamma_A} \tag{2.14}$$

where Γ_A is the Gaussian factor defined by the ratio of the average power of the Gaussian component to the average power of the non-Gaussian components. To approximate the desired impulsive nature in this section, small overlap index and Gaussian factor are suggested to provide a heavy-tailed distribution for the noise simulation.

In the meantime, Vastola proposed to approximate the Middletons class A model through a mixture of Gaussian noises (Vastola, 1984). The conclusion was drawn that the Gaussian

Mixture Model (GMM) provides a close approximation to the Millertons class A model while being computationally much more efficient. The PDF of the GMM mode is given by

$$f_\omega(x) = \sum_{k=1}^{K} \frac{\lambda_k}{2\pi\sigma_k^2} e^{-\frac{|x|^2}{2\sigma_k^2}} \tag{2.15}$$

where K is the total number of Gaussian components, λ_k is the probability of the noise being chosen from the kth component, and σ_k^2 is the variance of the kth component. As the GMM will be used as the primary model for impulsive noise, there we derive the PDFs of received signals in the non-Gaussian channel with a GMM noise model. Assume the GMM uses components where the probability and variance for each component are either known or estimated. The PDF of complex signal in the non-Gaussian channel can be derived as

$$f_r(x) = \sum_{m=1}^{M} \frac{1}{M} \sum_{k=1}^{K} f_r(x|A_m, \lambda_k, \sigma_k) = \sum_{m=1}^{M} \frac{1}{M} \sum_{k=1}^{K} \frac{\lambda_k}{2\pi\sigma_k^2} e^{-\frac{|x-A_m|^2}{2\sigma^2}} \tag{2.16}$$

with the corresponding variation for signal I-Q segments given by

$$f_{I(r)}(x) = \sum_{m=1}^{M} \frac{1}{M} \sum_{k=1}^{K} f_{I(r)}(x|A_m, \lambda_k, \sigma_k) = \sum_{m=1}^{M} \frac{1}{M} \sum_{k=1}^{K} \frac{\lambda_k}{\sigma_k\sqrt{2\pi}} e^{-\frac{|x-I(A_m)|^2}{2\sigma^2}} \tag{2.17}$$

2.5 Likelihood based classifiers

Likelihood Based (LB) modulation classifiers are by far the most popular modulation classification approaches. The interest in LB classifiers is motivated by the optimality of its classification accuracy when perfect channel model and channel parameters are known to the classifiers. The common approach of a LB modulation classifier consists of two steps. In the first step, the likelihood is evaluated for each modulation hypothesis with observed signal samples. The likelihood functions are derived from the selected signal model and can be modified to fulfil the need of reduced computational complexity or to be applicable in non-cooperative environments. In the second step, the likelihood of different modulation hypothesizes are compared to conclude the classification decision.

2.5.1 Maximum likelihood classifier

Likelihood evaluation is equivalent to the calculation of probabilities of observed signal samples belonging to the models with given parameters. In a maximum likelihood classifier (Wei and Mendel, 2000), with perfect channel knowledge, all parameters are known except the signal modulation. Therefore, the classification process can also be perceived as a maximum likelihood estimation of the modulation type where the modulation type is found in a finite set of candidates. Given that the likelihood of the observed signal sample $r[n]$ belongs to the modulation $\mathcal{M}$ is equal to the probability of the signal sample $r[n]$ being observed in the AWGN channel modulated with $\mathcal{M}$,

$$\mathcal{L}(r[n]|\mathcal{M},\sigma) = p(r[n]|\mathcal{M},\sigma) \tag{2.18}$$

as we recall the complex form PDF of received signal in AWGN channel, the likelihood function can be found as

$$\mathcal{L}(r[n]|\mathcal{M},\sigma) = \sum_{m=1}^{M} \frac{1}{M} \frac{1}{2\pi\sigma^2} e^{-\frac{|r[n]-A_m|^2}{2\sigma^2}} \tag{2.19}$$

Without knowing which modulation symbol the signal sample $r[n]$ belong to, the likelihood is calculated using the average of the likelihood value between the observed signal sample and each modulation symbol A_m. The joint likelihood given multiple observed samples is calculated with the multiplication of all likelihood of individual samples.

$$\mathcal{L}(\boldsymbol{r}|\mathcal{M},\sigma) = \prod_{n=1}^{N} \sum_{m=1}^{M} \frac{1}{M} \frac{1}{2\pi\sigma^2} e^{-\frac{|r[n]-A_m|^2}{2\sigma^2}} \tag{2.20}$$

For analytical convenience in many cases, the natural logarithm of the likelihood is used as likelihood value to be compared in a maximum likelihood classifier.

$$\begin{aligned} \log \mathcal{L}(\boldsymbol{r}|\mathcal{M},\sigma) &= \log \left(\prod_{n=1}^{N} \sum_{m=1}^{M} \frac{1}{M} \frac{1}{2\pi\sigma^2} e^{-\frac{|r[n]-A_m|^2}{2\sigma^2}} \right) \\ &= \sum_{n=1}^{N} \log \left(\sum_{m=1}^{M} \frac{1}{M} \frac{1}{2\pi\sigma^2} e^{-\frac{|r[n]-A_m|^2}{2\sigma^2}} \right) \end{aligned} \tag{2.21}$$

The likelihood, in the meantime, can be derived from probabilities of different aspects of sampled signals. As we have derived the PDF for In-phase segments of received signal in

AWGN channel, the corresponding likelihood function of the in-phase segments of a signal can be found as

$$\mathcal{L}_{I(r)}(\boldsymbol{r}|\mathcal{M},\sigma) = \prod_{n=1}^{N}\sum_{m=1}^{M}\frac{1}{M}\frac{1}{\sigma\sqrt{\pi}}e^{-\frac{|I(r[n])-I(A_m)|^2}{\sigma^2}}. \tag{2.22}$$

Having established the likelihood functions in AWGN channel, the decision making in a ML classifier becomes rather straightforward. Assuming a pool $\mathfrak{M}$ with finite number of I modulation candidates, among which hypothesis $\mathcal{H}_{\mathcal{M}(i)}$ of each modulation $\mathcal{M}(i)$ is evaluated using estimated channel parameters $\hat{\Theta}_{\mathcal{M}(i)}$ and suitable likelihood function to obtain its likelihood evaluation $\mathcal{L}(\boldsymbol{r}|\mathcal{H}_{\mathcal{M}(i)})$. With all the likelihood collected the decision made simply by finding the hypothesis with the highest likelihood.

$$\hat{\mathcal{M}} = \underset{\mathcal{M}(i)\in\mathfrak{M}}{\arg\max}\,\mathcal{L}(\boldsymbol{r}|\mathcal{H}_{\mathcal{M}(i)}) \tag{2.23}$$

2.5.2 Likelihood ratio test classifier

The issue of unknown parameter in a ML classifier is pivotal as the likelihood function is unable to handle any missing parameter. Average Likelihood Ratio Test (ALRT) is one way to overcome such limitation of a ML classifier. Polydoros and Kim first applied ALRT on modulation classification (Polydoros and Kim, 1990) which was later adopted by Huang and Polydoros (Huang and Polydoros, 1995), Beidas and Weber, Sills (Sills, 1999), Hong and Ho (Hong and Ho, 2000). Different from the ML likelihood function, the ALRT likelihood function replaces unknown parameters with the integral of all its possible values and their corresponding probabilities. Assuming that the channel parameters set Θ consisting channel gain α, noise variance σ^2, and phase offset θ_o is unknown to the classifier, the ALRT likelihood function is given by

$$\begin{aligned}\mathcal{L}_{ALRT}(\boldsymbol{r}) &= \int_{\Theta}\mathcal{L}(r|\Theta)f(\Theta|\mathcal{H})d\Theta \\ &= \int_{\Theta}\prod_{n=1}^{N}\sum_{m=1}^{M}\frac{1}{M}\frac{1}{2\pi\sigma^2}e^{-\frac{\left|r[n]-\alpha e^{-j\theta_o}A_m\right|^2}{2\sigma^2}}f(\alpha,\sigma,\theta_o|\mathcal{H})d\Theta\end{aligned} \tag{2.24}$$

where $\mathcal{L}(r|\Theta)$ is the likelihood given the channel parameter set Θ, $f(\Theta|\mathcal{H})$ is the probability of the parameters Θ under modulation hypothesis $\mathcal{H}$. The probability depends on deification

of prior probability of the unknown parameters. The common assumption of prior PDFs of different channel parameters are given below

$$f(\alpha|\mathcal{H}) \sim \mathcal{N}(\alpha|\mu_\alpha, \sigma_\alpha) \tag{2.25}$$

$$f(\sigma^2|\mathcal{H}) \sim Gamma(\sigma^2|a_\sigma, b_\sigma) \tag{2.26}$$

$$f(\theta_o|\mathcal{H}) \sim \mathcal{N}(\theta_o|\mu_{\theta_o}, \sigma_{\theta_o}) \tag{2.27}$$

where channel gain α is given a normal distribution with mean μ_α, variance σ_α^2, noise variance is given a Gamma distribution with shape parameter a_σ and scale parameter b_σ, and phase offset is given a normal distribution with mean μ_{θ_o} and variance $\sigma_{\theta_o}^2$. All the additional parameters associated with PDF of channels parameters are often called hyperparameters. The estimation of hyperparameters is not discussed in this research. Suitable schemes have been proposed by Roberts and Penny using variational Bayes estimator (Roberts and Penny, 2002).

The likelihood ratio test required for the classification decision making is conducted with the assistance of a threshold γ_A. The actual likelihood ratio is calculated as follows

$$\Lambda_A(i,j) = \frac{\int_\Theta \mathcal{L}(r|\theta) f(\theta|\mathcal{H}_{\mathcal{M}(i)}) d\theta}{\int_\Theta \mathcal{L}(r|\theta) f(\theta|\mathcal{H}_{\mathcal{M}(j)}) d\theta} \tag{2.28}$$

where the classification result is given using the conditional equation

$$\hat{\mathcal{M}} = \begin{cases} \mathcal{M}(i) & \text{if } \Lambda_A(i,j) \geq \gamma_A \\ \mathcal{M}(j) & \text{if } \Lambda_A(i,j) < \gamma_A \end{cases} \tag{2.29}$$

An easy assignment of the ratio test threshold is to define all thresholds to be one. The decision making becomes simple process of comparing the average likelihood of two hypotheses.

$$\hat{\mathcal{M}} = \begin{cases} \mathcal{M}(i) & \text{if } \mathcal{L}_{ALRT}(r|\mathcal{H}_{\mathcal{M}(i)}) \geq \mathcal{L}_{ALRT}(r|\mathcal{H}_{\mathcal{M}(j)}) \\ \mathcal{M}(j) & \text{if } \mathcal{L}_{ALRT}(r|\mathcal{H}_{\mathcal{M}(i)}) < \mathcal{L}_{ALRT}(r|\mathcal{H}_{\mathcal{M}(j)}) \end{cases} \tag{2.30}$$

Using the same assignment, the maximum likelihood decision making can also be applied using (2.23) with the likelihood function with average likelihood.

It is not difficult to see that the ALRT likelihood function has a much more complex form when unknown parameters are introduced. The requirement of underlining models

for unknown parameters rules that successful classification depends on the accuracy of the models. Consequently, if an accurate channel model is not known, the method becomes suboptimal and only an approximation to the optimal ALRT classifier. The additional requirement of the estimation hyperparameters adds yet another level of complexity and inaccuracy to the overall performance of the ALRT classifier. This is without mentioning that the likelihood function is more complex through an added integration operation.

For the above reason, Panagiotou, Anastasopoulos, and Polydoros proposed the General Likelihood Ratio Test (GLRT) as an alternative (Panagiotou et al., 2000). The GLRT in essence is a combination of a maximum likelihood estimator and a maximum likelihood classifier. The likelihood function, unlike the ALRT, replaces the integration of unknown parameters with a maximization of the likelihood over a possible interval for the unknown parameters. The likelihood function of the GLRT method is given by

$$\mathcal{L}_{GLRT}(r) = \max_{\Theta} \mathcal{L}(r|\alpha, \sigma, \theta_o) = \max_{\Theta} \prod_{n=1}^{N} \max_{A_m \in A} \frac{1}{M} \frac{1}{2\pi\sigma^2} e^{-\frac{\left|r[n]-\alpha e^{-j\theta_o} A_m\right|^2}{2\sigma^2}} \tag{2.31}$$

The complexity is notably further reduced. However, the classifier based on the modified GLRT likelihood function now becomes biased in both low SNR and high SNR scenarios. Assuming the modified GLRT likelihood function is used to classify among 4-QAM and 16-QAM signals. At low SNR, when signals are well spread, a 4-QAM modulated signal is always more likelihood to produce higher likelihood to a 16-QAM symbol, because the 16-QAM has more symbols and they are more densely populated under the assumption of unit power. At high SNR, when the signal is tight around the transmitted symbol, the maximization of the likelihood through channel gain is likely to be scaled the 16-QAM alphabets so that four symbols in the alphabet will be overlapping with the alphabet of the 4-QAM modulation. Such phenomenon observed in nested modulations produces equal likelihood between low order modulations and high order modulations when low order modulations are being classified. Therefore, the method is clearly biased for high order modulations in most scenarios.

While GLRT likelihood function provides alternative to ALRT, the fact that it is a biased classifier, as discussed in the previous section, makes it unsuitable for modulation with nested

modulations (e.g. QPSK, 8-PSK; 16-QAM, 64-QAM). For this reason, Panagiotou et al. proposed another likelihood ratio test named Hybrid Likelihood Ratio Test (HLRT). In the original publication, the HLRT is suggested as a LB classifier for unknown carrier phase offset. The likelihood in HLRT is calculated by averaging over the transmitted symbols and then maximizing the resulting likelihood function with respect to the carrier phase. The likelihood function is thus derived as

$$\mathcal{L}_{HLRT}(r) = \max_{\theta_o \in [0,2\pi]} \mathcal{L}(r|\theta_o) = \max_{\theta_o \in [0,2\pi]} \prod_{n=1}^{N} \sum_{m=1}^{M} \frac{1}{M} \frac{1}{2\pi\sigma^2} e^{-\frac{\left|r[n]-\alpha e^{-j\theta_o} A_m\right|^2}{2\sigma^2}}. \tag{2.32}$$

It is clear that the HLRT likelihood function calculates the likelihood of each signal sample belong to each alphabet symbol. Therefore, the case where a nested constellation creates a biased classification is of no existence. In addition, the maximization process replaces the integral of the unknown parameters and there PDFs for much lower analytical and computational complexity.

2.6 Distribution test based classifiers

When the observed signal is of sufficient length, the empirical distribution of the modulated signal becomes an interesting subject to study for modulation classification. In the beginning of this chapter, the signal distributions in various channels are given. It is clear that the signal distributions are mostly determined by two factors namely modulation symbol mapping and channel parameters. Assuming that the channel parameters are pre-estimated and available, the only variable in the signal distribution becomes the symbol mapping which is directly associated with the modulation scheme.

By reconstructing the signal distribution using the empirical distribution, the observed signals can be analysed through their signal distributions. If the theoretical distribution of different modulation candidates is available, there will exist one which best matches the underlying distribution of the signal to be classified. The evaluation of equality between difference distributions is also known as Goodness of Fit (GoF) which indicates how the sampled data fit the reference distribution. Ultimately, the classification is completed by finding the hypothesised signal distribution that has the best goodness of fit.

2.6.1 One-sample KS test

Kolmogorov-Smirnov test is a goodness of fit test which evaluates the equality of two probability distributions (Conover, 1980). The reference probability distributions can be sampled or theoretical Cumulative Distribution Function (CDF). There are two types of of KS test: one-sample KS test and two-sample test. In this section, we start with one-sample KS test which samples only the observed signal. In the next section, the two-sample KS test which samples both the observed signal and the reference signal is presented.

Massey first introduced the KS test (Massey 1951) building on theories developed by Kolmogorov (Kolmogorov, 1933) and Smirnov (Smirnov, 1939). The KS test has since been applied in many signal processing problems. F. Wang and X. Wang (Wang and Wang, 2010) first adopted the KS test for modulation classification highlighting its low complexity against likelihood based classifiers and high robustness versus cumulant based classifiers. Urriza, et al modified F. Wang and X. Wang's method for improved computational efficiency (Urriza et al., 2011).

In the context of modulation classification, we assume there are N number of received signal samples $r[1], r[2], ..., r[N]$ in the AWGN channel. The signal samples are first normalized to zero mean and unit power. The normalization is implemented on both the in-phase and quadrature segments of the signal samples separately.

$$r_I[n] = \frac{\Re(r[n]) - \overline{\Re(r)}}{\sigma(\Re(r))} \tag{2.33}$$

$$r_Q[n] = \frac{\Im(r[n]) - \overline{\Im(r)}}{\sigma(\Im(r))} \tag{2.34}$$

Where $\overline{\Re(r)}$ and $\overline{\Im(r)}$ are the mean of the real and imaginary part of the complex signal with $\sigma(\Re(r))$ and $\sigma(\Im(r))$ being the standard deviation of the real and imaginary part of the complex signal. In the case of non-blind modulation classification, the effective channel gain and noise variance after normalization is assumed to be known. The assumption is demanding whilst an alternative is found where these parameters are estimated as part of a blind modulation classification.

For the hypothesis modulation $\mathcal{M}(i)$ (with alphabet set $A_m \in A, m = 1, .., M$) in the

AWGN channel with effective gain α and noise variance σ^2, the hypothesis cumulative distribution function can be derived from the PDF of signal I-Q segments in (2.6).

$$F_i^I(x) = \int_{-\infty}^{x} \sum_{m=1}^{M} \frac{1}{M} \frac{1}{\sigma\sqrt{2\pi}} e^{-\frac{|x-\Re(\alpha A_m)|^2}{2\sigma^2}} dx \tag{2.35}$$

$$F_i^Q(x) = \int_{-\infty}^{x} \sum_{m=1}^{M} \frac{1}{M} \frac{1}{\sigma\sqrt{2\pi}} e^{-\frac{|x-\Im(\alpha A_m)|^2}{2\sigma^2}} dx \tag{2.36}$$

As only the cumulative distribution at the signal samples is needed, the cumulative distribution values are calculated for $F_i^I(\Re(r[1]))$, $F_i^I(\Re(r[2]))$,..., $F_i^I(\Re(r[N]))$ and $F_i^Q(\Im(r[1]))$, $F_i^Q(\Im(r[2]))$,..., $F_i^Q(\Im(r[N]))$. These values are calculated during the classification process and therefore the computation complexity should be included as part of the classifier. The empirical cumulative distribution function is calculated as

$$\hat{F}^I(x) = \frac{1}{N} \sum_{n=1}^{N} \mathbb{I}(\Re(r[n]) \leq x) \tag{2.37}$$

and

$$\hat{F}^Q(x) = \frac{1}{N} \sum_{n=1}^{N} \mathbb{I}(\Im(r[n]) \leq x) \tag{2.38}$$

where $\mathbb{I}(\cdot)$ is an indicator function which outputs of 1 if the input is true and 0 if the input is false. It is worth noting that the empirical cumulative distribution is independent of the test hypothesis. Therefore the collected values can be reused for all modulation hypotheses. With both the hypothesised cumulative distribution function and empirical cumulative distribution function ready, the test statistics of the one-sample Kolmogorov-Smirnov test can be found for each signal I-Q segments

$$D_i^I = \max_{1 \leq n \leq N} \left| \hat{F}^I(\Re(r[n])) - F_i^I(\Re(r[n])) \right| \tag{2.39}$$

$$D_i^Q = \max_{1 \leq n \leq N} \left| \hat{F}^Q(\Im(r[n])) - F_i^Q(\Im(r[n])) \right| \tag{2.40}$$

To accommodation the multiple test statistics calculated from multiple signal segments, they are simply averaged to create a single test statistics for the modulation decision making.

$$D_i = \frac{1}{2} \left(\max_{1 \leq n \leq N} \left| \hat{F}^I(\Re(r[n])) - F_i^I(\Re(r[n])) \right| + \max_{1 \leq n \leq N} \left| \hat{F}^Q(\Im(r[n])) - F_i^Q(\Im(r[n])) \right| \right) \tag{2.41}$$

In some cases when the modulation candidates have identical distribution (e.g. M-PSK, M-QAM) on their in-phase and quadrature segments their empirical cumulative distribution can be combine to form an empirical cumulative distribution function with larger statistics.

$$\hat{F}(x) = \frac{1}{2N} \sum_{n=1}^{N} \mathbb{I}(\Re(r[n]) \leq x) + \mathbb{I}(\Im(r[n]) \leq x) \tag{2.42}$$

Since the signal samples are complex, the multi-dimensional version of the KS test has been discussed in (Peacock, 1983; Fasano and Franceschini, 1987). We suggest to that corresponding test statistics can be modified to

$$D_i = \max_{1 \leq n \leq 2N} \left| \hat{F}(z[n]) - F_i^I(z[n]) \right| \tag{2.43}$$

where the test sampling locations are a collection of the in-phase and quadrature segments of the signal samples

$$z_{2n-1} = \Re(r[n]), z_{2n} = \Im(r[n]) \tag{2.44}$$

Regardless the format of test statistics the classification decision is based on the comparison of the test statistics of all modulation hypotheses. The modulation decision is assigned to the hypothesis with a smallest test statistics.

$$\hat{\mathcal{M}} = \arg\min_{\mathcal{M}_i \in \mathfrak{M}} D_i \tag{2.45}$$

2.6.2 Two-sample KS test

When the channel is relatively complex and the hypothesis cumulative distribution function is difficult to be modelled accurately, the two sample Kolmogorov-Smirnov test maybe much easier to implement. However, training/pilot samples are needed to construct the reference empirical cumulative distribution functions. Without any prior assumption on the channel state, K number of training samples $x[1], x[2], ..., x[K]$ are transmitted using modulation $\mathcal{M}(i)$. The empirical cumulative distribution function can be found following (2.37) and (2.38)

$$\hat{F}_i^I(x) = \frac{1}{N} \sum_{n=1}^{N} \mathbb{I}(\Re(x[n]) \leq x) \tag{2.46}$$

$$\hat{F}_i^Q(x) = \frac{1}{N}\sum_{n=1}^{N}\mathbb{I}(\Im(x[n]) \leq x) \tag{2.47}$$

The empirical cumulative distribution function of the N number of testing signal samples $r[1], r[2], ..., r[N]$ are formulated in the same way as (2.37) and (2.38). Using the two-sample test statistic, the two-sample test statistics for modulation classification can be found as

$$D_i = \frac{1}{2}\left(\max_{-\infty<x<\infty}\left|\hat{F}^I(x) - \hat{F}_i^I(x)\right| + \max_{-\infty<x<\infty}\left|\hat{F}^Q(x) - \hat{F}_i^Q(x)\right|\right) \tag{2.48}$$

In a practical implementation, it is easier to quantize the testing range of into a set of evenly distributed sampling locations. The classification rule is the same as the one-sample Kolmogorov-Smirnov test where the modulation hypothesis with the smallest test statistics is assigned as the classification decision.

2.7 Feature based classifiers

In this section, we list some of the well-recognised features designed for modulation classification. We first investigate the spectral based feature which exploits the spectral properties of different signal components. The high order static features are examined as opposed to classifier digital modulations of different type and orders.

2.7.1 Signal spectral based features

Nandi and Azzouz proposed some key signal spectral based features in the 1990s for the classification of basic analogue and digital modulations (Azzouz and Nandi, 1995, 1996b; Nandi and Azzouz, 1995). These key features generalized and advanced the works of Fabrizi et al. (Fabrizi et al., 1986); Chan and Gadbois (Chan and Gadbois, 1989); Jovanovic et al. (Jovanovic et al., 1990); which suggested different feature extraction method. The features exploit the unique spectral characters of different signal modulations in three key signal aspects namely the amplitude, phase, and frequency. Since different signal modulations exhibit different properties in their amplitude, phase, and frequency, a complete pool of modulation candidates are broken down to sets and subsets which can be discriminated with the most effective features. A decision tree, consisting of nodes of sequential tests

dedicated by different features, is often employed to give a clear guideline for the classification procedure.

The first feature, γ_{max}, is the maximum value of the spectral power density of the normalized and centred instantaneous amplitude of the received signal (Azzouz and Nandi, 1996b).

$$\gamma_{max} = \max |\mathrm{DFT}(A_{cn})|^2/N \tag{2.49}$$

where $\mathrm{DFT}(\cdot)$ is the discrete Fourier transform (DFT), A_{cn} is the normalized and centred instantaneous amplitude of the received signal $\boldsymbol{r}$, and N is the total number signal samples. The normalization is achieved by

$$A_{cn}[n] = A_n[n] - 1, \quad \text{where} \quad \mathrm{A_n[n]} = \frac{\mathrm{A[n]}}{\mu_{\mathrm{A}}}, \tag{2.50}$$

where μ_A is the mean of the instantaneous amplitude one signal segment.

$$\mu_A = \frac{1}{N}\sum_{n=1}^{N} a[n] \tag{2.51}$$

The normalization of the signal amplitude is designed to compensate the unknown channel attenuation.

The second feature, σ_{ap}, is the standard deviation of the absolute value of the non-linear component of the instantaneous phase.

$$\sigma_{ap} = \sqrt{\frac{1}{N_c}\left(\sum_{A_n[n]>A_t} \phi_{NL}^2[n]\right) - \left(\frac{1}{N_c}\sum_{A_n[n]>A_t} |\phi_{NL}[n]|\right)^2} \tag{2.52}$$

where N_c is the number of sample that meets the condition: $A_n[n] > A_t$. The variable A_t is a threshold value which filters out the low amplitude signal sample because of their high sensitivity to noise. $\phi_{NL}[n]$ denotes the non-linear component of the instantaneous phase of the nth signal sample.

The third feature, σ_{dp}, is the standard deviation of the non-linear component of the direct instantaneous phase.

$$\sigma_{dp} = \sqrt{\frac{1}{N_c}\left(\sum_{A_n[n]>A_t} \phi_{NL}^2[n]\right) - \left(\frac{1}{N_c}\sum_{A_n[n]>A_t} \phi_{NL}[n]\right)^2} \tag{2.53}$$

where all parameter remains same as in the expression for σ_{ap}. However, it is noticeable that the absolute operation on the non-linear component of the instantaneous phase is removed.

The fourth feature, P, is an evaluation of the spectrum symmetry around the carrier frequency.

$$P = \frac{P_L - P_U}{P_L + P_U} \tag{2.54}$$

where

$$P_L = \sum_{n=1}^{f_{cn}} |X_c[n]|^2 \tag{2.55}$$

$$P_U = \sum_{n=1}^{f_{cn}} |X_c[n + f_{cn} + 1]|^2 \tag{2.56}$$

$X_c[n]$ is the Fourier transform of the signal $x_c[n]$. $(f_{cn}+1)$ is the sample number corresponding to the carrier frequency f_c. f_s is the sampling rate.

$$f_{cn} = \frac{f_c N}{f_s} - 1 \tag{2.57}$$

The fifth feature, σ_{aa}, is the standard deviation of the absolute value of the normalized and centred instantaneous amplitude of the signal samples.

$$\sigma_{aa} = \sqrt{\frac{1}{N}\left(\sum_{n=1}^{N} A_{cn}^2[n]\right) - \left(\frac{1}{N}\sum_{n=1}^{N} |A_{cn}[n]|\right)^2} \tag{2.58}$$

The sixth feature, σ_{af}, is the standard deviation of the absolute value of the normalized and centred instantaneous frequency.

$$\sigma_{af} = \sqrt{\frac{1}{N_c}\left(\sum_{A_n[n]>A_t} f_N^2[n]\right) - \left(\frac{1}{N_c}\sum_{A_n[n]>A_t} |f_N[n]|\right)^2} \tag{2.59}$$

where the centred instantaneous frequency f_m is normalized by the sampling frequency f_s.

$$f_N[n] = f_m[n]/f_s \tag{2.60}$$

The instantaneous frequency is centred using the frequency mean μ_f

$$f_m[n] = f[n] - \mu_f \tag{2.61}$$

$$\mu_f = \frac{1}{N}\sum_{n=1}^{N} f[n] \tag{2.62}$$

The seventh feature, σ_a, is the standard deviation of the normalised and centred instantaneous amplitude.

$$\sigma_a = \sqrt{\frac{1}{N_c}\left(\sum_{A_n[n]>A_t} a_{cn}^2[n]\right) - \left(\frac{1}{N_c}\sum_{A_n[n]>A_t} a_{cn}[n]\right)^2} \tag{2.63}$$

The eighth feature, μ_{42}^a, is the kurtosis of the normalised and centred instantaneous amplitude.

$$\mu_{42}^a = \frac{E\{A_{cn}^4[n]\}}{\{E\{A_{cn}^2[n]\}\}^2} \tag{2.64}$$

The ninth feature, μ_{42}^f, is the kurtosis of the normalised and centred instantaneous amplitude.

$$\mu_{42}^f = \frac{E\{f_N^4[n]\}}{\{E\{f_N^2[n]\}\}^2} \tag{2.65}$$

Azzouz and Nandi designed decision trees for the classification analogue and digital modulations. The trees consist of an input node where all the features extracted and imported. The input node is followed by a sequence of conditional or decision steps facilitated with selected individual features. In this section, we have reorganized these decision trees and created a decision tree in Figure 2.1 for the classification of the aforementioned modulations. The diamond block in Figure 2.1 represents a conditional sub-stage classification, with $t(\cdot)$ being the suitable threshold for different features.

2.7.2 High-order statistics based features

Hipp was the first to adopt the third-order moment of the demodulated signal amplitude as a modulation classification feature (Hipp, 1986). Since we consider the demodulated signal as a luxury for any modulation classifier, this moment based feature is not investigated in this section. The usage of moment of moments in modulation classification is later extended by Soliman and Hsue who investigated the high-order moments of the signal phase for the classification of M-PSK modulations (Soliman and Hsue, 1992). They derived the theoretical kth moment of signal phase in Gaussian channel which leads to the conclusion that the

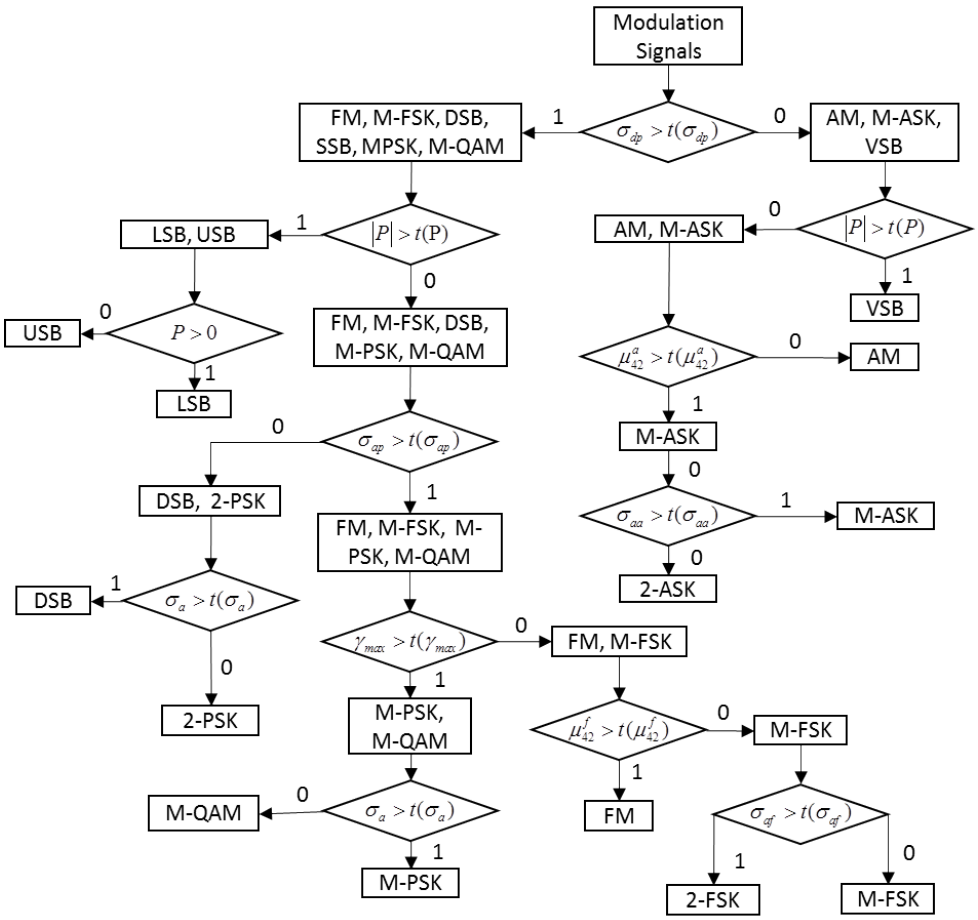

Figure 2.1: Decision tree for signal spectral based features.

moments are monotonically increasing function with respect to the order of the M-PSK modulation. Thus, high order M-PSK modulations have higher moment values which provide the condition for the classification of M-PSK modulations of different orders. Meanwhile, Soliman and Hsue also made the observation that the difference in moment values between higher order modulations is not distinct for lower-order moments. Therefore, they conclude that the effective classification of M-PSK modulation with higher order requires the moments of higher-order. The calculation of the kth order moment of the signal phase is defined as

$$\mu_k(r) = \frac{1}{N}\sum_{n=1}^{N}\phi^k(n) \tag{2.66}$$

where $\phi(n)$ is the phase of the nth signal sample. Azzouz and Nandi, proposed the kurtosis of the normalized-centred instantaneous amplitude μ_{42}^a and the kurtosis of the normalized-centred instantaneous frequency μ_{42}^f for the classification of M-ASK and M-FSK modulations. The expressions for these two features are given in (5.16) and (5.17). Hero and Hadinejad-Mahram generalized the moment based features to include the high order moment of signal phase and frequency magnitude (Hero and Hadinejad-Mahram, 1998). Spooner employs high-order cyclic moments as features (along with cyclic moments) for the classification of modulation with identical cyclic autocorrelation functions (Spooner, 1996). In later chapter, we use the following formula to calculate different kth moment of the complex-valued signal

$$\mu_{xy}(r) = \frac{1}{N}\sum_{n=1}^{N} r^x[n]\cdot r^{*y}[n] \tag{2.67}$$

where $x + y = k$ and $r^*[n]$ is the complex conjugate of $r[n]$.

Swami and Sadler suggested the fourth-order cumulant of the complex-valued signal as features for the classification of M-PAM, M-PSK, and M-QAM modulations (Swami and Sadler, 2000). For signal the second-order moments can be defined in two different ways. The two-digit subscript describes the order of the cumulant and the number of complex conjugate involved.

$$C_{20} = E\{r^2[n]\} \tag{2.68}$$

$$C_{21} = E\{|r[n]|^2\} \tag{2.69}$$

Likewise, the fourth-order moments and cumulants can be expressed in three different ways using different placement of conjugation,

$$C_{40} = \text{cum}(r[n], r[n], r[n], r[n]) \tag{2.70}$$

$$C_{41} = \text{cum}(r[n], r[n], r[n], r*[n]) \tag{2.71}$$

$$C_{42} = \text{cum}(r[n], r[n], r*[n], r*[n]) \tag{2.72}$$

where cum$(\cdot)$ is joint cumulant function defined by

$$\text{cum}(w, x, y, z) = E(wxyz) - E(wx)E(yz) - E(wy)E(xz) - E(wz)E(xy) \tag{2.73}$$

Meanwhile, the estimation of the second and fourth cumulants is achieved using the following processes,

$$\hat{C}_{20} = \frac{1}{N}\sum_{n=1}^{N} r^2[n] \tag{2.74}$$

$$\hat{C}_{21} = \frac{1}{N}\sum_{n=1}^{N} |r[n]|^2 \tag{2.75}$$

$$\hat{C}_{40} = \frac{1}{N}\sum_{n=1}^{N} r^4[n] - 3\hat{C}_{20} \tag{2.76}$$

$$\hat{C}_{41} = \frac{1}{N}\sum_{n=1}^{N} r^3[n]r*[n] - 3\hat{C}_{20}\hat{C}_{21} \tag{2.77}$$

$$\hat{C}_{42} = \frac{1}{N}\sum_{n=1}^{N} |r[n]|^4 - \left|\hat{C}_{20}\right|^2 - 2\hat{C}_{21}^2 \tag{2.78}$$

Cumulant values for some noise free modulation signals are listed in Table 2.1. It is clear from Table 2.1 that different modulations have different cumulant values between each other. Thus the classification of these modulations can be realized. The classification decision making could be achieve with a decision where modulations are divided in to subgroups for each cumulant.

	C_{20}	C_{21}	C_{40}	C_{41}	C_{42}
2-PAM	1.0000	1.0000	-2.0000	-2.0000	-2.0000
4-PAM	1.0000	1.0000	-1.3600	-1.3600	-1.3600
8-PAM	1.0000	1.0000	-1.2381	-1.2381	-1.2381
BPSK	1.0000	1.0000	-2.0000	-2.0000	-2.0000
QPSK	0.0000	1.0000	1.0000	0.0000	-1.0000
8-PSK	0.0000	1.0000	0.0000	0.0000	-1.0000
4-QAM	0.0000	1.0000	1.0000	0.0000	-1.0000
16-QAM	0.0000	1.0000	-0.6800	0.0000	-0.6800
64-QAM	0.0000	1.0000	-0.6191	0.0000	-0.6191

Table 2.1: Decision tree for modulations classification using spectral based features

2.8 Summary

In this chapter, the signal models in the AWGN channel, fading channel, and non-Gaussian are defined. The received signals are expressed using the the corresponding channel parameters, additive noise and transmitted signals. The resulting probability density functions are derived for the received signals the corresponding channels. Three main categories of classifiers are presented in the later part of the chapter. For likelihood based classifiers, maximum likelihood classifier and classifiers based on likelihood ratio tests are discussed in details. For distribution test based classifiers, the one-sample and two-sample Kolmogorov-Smirnov tests are illustrated with their implementation in modulation classification. Some of the modulation classification features are listed including signal spectral based features and high order statistics features.

Chapter 3

Machine Learning for Modulation Classification

3.1 Introduction

In Chapter 2, we list a collection of signal features for modulation classification. Some of the classification decision making is based on multi-stage decision trees where each stage utilizes a different feature. However, the need for designing the decision tree and optimization of multiple decision thresholds is not very convenient. To overcome these problems, various machine learning techniques have been employed to accomplish two major tasks in feature based modulation classification. First, the machine learning techniques can provide a classification decision making process that is much easier to implement. Second, the machine learning techniques can reduce the dimension of the feature set. It is achieved by feature selection and feature generation, which enables the consideration of a more versatile feature set while maintaining the computational efficiency of the classifier.

In this chapter, we first give two machine learning based classifiers namely k-nearest neighbour classifier and support vector machine classifier for modulation classification in combination with the features listed in Chapter 2. Next, the issue of feature space dimension reduction is explored through different algorithms including linear regression, genetic

algorithm, and genetic programming.

3.2 Machine learning based classifiers

3.2.1 K-nearest neighbour classifier

The K-nearest Neighbour (KNN) classifier is a non-parametric algorithm which assigns the class to a testing signal by analysing the number of nearest reference signals in the feature space. It has been used to solve many different classification problems (Espejo et al., 2010; Guo and Nandi, 2006).There are three mains steps in a KNN classifier.

To enable KNN classification, a reference feature space must be established first. The features space should include M reference values of each feature from each modulation class. The selection of M depends on the problem and is normally optimized heuristically. The motivation for a larger number of M is that the reference feature space provides a more accurate representation of the likely distribution of the testing signal features. On the other hand, a larger M value is likely to impose a higher computational complexity in the later steps of the KNN classifier.

For modulation classification, Zhu et al. suggested the use of training data from the same signal source for the generation of reference feature values (Zhu et al., 2010). The advantage of this approach is that the training signal shares the same source as the testing signal. Thus the reference feature space is an accurate representation of the feature distribution of the testing signal. Meanwhile, the construction of the reference feature space is really easy as the only step required is to calculate the feature values for the training signals. However, because of the random nature of the training signal, one cannot guarantee the accuracy of the feature space to be high enough. Synthesised reference values are more controlled over the construction of the reference feature space. Nevertheless, there need to be a hypothesised feature distribution which is often not reliable.

Since the classifier requires the evaluation of distances between the test signal and reference signals, a distance metric must be defined before the search of neighbouring reference signals can be achieved. There are many different metric systems that can be used for

distance measurement in a KNN classifier. Euclidean distance is one of the most common distance metrics for KNN classifier. Given a feature set $\mathbb{F} = \{\mathbb{f}_1, \mathbb{f}_2 ... \mathbb{f}_L\}$ with L number of features, the Euclidean distance between feature set of signal A and B is calculated as

$$D(\mathbb{F}(A), \mathbb{F}(B)) = \sqrt{\sum_{l=1}^{L} [\mathbb{f}_l(A) - \mathbb{f}_l(B)]^2} \tag{3.1}$$

Having established the distance measurement, the classification decision is achieved by finding the nearest number of reference samples and analysing the demography with these k number of samples.

When the distances between test signal and all reference signals are evaluated, k number of the reference signals are recorded as the k nearest neighbour. The selection of the value of k should follow these rules:

- The value should ideally be a prime number, to avoid the case where the k neighbour consisting of an equal number of reference signals from different classes.
- The value should be less than the total number of reference signals from a signal class.
- The value of k should be big enough to avoid false classification caused by outliers.

The actual optimization of the value k can be heuristic because it has been shown that the classification does not vary much if the k value is in a reasonable range. The end classification result is achieved by finding the majority of the k-nearest neighbour that share the same class. This class will be assigned to the testing signal as the classification result. A pseudo code for the KNN classifier implementation is given below.

The KNN is non-parametric and capable of multi-class classification. However it suffers with increasing number of features which raises the dimension of the feature space and the complexity of the distance calculation. Therefore, some sort of dimension reduction is needed to make this method viable. Another disadvantage of the KNN classifier is that the features contribution to the classification decision making is not weighted. There maybe cases where the final distance is mostly affected by only one feature, if the distribution of this feature is sparse and the distance between the testing sample and the reference sample on this feature

Algorithm 1: K-nearest Neighbour Classifier

Input: M reference signals from every candidate modulation $\mathcal{M}(i)$, $i = 1, 2, ..., I$, each with a set of extracted features $\mathbb{F}^i(m)$, an observed unknown signal with extracted feature set $\mathbb{F}$, a pre-defined k value

begin

Distance between and every reference feature set is calculated using (3.1)

The resulting distances $D(\mathbb{F}, \mathbb{F}^i(m))$ are sorted in descending order

The first k distances are selected

The modulation label for each distance $D(\mathbb{F}, \mathbb{F}^i(m))$ is extracted

The mode of the set extracted label set i' is used to identify the modulation

Output: classified modulation type $\hat{\mathcal{M}}$

dimension is on a larger scale compared to other feature dimensions. The classification of some modulations relaying on other features may be affected.

In AWGN channel, BPSK, QPSK, 16-QAM and 64-QAM signals are simulated using (2.4) to evaluate the performance of a KNN classifier. A set of 16 different signal length and SNR combinations are simulated with each consisting 10,000 signal realizations from each modulation. In addition, 50 realizations of each modulation signal are generated to form the reference feature space in each channel setting. The k value is set to 11. High order cumulants including C_{40}, C_{41}, C_{42}, C_{60}, C_{61}, C_{62} and C_{63} are extracted from each testing signals as classification features. The classification accuracy P_{cc} for each signal modulation is calculated using the following formula,

$$P_{cc} = \frac{L_s}{L} \ (\%) \tag{3.2}$$

where L_s is the number of signal realizations been successfully classified. The classification of all modulations are averaged to produce the classification accuracy in Table 3.1.

It is clear that the percentage of correct classification increases with higher SNR and longer signal length. It is a phenomenon commonly observed in most modulation classifiers. This KNN classifier is a rather simple approaches to the problem. The improved KNN classifier with feature enhancement and multi-stage classification is given more detailed discussion

	Number of Samples			
SNR	512	1024	2048	4096
5 dB	79%	81%	91%	96%
10 dB	88%	93%	99%	100%
15 dB	90%	97%	100%	100%
20 dB	93%	98%	100%	100%

Table 3.1: Modulation classification performance of a KNN classifier in AWGN channels

in Section 3.3.3.

3.2.2 Support vector machine classifier

Support Vector Machine (SVM) provides another way to achieve classification in the existing multi-dimensional feature space. It has been adopted for the classification of many different data sets (Mustafa and Doroslovacki, 2004; Polat and Güne, 2007; Akay, 2009). SVM achieve classification by finding the hyperplane that separates data from different classes. The hyperplane, meanwhile, is optimized by maximizing its distance to the signal samples on each side of the hyper-plane. Depending on the nature of the signal being classified, the SVM classifiers can be divided into linear and non-linear versions.

The linear SVM classifiers have linear kernels. The kernel is defined by

$$K(\boldsymbol{x}, \boldsymbol{w}) = \boldsymbol{x}^T \boldsymbol{w} \tag{3.3}$$

where $\boldsymbol{x} = [x_1 ... x_K]$ is the input feature vector and is the weight vector to be optimized. The kernel defines a linear separation hyperplane (Theodoridis, 2008)

$$g(\boldsymbol{x}) = \boldsymbol{x}^T \boldsymbol{w} + w_0 \tag{3.4}$$

where w_0 is a constant. The classification of a two-class (between modulation candidate $\mathcal{M}(a)$ and $\mathcal{M}(b)$) problem is achieved by simply using the sign of $g(\boldsymbol{x})$

$$\hat{\mathcal{M}} = \begin{cases} \mathcal{M}(a), g(\boldsymbol{x}) = \boldsymbol{x}^T \boldsymbol{w} + w_0 \geq 0 \\ \mathcal{M}(b), g(\boldsymbol{x}) = \boldsymbol{x}^T \boldsymbol{w} + w_0 < 0 \end{cases} \tag{3.5}$$

To obtain the weight through training, the following optimization process is exercised

$$\text{maximize} \quad \mathrm{J}(w, w_0) = \frac{2}{\|w\|^2} \tag{3.6}$$

$$\text{subject to} \quad y_i(w^T x_i + w_0) \geq 1, \quad i = 1, 2, ..., N \tag{3.7}$$

where y_i is the class indicator for the ith feature vector (+1 for $\mathcal{M}(a)$ and -1 for $\mathcal{M}(b)$). An illustration of a SVM for a two-class problem is given in Figure 3.1.

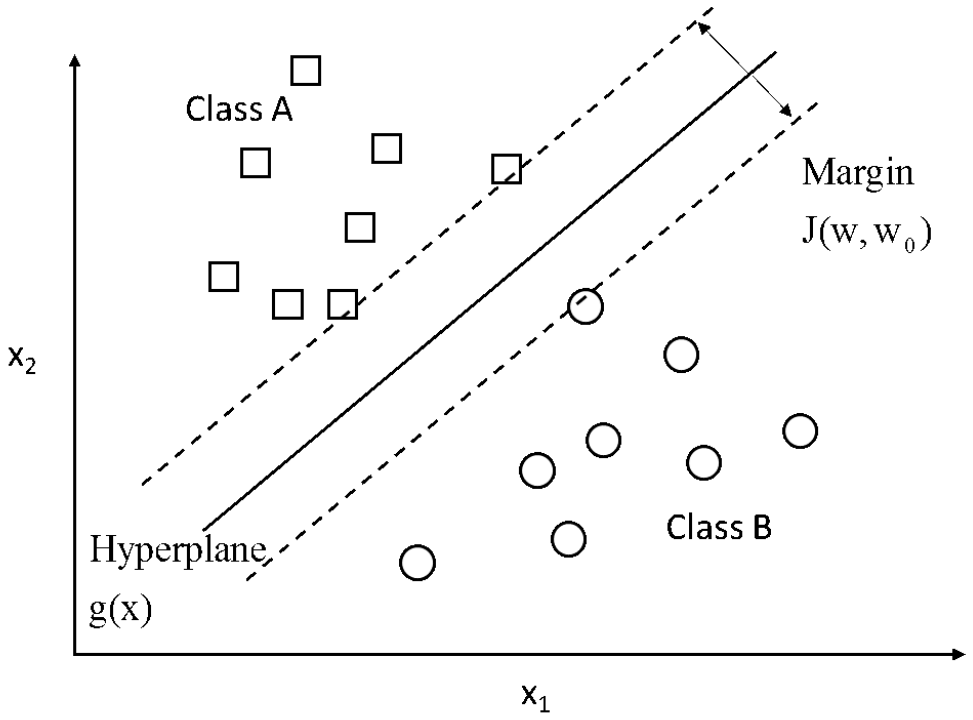

Figure 3.1: Feature space and SVM with linear kernel and X_1 and X_2 representing two separate feature dimensions.

The non-linear version of the SVM classifier shares the same training and classification process as the linear SVM classifier. Except, the kernel used for hyper-plane is replaced by a non-linear kernel. We have tested in the past that a polynomial kernel is enough to provide effective classification. The polynomial kernel is given by

$$K(\boldsymbol{x}, \boldsymbol{w}) = (\boldsymbol{x}^T \boldsymbol{w})^d \tag{3.8}$$

where d is the degrees of the polynomials. A general procedure of the SVM classifier for AMC described using pseudo code in Algorithm 2.

Algorithm 2: Support Vector Machine Modulation Classifier

Input: M reference signals from two candidate modulation $\mathcal{M}(i)$, $i = 1, 2$ each with a set of extracted feature set $\mathbb{F}^i(m)$, an observed unknown signal with extracted feature set $\mathbb{F}$, a pre-defined value d if using non-linear SVM classifier

begin

initialize weights $\boldsymbol{w}$ and w_0

repeat

update the weights through (3.6) and (3.7) using $\mathbb{F}^i(m)$

until *maximum number iteration reached*

$K(\mathbb{F}, \boldsymbol{w}) + w_0$ is calculated

if $K(\mathbb{F}, \boldsymbol{w}) + w_0 \geq 0$ **then**

$\mathcal{M}(1)$ is given as classification decision $\hat{\mathcal{M}}$

if $K(\mathbb{F}, \boldsymbol{w}) + w_0 < 0$ **then**

$\mathcal{M}(2)$ is given as classification decision $\hat{\mathcal{M}}$

Output: classified modulation type $\hat{\mathcal{M}}$

Compared to the KNN classifier, the SVM classifier only needed to use the training signal when establishing the separating hyperplane. Once the hyperplane is optimized, there is no need to involve the training signal in any sort of further calculation. The benefit is that the computation needed at the testing stage is relatively inexpensive compared to KNN. However, the SVM classifier is most natural for two-class classification. There are implementations of a multi-classes classification using SVM however the implementation is much less intuitive than the two-class case. Gunn first suggested SVM for modulation classification (Gunn, 1998). It was later extended by several other studies (Mustafa and Doroslovacki, 2004; Dan et al., 2005; Wu et al., 2005). In this research, we incorporated the SVM classifier as part of the fitness evaluation process in genetic programming. More details on the implementation, performance and analysis are given in Section 3.3.3.

3.3 Feature selection and combination

For both KNN and SVM classifier, it is always preferable to have as many features as possible for improving the classification accuracy. However, both classifiers suffer when the number of features increase. That is why reducing the feature space dimension is necessary. Using machine learning algorithms, there are two ways to do so. First, feature space dimension can be reduced by eliminating some of the features which make less or no contribution to the classification task. Second, feature space dimension can be reduced by combining the existing feature into fewer new features.

3.3.1 Logistic regression

While feature selection is an effective way to reduce the complexity for a feature based modulation classifier, the elimination of a feature can sometimes be destructive. That is without mentioning that sometime the features are all useful to some degree and the elimination of any feature can be destructive for the classification performance. In this case, a more conservative approach is needed for dimension reduction. That is why feature combination has been considered for not just the reduction of feature dimension but also for enhancing the performance of these features.

To begin with, linear combination of the features is the simplest but often effect way of the combining the features. Assuming we are combining number of existing features into a single new feature, the linear combination is given by

$$\mathbb{f}_{new} = w_0 + \sum_{k=1}^{K} w_k \mathbb{f}_k \tag{3.9}$$

where w_k is the weight of the kth feature , w_0 is a constant, and K is the total number of features available for combination. The process to optimize these weights is called logistic regression which aims to maximize the difference of the new feature value between different classes. It has been adopted by Zhu et al. in the dimension reduction for distribution based features (Zhu et al., 2013c).

There are two common logistic regression tools in the family of generalized linear regression algorithms namely binomial logistic regression and multinomial logistic regression. The

binominal logistic regression is designed to project the signal using a logistic function $p(\cdot)$ so that $p(\cdot)$ equals to 1 when the signal is modulated using $\mathcal{M}(i)$ and 0 if the signal modulation using $\mathcal{M}(j)$.

$$p(\mathbb{F}) = \frac{1}{1 + e^{-g(\mathbb{F})}} \tag{3.10}$$

where $\mathbb{F}$ is the collection of existing features and $g(\cdot)$ is the logit function, the inverse of the logistic function $p(\cdot)$, given by

$$g(\mathbb{F}) = B_0 + \sum_{k=1}^{K} B_k \mathbb{f}_k \tag{3.11}$$

The estimation of each of the parameter B_0 and B_k is often achieved using iterative processes such as Newton-Raphson method (Hosmer and Lemeshow, 2000). The resulting estimation of B_0 and B_k can be used to substitute the weights w_0 and w_k in (3.9). Logistic regression provides a basic tool for feature selection and combination. However, multi-class classification is not always suited for linear regression assisted feature selection and combination. It is sometimes better to divide the classification into multiple steps.

In this research, we applied logistic regression on for the enhancement of distribution based features. More details are given in Chapter 4.

3.3.2 Genetic algorithm

To overcome the issue of high dimensionality in the feature space, Wong and Nandi suggested Genetic Algorithm (GA) as a tool for reducing the number of features (Wong and Nandi, 2004). They used binary strings to represent the selection of different features. If there are 5 existing feature, a binary string example could be 11000, which means that the first two features are selected for classification and the last three features are neglected.

The training of such binary strings begins with a randomly generated string. According to the initial binary string, features are selected for modulation classification with some training data. The resulting classification performance achieved by these selected features is then used as a criterion for evaluating the performance of the binary string. Based on their performance, better binary strings are selected for the evolutionary process of producing new binary strings are migrates toward the optimal solution or optimal selection of features. The

two genetic operators used are crossover and mutation.

For crossover, we assume there are two parent binary strings 11011 and 01000. The crossover would randomly choose equal number of bits in both parents and swap their values. In the given case, if the first four digits are selected. The children of the crossover operation would be 01001 and 11010 which represents two new sets of selected features.

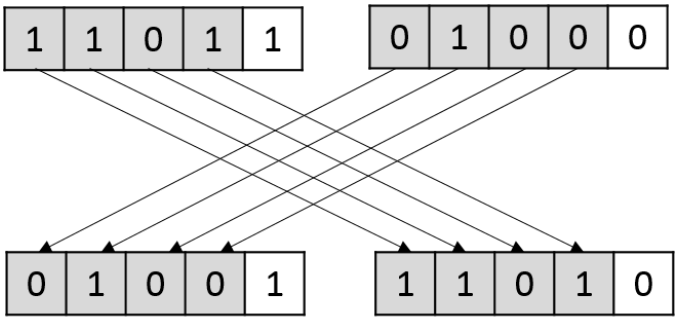

Figure 3.2: Crossover operation in genetic algorithm.

Meanwhile, mutation utilizes only one parent e.g. 11011. The operation is the process of selecting random digits in the parent string and generating a random value for that digit. Using the example, if the mutation operation selects the first, third, and fourth digit of the binary string, the resulting child string would become 01111. Since the new value is randomly generated they could be same as the parent value as seen in the fourth digit or different as seen in the first and third digit.

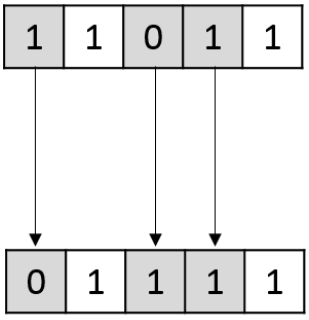

Figure 3.3: Mutation operation in genetic algorithm.

The processes of fitness evaluation, parent selection, and reproduction are repeated for

a pre-defined number of generations, after which the GA is terminated. Termination can also be triggered if the average or best fitness in the current generation reaches a pre-defined threshold or the improvement over the last few generations becomes lower than a pre-defined threshold. In the end, the binary strings in all generations are ranked by their fitness. The string with the highest fitness is selected as the final product of the GA process. According the binary string, the features can be selected subsequently. It is worth mentioning that the GA process can be highly random because of the random initialization and mutation operation. It is sometimes recommended to repeat the GA process several times and to produce a few sets of different feature selections from which the best feature selection can a determined by another test.

GA has been used in this research for the optimization of sampling locations in the optimized distribution sampling classifier. More details on its implementation is given in Chapter 4.

3.3.3 Genetic programming

Koza popularized the Genetic Programming (GP) as another evolutionary machine learning algorithm (Koza, 1992). It has since been used for classification of many different types of data and signal (Espejo et al., 2010). Zhu et al. first employed GP for modulation classification feature selection and combination (Zhu et al., 2010). Zhu et al. also extended the application of GP in modulation classification by combine GP with other machine learning algorithms to achieve improved classification performance (Zhu et al., 2011; Aslam et al., 2012).

GP belongs to the class of evolutionary algorithms which attempt to emulate Darwinian model of natural evolution. It is a machine learning methodology which is used to optimize a population of individuals (computer programs) with the help of tness values. GP develops the solution of a problem in the form of a mathematical formula. Each solution is a computer program and can be represented in the form of tree. Each tree has terminal nodes (data nodes) and internal nodes (function nodes). Each individual is given a tness value which quanties its ability to solve the given problem. The tness value is computed using a user-

dened tness function. This tness function used depends upon the nature of the problem. The advantages GP have on other machine learning methods are listed below. (a) No prior knowledge about the statistical distribution of data is needed. (b) Pre-processing of data is not required and data can be used directly by GP in its original form. (c) GP returns mathematical function as output which can be used directly in application environment. (d) GP has the inherent capability to select useful features and ignore others. Typically GP implementation follows the following steps: (a) GP starts with a randomly generated population of user dened size. (b) Each individual is assigned a tness value which represents the strength of the individual to solve the given problem. (c) A genetic operator is applied on current generation to give birth to individuals of next generation. Genetic operators are explained in the next section. (d) All the individuals are given tness values and those individuals having better tness values get transferred to the next generation. (e) Step (c) and (d) are repeated till a desired solution is achieved. Otherwise GP is terminated after a certain number of generations set by the user.

There are different ways to represent the individuals (computer programs) in GP. One of the common representations is a tree representation and the same representation has been used here as well. A tree has terminal nodes, internal nodes and output node. Terminal nodes represent the inputs, and internal nodes represent the functions operating on inputs while the output node gives the output of the tree. An example of a tree structures mathematical formula $(A + B) \times C$ is given in Figure 3.4. In the case of modulation classification feature selection and combination, the input nodes are the selected raw feature. The output node represents the desired new feature combination.

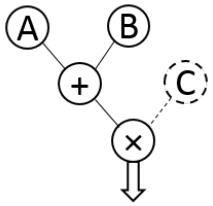

Figure 3.4: Genetic programming individuals in the form of a tree structure.

Genetic operators are used for reproducing new individuals from older individuals. The

operation mimics the genetic processes observed in genetic science. The tradition operators included in a standard GP are crossover and mutation. Semantically, crossover is intended for the sharing of fitter parts of two different individuals in order to create a new individual which is fitter than both parents. Meanwhile, mutation generates new individual by replacing a random branch of a parent with a randomly generated new branch in hope of the child to have better fitness than the parent. Practically, the sematic motive of crossover and mutation is implemented with random symbolic process. We shall use a simple example to illustrated how crossover and mutation is achieved in standard GP.

Let us assume that there are two parent trees each representing a mathematical formula as shown in Figure 3.5. The first step of crossover randomly selects a branch in each parent

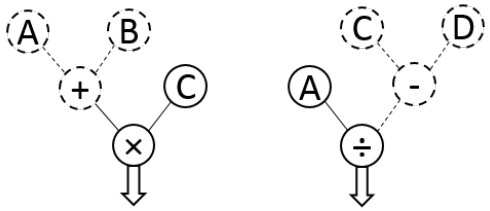

Figure 3.5: Parents selected for crossover operation in genetic programming.

three. The selected branch is highlighted in Figure 3.5 with dash lines. In the second step, the selected branches are swapped between the two parents creating two new individuals as shown in Figure 3.6.

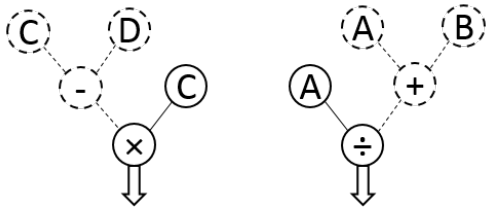

Figure 3.6: Children produced by the crossover operation in genetic programming.

For mutation, we use select only one tree as shown in Figure 3.7. The first step of the mutation selects a random branch from the parent tree. In the second step, a new branch is randomly generated. Finally, the mutation is completed by attaching the randomly generated

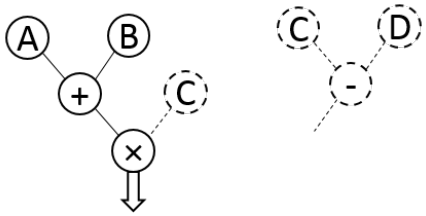

Figure 3.7: Parent selected for mutation operation and a randomly generated branch.

new branch to the same position where the old branch is removed from. The resulting tree is the child three of a mutation operation.

Fitness evaluation is the most important design component because it is directly linked to the evaluation of how well an individual in the evolution solves the given problem. If a miss fitting fitness criterion is used, regardless of how efficient the GP is, the end solution will deviated from the goal of the entire system.

For modulation classification, as we dedicated GP as a feature selector and generator, the goal is to generate a combination of selected features which provides fast and accurate modulation classification. Because of the nature of the task, there has been two different approaches to define the fitness function. The first approach is to evaluate the quality of the new feature by measuring the inter-class tightness and intra-class separation given some training signals. To achieve such evaluation, Aslam et al. proposed to use Fisher's criterion as the fitness function for GP (Aslam et al., 2011). Assuming there are number of signal realizations from two different modulations A and B, a new feature acquired through GP can be calculated for each signal realization. Therefore, we have two sets of feature values $\mathbb{f}_A(1), \mathbb{f}_A(2)...\mathbb{f}_A(L)$ and $\mathbb{f}_B(1), \mathbb{f}_B(2)...\mathbb{f}_B(L)$. To calculate the fitness of this new feature, the following fitness function is employed base on Fisher's criterion,

$$\mathcal{F}(\mathbb{f}) = \frac{|\mu_A - \mu_B|}{\sqrt{\sigma_A^2 + \sigma_B^2}} \tag{3.12}$$

where μ_A and μ_B are the means of the two set of the feature values and σ_A^2 and σ_B^2 are the corresponding variances.

$$\mu_A = \frac{1}{L}\sum_{l=1}^{L} \mathbb{f}_A(l) \quad \text{and} \quad \mu_B = \frac{1}{L}\sum_{l=1}^{L} \mathbb{f}_B(l) \tag{3.13}$$

$$\sigma_A^2 = \frac{1}{L}\sum_{l=1}^{L}[\mathbb{f}_A(l) - \mu_A]^2 \quad \text{and} \quad \sigma_B^2 = \frac{1}{L}\sum_{l=1}^{L}[\mathbb{f}_B(l) - \mu_B]^2 \tag{3.14}$$

It is obvious that the nominator measures the separation of the features from different modulation signal and the denominator measure the tightness of the features from the same modulation signals. Therefore, the fitness function matches the desired property of an effective feature for modulation classification. However, there are two drawbacks of the Fisher's criterion for fitness evaluation. First, the criterion is developed with the assumption of the statistic being normally distributed. In the case of GP generated features, it is very difficult to establish the distribution of a new feature because the features can be a very complicated combination of many existing features. That is without mentioning the normality need to be met for each new feature which various dramatically because of the random nature of GP. The genetic operators constantly maintain the diversity in the populations resulting in new features of diverse distributions. Secondly, in practice, there are cases where the trained new feature may converge to have minimum amount of difference in their mean difference while having very small variance. In other cases, the new feature can have very big mean difference while the variance also being infinitely big.

Meanwhile, there is another approach which does not share the flaws of the Fisher's criterion based fitness evaluation. As the ultimate goal for the new feature is to enhance the classification performance, we used a small set of training signals in the GP evaluation and incorporated a computational efficient classifier in the fitness evaluation (Zhu et al., 2010). The fitness, in this case, is evaluated by directly classifying the training signals with a classifier from which the average classification accuracy is used as the fitness value.

In the first case, we employed the KNN classifier for the fitness evaluation. Different from conventional fitness evaluation, the tree output from each individual is not directly utilized for fitness calculation having employed the target value from the training input. Instead, the output is used as a new feature for the KNN classifier with some of the training data used as reference samples and the remaining training data used for evaluating trees. The classification results from KNN classifier are obtained as described in earlier in this section. Once the classification is finished, the result is returned to the fitness calculation function

to be checked with the correct class information. The number of correct classifications and incorrect classifications are calculated for the fitness calculation. The fitness $\mathcal{F}$ is given by

$$\mathcal{F}(\mathbb{f}) = \sum_{i=1}^{I} w^i P_{cc}^i \tag{3.15}$$

where I is the number of candidate modulations, and P_{cc}^i is the number of classification errors for class i. Because this is a multi-class classification, errors from different classes are recorded separately and can be assigned with different penalty weight w^i. By setting different w^i, the program can adjust its classification performance for different classes. The larger penalty given to a class, the evolution will be more biased to correctly classify this class. Ultimately, the individuals with high fitness values, which indicate better classification performance and better fitness, will have an increased chance of joining the evolution of the next generation via different operations.

Initially GP was used to classify all modulations in a single stage but as the classification of BPSK and QPSK are easier compared to other two modulations, a drift was seen in GP to the classification of BPSK and QPSK and the improvement in classification of M-QAM(M>4) was minimal. Therefore, in order to achieve the better performance for all classes, a two-stage genetic programming has been used here to counter this problem. At the first stage, classification of BPSK, QPSK and M-QAM(M>4) is performed. At the second stage, GP is used again to do the classification of remaining two classes. So at the second stage GP creates a new tree for the classication of remaining classes. As this tree is independent from the first tree and it is solely devoted for the classification of M-QAM(M>4) modulations, the accuracy would be better. The two stages are shown in Figure 3.8. The performance of GP for these two stages for classification of different classes is shown in Figure 3.9 and Figure 3.10.

To evaluate the combination of GP and KNN, the following simulation is set up in MATLAB environment. The GP programs are developed based on Silva's GPLAB toolbox (Silva, 2007). The parameters used for the experiments are given in detail in Table 3.2. The number of generations used for all the experiments were 100. It is determined by 10 trail runs with 500 number of generation in which convergence was observed in the first 100

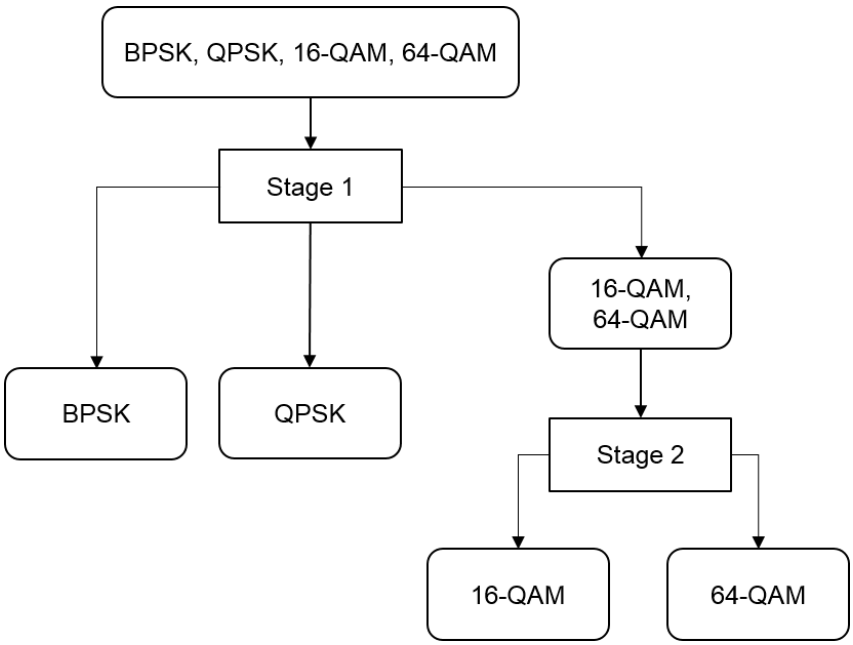

Figure 3.8: Two stage classification of BPSK, QPSK, 16-QAM and 64-QAM signals.

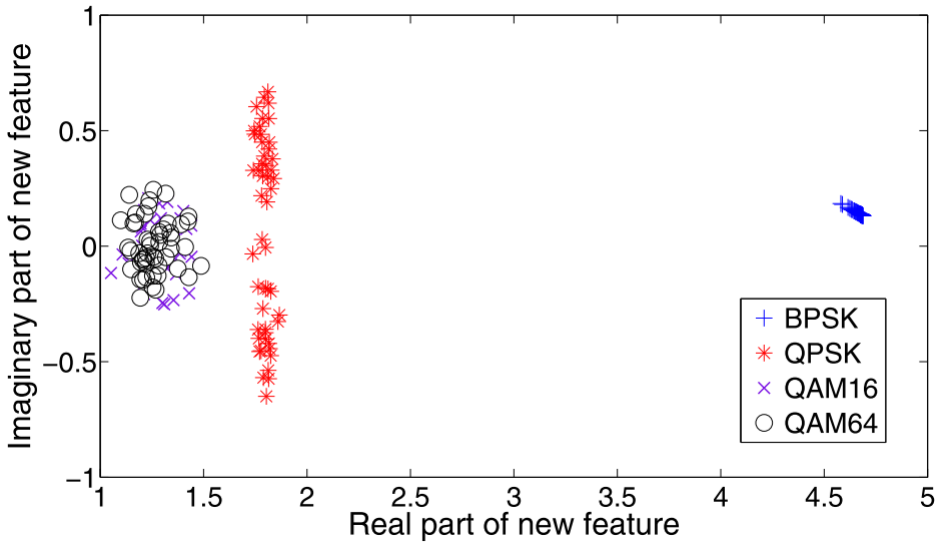

Figure 3.9: New GP feature space for stage 1 of the GP-KNN classifier.

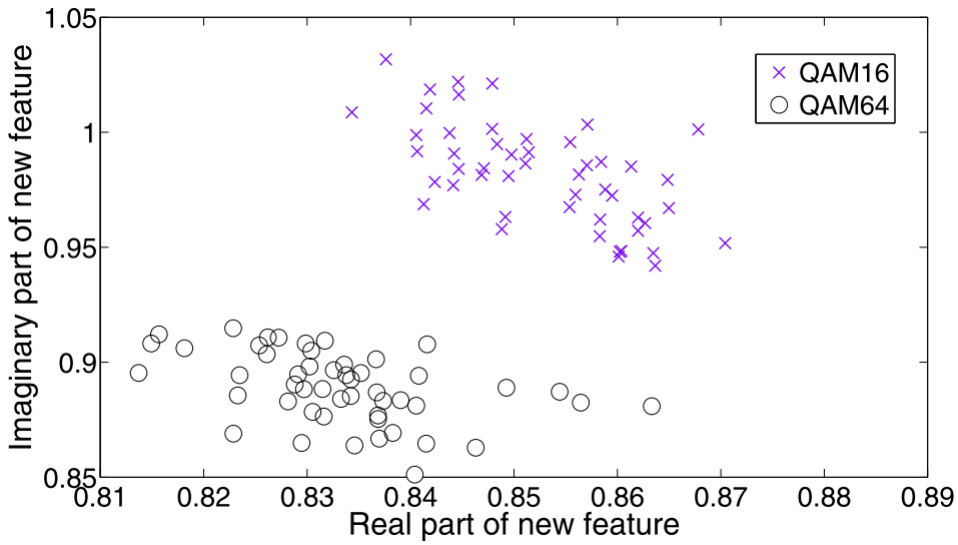

Figure 3.10: New GP feature space for stage 2 of the GP-KNN classifier.

Parameters	Values
Number of generations	100
Population size	25
Function pool	plus, minus, times, reciprocal, negator, abs, sqrt, sin, cos, tan, asin, acos, tanh, mylog
Terminal pool	HOS features
Genetic operators	crossover and mutation
Operator probabilities	90% and 10%
Tree generation	ramped half-and-half
Initial maximum depth	28
Selection operator	lexictour
Elitism	replace

Table 3.2: Parameters used in genetic programming and KNN classifier.

generations. The number of individuals in each of the experiments were 25. Total number of training experiments done is also 25. So the total number of individuals or solutions created were 625. The best tree out of these 625 trees was tested with test data and results are analysed here. The number of samples used are 512, 1024, 2048 and 4096 respectively, and the SNRs used are 5 dB, 10 dB, 15 dB and 20 dB. For each value of SNR and number of samples, 10,000 signal realizations are produced. These 10,000 realizations are tested with the best tree and results are summarized.

	Number of Samples			
SNR	512	1024	2048	4096
5 dB	84±4 %	88±3 %	93±3 %	97±2 %
10 dB	94±2 %	98±0 %	100±0 %	100±0 %
15 dB	97±2 %	99±0 %	100±0 %	100±0 %
20 dB	98±1 %	100±0 %	100±0 %	100±0 %

Table 3.3: Classification performance of a GP-KNN classifier in AWGN channels

Table 3.3 shows the results obtained for particular combination of SNRs and number of samples. The results for simple KNN in the same setting can be found in Table 3.1. It is clear from these results that GP-KNN produces better results compared to the simple KNN classifier. Meanwhile, the performance of GP for different SNRs and at 1024 number of samples is given in Table 3.4 in the form of confusion matrix. It is clear from this Table that classication of BPSK and QPSK is easier as compared to other two modulations. The classification performance for BPSK and QPSK is 100% in all the cases as shown in matrix. Figure 3.11 shows the performance against SNR for different values of number of samples. It is clear from the Figure that performance reaches to 100% at an SNR of 8 dB and 4096 number of samples. One can see from the Figure that the greater the number of samples the better is the performance. In all the curves shown in Figure 3.11 there is a dip in performance at 3 dB. Table 3.5 explains the reason behind this dip. Table 3.5 gives the range of values of new feature created by GP at 2, 3, 4 and 5 dB for BPSK, QPSK, 16-QAM and 64-QAM respectively. At 2 dB the values of 16-QAM and 64-QAM are in between the values of BPSK

SNR	Modulation Candidates	BPSK	QPSK	16-QAM	64-QAM
5 dB	BPSK	10000	0	0	0
	QPSK	0	10000	0	0
	16-QAM	0	0	8091	3404
	64-QAM	0	0	1909	6596
10 dB	BPSK	10000	0	0	0
	QPSK	0	10000	0	0
	16-QAM	0	0	9557	423
	64-QAM	0	0	443	9577
15 dB	BPSK	10000	0	0	0
	QPSK	0	10000	0	0
	16-QAM	0	0	9870	145
	64-QAM	0	0	130	9855
20 dB	BPSK	10000	0	0	0
	QPSK	0	10000	0	0
	16-QAM	0	0	9924	104
	64-QAM	0	0	76	9896

Table 3.4: Classification confusion matrix of a GP-KNN classifier in AWGN channels

	Number of Samples			
SNR	BPSK	QPSK	16-QAM	64-QAM
2 dB	3.2-5.5	0.6-1.3	1.2-1.5	1.3-1.5
3 dB	4.5-6.6	0.6-1.3	1.2-1.5	1.3-1.5
4 dB	5.8-7.7	1.3-1.9	0.7-1.4	0.9-1.5
5 dB	7.2-8.8	1.6-2.2	0.6-1.3	0.7-1.4

Table 3.5: Range of new GP generated feature values for different modulations between 2 dB and 5 dB.

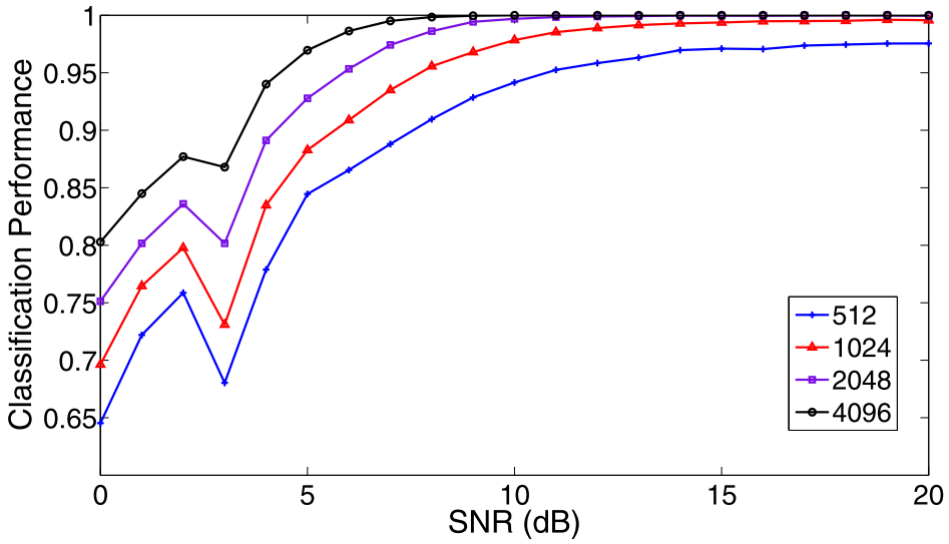

Figure 3.11: Parent selected for mutation operation and a randomly generated branch.

and QPSK. As the SNR increases the feature values of BPSK and QPSK increase while the values of 16-QAM and 64-QAM decrease a little. At the 3 dB SNR, QPSK crosses both 16-QAM and 64-QAM, and that is the reason why the performance is low at this particular SNR. As the SNR goes above 3 dB, QPSK feature value starts going above the feature values of both 16-QAM and 64-QAM. This new feature value of QPSK continues to increase with increase in SNR. At 5 dB the feature value of QPSK is greater than the values of 16-QAM and 64-QAM so the performance always increases after this SNR. It is to be mentioned that these feature values are taken from the first stage where 16-QAM and 64-QAM are treated as one class. That is why their values are completely overlapping with each other in this Table.

As concluded previously, the classification of 16-QAM and 64-QAM is more difficult and the performance curves for these two modulations are presented separately. Figure 3.12 shows the performance of 16-QAM and 64-QAM for different SNRs. It is clear from this figure that the performance reaches 100% at an SNR of 8 dB at 4096 number of samples. As the dip at 3 dB in Figure 3.11 was due to the overlap of QPSK with M-QAM(M>4), that dip is not present in this Figure which considers only 16-QAM and 64-QAM. Figure 3.13 shows

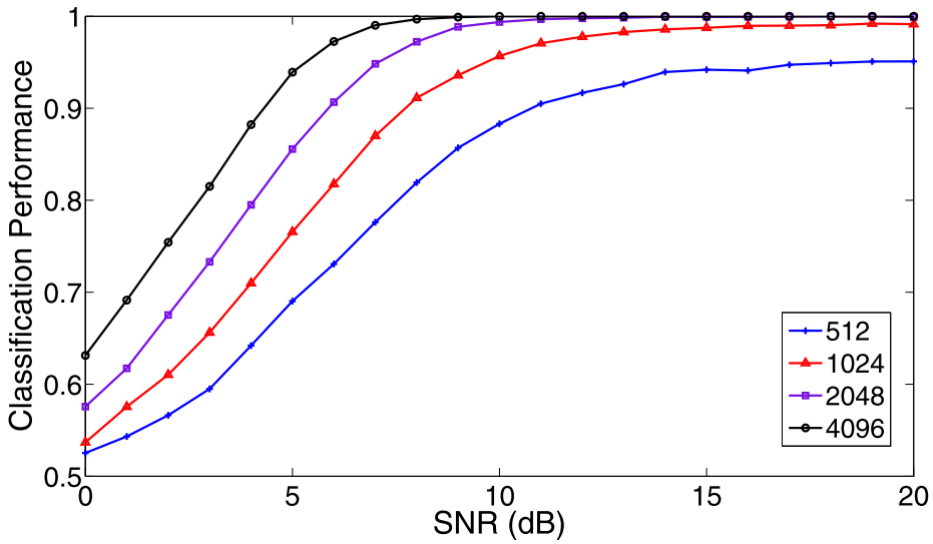

Figure 3.12: Classification accuracy of 16-QAM and 64-QAM using GP-KNN in AWGN channels.

the standard deviation of performance for different SNRs. It is clear from the Figure that standard deviation of performance is very low which proves the robustness of the classier.

To better understand the performance of GP-KNN classifier, the simulations results are compared with existing methods including the maximum likelihood classifier (Wei and Mendel, 2000), the SVM classifier (Wong et al., 2008), and the Navie-Bayes classifier (Wong et al., 2008). The same experiments are conducted for the maximum likelihood classifier in the same test environment. For the SVM classifier and the Navie-Bayse classifier, since the experiments in (Wong et al., 2008) is very similar to this research, results reported in (Wong et al., 2008) are directed used in our comparison. The results are listed in Figure 3.14.

In (Wong et al., 2008), Wong, Ting and Nandi presented results for the same modulations that we have used in this research. At an SNR of 10 dB they achieved performance of 90.2%, 94.4% and 97.9% at 512, 1024 and 2048 respectively using Naive Bayes classifier. For the same SNR and number of samples the performance achieved through SVM was 91.2%, 94.8% and 97.9% respectively. They also used SVM and ML for classification. We have produced ML results ourselves as the results reported in their research do not look correct. Figure 3.14 shows the comparison of our results with other methods. ML gives the upper bound

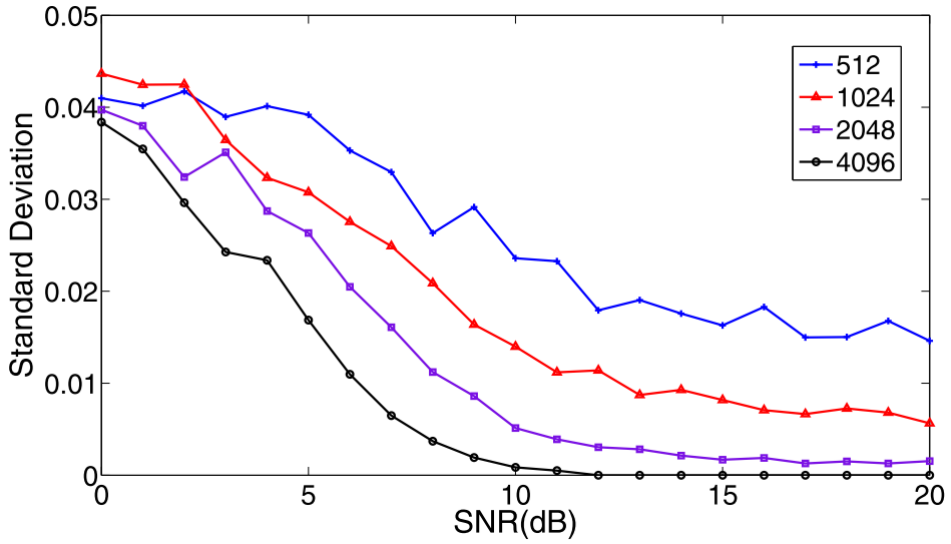

Figure 3.13: Standard deviations of classification accuracy for 16-QAM and 64-QAM using GP-KNN in AWGN channels.

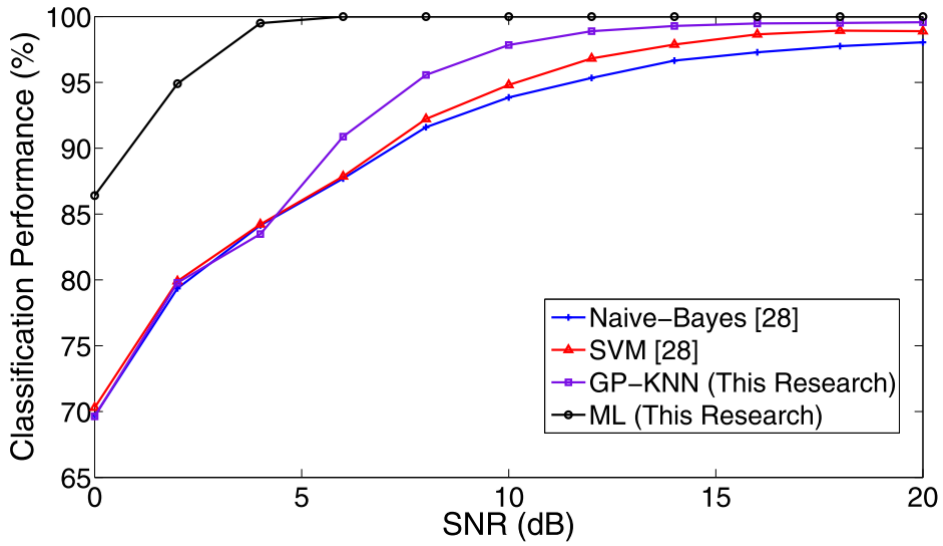

Figure 3.14: Performance comparison of GP-KNN and other methods in AWGN channels.

performance but have more computational complexity. It is clear from the figure that our method gives better results compared to SVM and Naive Bayes method. Up to 4 dB SNR, the performance of our method is same as the other two methods but after 4 dB, the performance of our method improves compared to the other two. The maximum likelihood classifier (Wei and Mendel, 2000), known to be optimum with perfect channel knowledge, is superior to all other methods. However, its computational complexity also known to be high compared to feature based classifiers.

Although many think that GP classifier will take a long time for classification as the time for evolution could be very long. However, the computational complexity of the final classifier is not to be confused with the training time of the classifier. Once we get the final solution from training a GP, that final solution is used for classification and the computational complexity of training a GP does not come into account while using the final solution. The final solution produced by GP has inputs as cumulants and some functions from the function pool. So the complexity of this particular solution really depends on the particular cumulants and functions used by final GP solution. We have used sixth order cumulants and the complexity of calculating these cumulants is lower than higher-order cumulants. The function pool used has been presented in Table 3.2. Also the output used by this solution is tested through KNN classifier which has complexity of $\mathcal{O}(nd)$ where n is the number of reference samples and d represents dimensions of reference data. Here we have used two dimensional data in the form of complex numbers but the function pool contains an abs function which returns the magnitude of complex number as the output when the input is a complex number. If the final solution is using the abs function in the last stage the final output could be a real value. In a nutshell the complexity of our final classifier is $\mathcal{O}(nd)+$ complexity of final solution.

3.4 Summary

In this chapter, we suggested different machine learning techniques for modulation classification. The KNN classifier and SVM classifier are developed for feature based modulation

classifier with supervised threshold optimization and decision making. Both classifiers can be further enhanced using logistic regression, genetic algorithm, and genetic programming for feature selection and combination. The simulation results show that the combination of GP and KNN classifier is able to improve the classification accuracy of digital modulations over existing classifier using the same features. While, the training stage is relatively complex, the actual testing is much simpler and faster.

Chapter 4

Distribution Test Based Classifiers

4.1 Introduction

For the purpose of reducing the computational complexity, algorithms based on distribution tests have been developed and presented in some recent publications. F. Wang and X. Wang (Wang and Wang, 2010) used Kolmogorov-Smirnov test (Massey, 1951) to formulate a solution by comparing the testing signal cumulative distribution functions with the reference modulation's CDFs. This method successfully achieved an improved performance especially when limited signal length was available. It was pointed out in (Urriza et al., 2011) that the K-S test approach requires the complete construction of signal CDFs which is relatively complex and has the potential to be simplified. In the same paper, an optimized approach was presented which reduced the complexity of KS classifier by analysing the CDFs between two modulations at a single given location. When more than two modulations are considered, multiple sets of sampling locations, each responsible for the classification of two modulations, have been used. The classification accuracy is comparable to the KS classifier and the complexity of the algorithm is reduced significantly. However, it is clear that the embedded information in CDFs is underutilized and the robustness of this approach can be improved. To overcome these limitations, we have developed the Optimized Distribution Sampling Test (ODST) classifier which conducts simplified distribution tests at multiple optimized sampling locations to achieve the balance between simplicity and performance. In addition,

the signal distributions are extended to signal phase and magnitude where sampled statistics are treated as features.

4.2 Optimized distribution sampling test

The classification procedure starts with the selection of the optimum sampling locations. Once the optimum sampling locations are established, distribution parameters can be collected at different locations and used for decision making. The exact procedure in each step will be discussed in the following subsections. It is worth mentioning that we only considered four modulation types namely: BPSK, QPSK, 16-QAM and 64-QAM. The multi-class classification problem is handled by dividing it into two 2-class classification steps. The actual decision procedure is demonstrated in Figure 4.1. As the proposed method exploits the different CDFs between different M-QAM signal modulations and it is the nature of M-QAM signals to exhibit different distribution on their real and imaginary components, the extension of the proposed method for other M-QAM modulations can be easily implemented following the sampling location optimization principle explained in Section 4.2.2 and the decision value calculation explained in Section 4.2.3. However, with different modulation candidates, the performance may vary depending on the specific M-QAM modulation being considered. Lower level M-QAM modulations are normally easier to classify. Modulations with similar constellation shape and similar number of symbols are more difficult to distinguish.

4.2.1 Phase offset compensation

In a fading channel, phase and frequency offsets are added along with some attenuation and additive noise. The received signal after matched filtering and sampling is given by

$$r(n) = \alpha e^{j(2\pi f_o n + \theta_o)} s(n) + \omega(n) \tag{4.1}$$

where the residual intersymbol interference is omitted and treated as noise. We first consider the phase offset. It is assumed here that fading is slow, thus the phase offset is consistent for all signal samples. Instead of constructing a signal model with phase offset in mind,

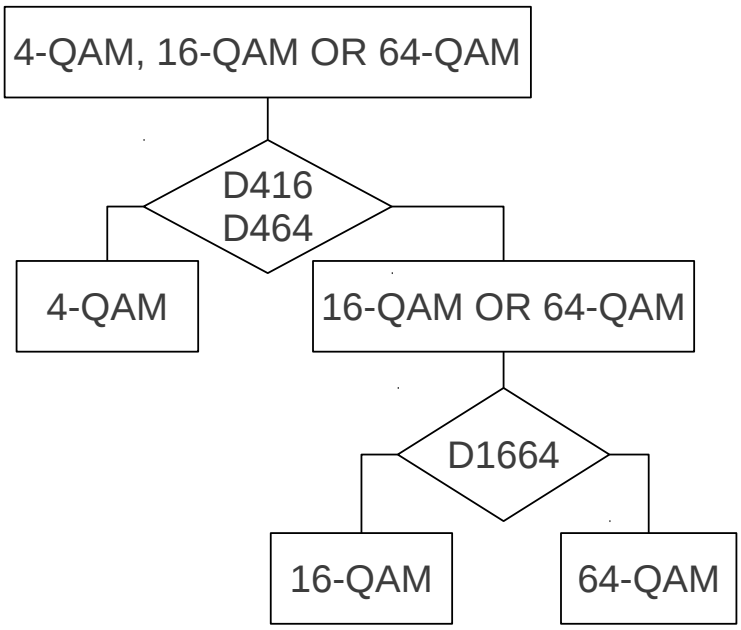

Figure 4.1: Two stage classification strategy in the ODST classifier.

it is easier to recover the received data from the transmitted form. As the rotation of the constellation mapping would cause a significant amount of mismatching with the established reference signal model, the Extended Maximum Likelihood (EML) estimator in (Zarzoso and Nandi, 1999) is used for pre-processing the signal to recover the phase offset. The phase estimation starts with the calculation of fourth-order complex statistics.

$$\hat{\xi} = \frac{1}{N}\sum_{n=1}^{N}\rho_n^4 e^{j4\phi_n} = \frac{1}{N}\sum_{n=1}^{N}(\Re\{r(n)\} + j\Im\{r(n)\})^4 \tag{4.2}$$

ρ_n and ϕ_n come from the polar expression of the nth signal sample $r(n) = \rho_n e^{j\phi_n}$ among the total number of N signal samples. The source kurtosis sum $\hat{\gamma}$ is also needed in the phase estimation.

$$\hat{\gamma} = \frac{1}{N}\sum_{n=1}^{N}\rho_n^4 - 8 = \frac{1}{N}\sum_{n=1}^{N}(\Re\{r^2(n)\} + \Im\{r^2(n)\})^2 - 8 \tag{4.3}$$

The phase offset $\hat{\theta}_{EML}$ is then estimated using the fourth-order complex statistics and source kurtosis sum calculated previously.

$$\hat{\theta}_{EML} = \frac{1}{4} angle(\hat{\xi} \cdot sign(\hat{\gamma})) \tag{4.4}$$

Once the phase offset is estimated, it can be easily recovered by conducting the following procedure

$$\hat{r}(n) = r(n)/e^{j\hat{\theta}_{EML}} \tag{4.5}$$

and the PDF could be treated in the same way as in AWGN channel

$$f_i(x) = \frac{1}{\hat{\sigma}\sqrt{2\pi}} e^{-\frac{(x-\hat{A}_i)^2}{2\hat{\sigma}^2}} \tag{4.6}$$

Frequency offset is added to the signal separately from the phase offset. Any frequency offset is treated as noise in the investigation.

4.2.2 Sampling location optimization

In Kolmogorov-Smirnov Test, the similarity of two distributions is tested by finding the maximum distance between the two distributions. However, it is limited by the fact that outliers and other irregularities in the test signal distribution can cause the maximum distance to occur at a location which does not exhibit the best characteristic difference between them. The effect becomes more significant when the signal length is reduced or the amount of noise added is increased. Ultimately, the classification accuracy from different tests could vary dramatically. To overcome this limitation, the ODST uses multiple sampling locations estimated with theoretical analysis to achieve a more robust performance.

As the later distribution test will be based on CDFs from different signal modulations, the main purpose of the sampling location optimization is to find locations where the two CDFs from different modulations exhibit the biggest difference. In this research, we propose to use the local optima on the CDFs' differences as sampling locations.

There are two parameters to consider when searching for sampling locations: the number of sampling points and their locations. Though more information from the distribution could always help to improve the understanding of the signal, some contribute significantly more

than the others. A simple example would be two adjacent sampling locations which are very close to each other. Though using both of them would better translate the nature of the signal as compared to using only one of them, any minor advantage using both is often difficult to justify the added complexity. Figure 4.2 gives some examples of signal constellations and differences between these cumulative distributions. With the proposed location optimization scheme, it can be seen in Figure 4.2d that there are eight local optima that can be used for distribution sampling test. These locations are evenly spread over the signal range and each of them presents distinct differences between two modulations. Both of these characteristics are desirable qualities when looking for sampling locations.

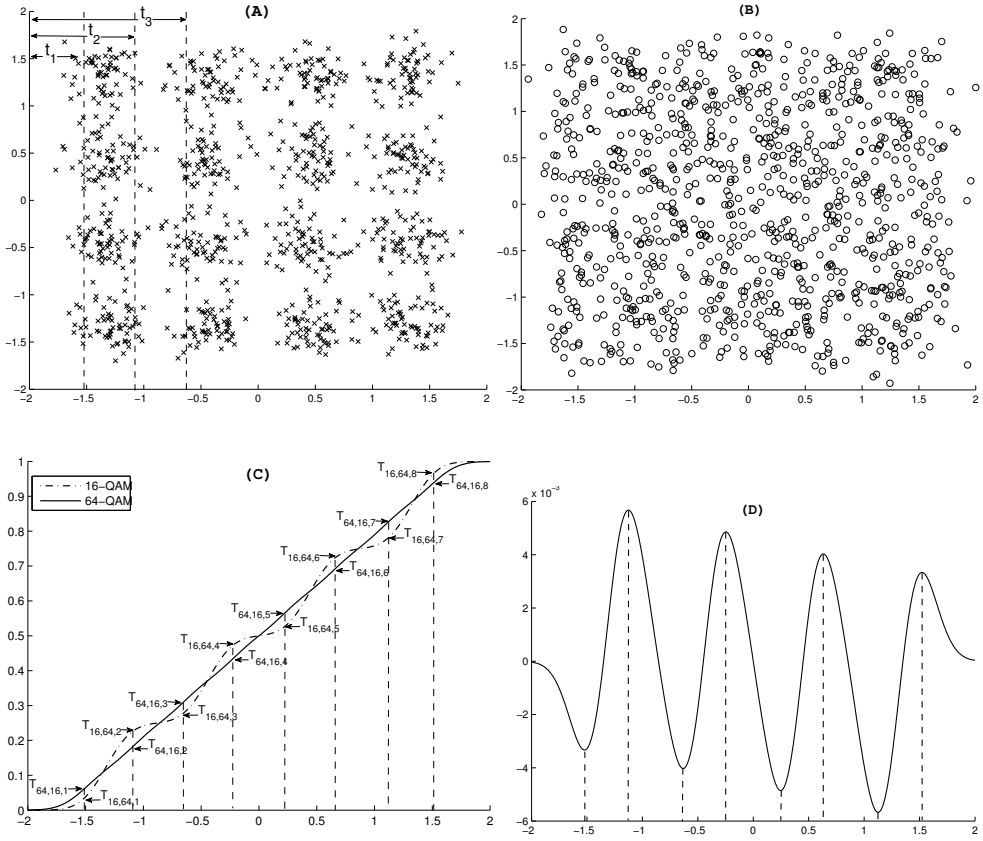

Figure 4.2: (A) 500 signal samples from 16-QAM at 15 dB, (B) 500 signal samples from 64-QAM at 15 dB, (C) The CDFs from 16-QAM and 64-QAM, and (D) The difference between the two CDFs. The dashed lines indicate the shared optimized sampling locations.

We define $\boldsymbol{l}$ as a collection of sampling locations with l_k being the individual points.

$$\boldsymbol{l} = \{l_k,\ for\ k = 1, .., K\} \tag{4.7}$$

Through extended observations of various type of signals and their distributions, we define the optimum sampling locations to occur when the difference between CDFs from two classes is locally optimum, for modulation A-QAM and B-QAM, this can be easily transformed into the calculation of first derivative of their CDFs' (F_A and F_B) difference

$$\frac{d}{dx}\left(F_A(\boldsymbol{l}) - F_B(\boldsymbol{l})\right) = 0 \tag{4.8}$$

The derivative of CDFs' difference can also be replaced by probability distribution for both modulations (f_A and f_B)

$$f_A(\boldsymbol{l}) - f_B(\boldsymbol{l}) = \sum_{i=1}^{I_A}(f_{Ai}(\boldsymbol{l})) - \sum_{i=1}^{I_B}(f_{Bi}(\boldsymbol{l})) = 0 \tag{4.9}$$

where the PDF for each signal centroids (f_{Ai} and f_{Bi}) are defined previously in (2.6). I_A and I_B correspond to the total number of centroids for each modulation on one signal dimension. After the optimization of the sampling locations, the theoretical CDF values at sampling locations for different modulations are collected for classification task as the reference data. The reference data for A-QAM while considering the classification between A-QAM and B-QAM is given as

$$T_{A,B} = [T_{A,B,1}, ..., T_{A,B,k}] \tag{4.10}$$

where

$$T_{A,B,k} = F_A(l_k) \tag{4.11}$$

F_A is the CDF of modulation A-QAM. These values will be stored for later distribution tests.

Once the sampling locations are established, the distribution sampling could be converted to simple counting tasks. The counted distribution parameter t_k can be written as

$$t_k = \frac{1}{2N}[\sum_{n=1}^{N}\mathbb{I}(r_X(n) < l_k) + \sum_{n=1}^{N}\mathbb{I}(r_Y(n) < l_k)] \tag{4.12}$$

where $\mathbb{I}(\cdot)$ is an conditional function which returns 1 if the input is true and 0 if input is false. The counting tasks at different locations are also illustrated in Figure 4.2a.

4.2.3 Test statistics and decision making

The counting results are put into the classification context by finding the difference Δt between the counted value and the theoretical value from candidate modulations.

$$\Delta t_{A,B,k} = |t_k - T_{A,B,k}| \tag{4.13}$$

where $\Delta t_{A,B,k}$ give the difference between testing signal distribution parameter and reference value $T_{A,B,k}$ from candidate A. Likewise the difference between testing signal and candidate B can be found as

$$\Delta t_{B,A,k} = |t_k - T_{B,A,k}| \tag{4.14}$$

In the standard uniformly weighted distance metric, the decision is made using all sampled results with the same weight. The decision values for different 2-class classification situations are defined as

$$D_{A,B} = \sum_{k=1}^{K} \Delta t_{A,B,k} - \sum_{k=1}^{K} \Delta t_{B,A,k} \tag{4.15}$$

where $D_{A,B}$ compares the distance between testing signal and candidate A and the distance between testing signal and candidate B. If $D_{A,B} \geq 0$, it means the tested signal is close to candidate A and thus have a higher probability of being classified as candidate A. However as there are more than two candidate modulations involved. The final decision can be made according to a set of decision values.

$$\hat{\mathcal{M}} = \begin{cases} \text{4QAM}, & D_{4,16} \leq 0 \ \& \ D_{4,64} < 0 \\ \text{16QAM}, & D_{4,16} > 0 \ \& \ D_{16,64} \leq 0 \\ \text{64QAM}, & D_{4,64} \geq 0 \ \& \ D_{16,64} > 0 \end{cases} \tag{4.16}$$

The resulting $\hat{\mathcal{M}}$ gives the estimated $\mathcal{M}$ value for the tested M-QAM signals. $D_{4,16}$, $D_{4,64}$ and $D_{16,64}$ are decision values gathered from the previous stage.

Given the distance definition in (4.15), it is worth questioning the actual contribution of each sampling locations. Though the optimization process attempts to find the best locations with maximum amount of separation while conveying the full characteristic of the CDFs, it is still possible for the local optima to be inefficient. For example, two local optimums

can be very close to each other and represent the same signal attribute. As can be seen in Figure 4.3, the four locations in the middle get closer when the SNR is less than 9 dB and become effectively same locations at around 7 dB. Then all four locations are no longer selected as optimum sampling locations. Based on the behaviour of these four optimized locations, it is easy to doubt their contribution to the classification task for SNRs between 7 dB to 9 dB. It is also verified in the simulation results that these locations are normally abandoned or given a lower weight.

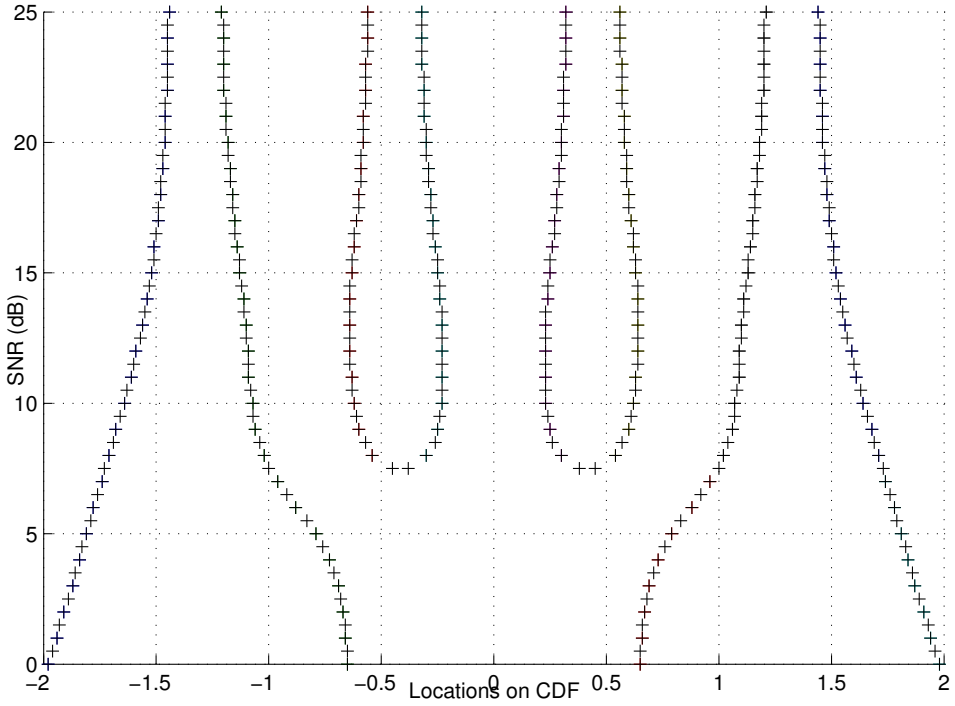

Figure 4.3: Two stage classification strategy in the ODST classifier.

To justify the use of specific sampling locations, GA has been used to find the best selection of these locations to enhance the decision making procedure. Here the distance metric is redefined with the addition of weights on each sampled distribution parameters.

$$D_{A,B} = \sum_{k=1}^{K} W_{A,B,k} \Delta t_{A,B,k} - \sum_{k=1}^{K} W_{A,B,k} \Delta t_{B,A,k} \tag{4.17}$$

There are two types of constraint considered while training the weights. The first limits the weights to binary values (GA-Bin), when $W_{A,B,k} = 0$ the distribution test result at location

k will not be included and when $W_{A,B,k} = 1$ the result would be considered. As the training phase evolves for a long time, the trained weights can be an indication of the best selection of sampling locations. The second type was experimented with the linear combinational weights limited to values between 0 and 1 (GA-Lin), so that the trained results could provide a more versatile combination of the decision values. Both cases share the same fitness evaluation approach. The fitness value is obtained through a small classification task using a small set of testing signals. The accuracy of the small classification is used directly as the fitness value. Therefore, fitter individuals always have higher fitness values. Other GA parameters can be found in Table 4.1.

Table 4.1: Parameters for the Genetic Algorithm

Parameters	Case 1	Case 2
Constraint	Binary	$0 \leq W \leq 1$
Generation	100	100
Population	20	20
Elite Count	2	2
Crossover Fraction	60%	80%
Mutation Type	Uniform	Uniform
Mutation Raete	60%	40%

4.2.4 Simulations and numerical results

All experiments are simulated in computer based environment and signals were first created as symbols, randomly drawn from specific modulation mapping in a uniform manner. If phase or frequency offset is to be considered, the native MATLAB function is used to implement the channel effects. Additive white Gaussian noise is also included under these channel conditions. Before classification, sampling locations and theoretical reference distribution test values for SNR range from 0 dB to 25 dB with 1 dB step are collected and stored. In the given SNR range, it is discovered that twelve sampling locations are found in each SNR

scenario between 0 dB and 7 dB, and sixteen sampling locations are found when SNR is between 8 dB and 25 dB. As two reference CDF values are needed at each sampling location to complete the decision value calculation, there are a total number of 768 reference values prepared for each given signal length.

During GA optimization, the fitness function is defined in the same way as in classification problems where the classification accuracy is used as the fitness value. To reduce the complexity of the training stage, only 1000 realizations from each modulation with a signal length of $N = 512$ samples are used in the fitness evaluation process. The training is repeated five times for each SNR value ranging from 0 dB to 10 dB. All signal data is generated randomly at every fitness evaluation, which avoids weights being over-trained for a specific set of signal data. In addition, with the two elites always being passed on to the next generation, the possibly best solutions are always protected to some degree. The training was repeated for five runs under each signal condition. The collections of weights which give the best performance were selected for performance assessment with larger statistics at a later stage.

When testing the performance of the proposed solution, maximum likelihood classifier, the KS test, culumant based Genetic programming and k-nearest neighbour classifiers were used for benchmarking purpose.

For the performance test in AWGN channel, two sets of experiments were conducted. The first set of experiments focused on the classification accuracy under different noise levels. Here, the signal length is fixed at 512 samples with the SNR ranging from 0 dB to 25 dB. Then classifications of 100,000 signal realizations from each modulation were tested using ML, KS test, GP-KNN and the proposed ODST classifier. The successful classification percentage was calculated based on the number of successful classifications and the total number of signal realizations. The results are presented in Figure 4.4. In the second set of experiments, we tried to understand how the signal length influences the classification performance. In this case, similar settings were used, except for SNR being fixed at 10 dB and sample size to vary from 100 to 1000. The results are presented in Figure 4.5.

The classification performance under different amount of additive noise has always been

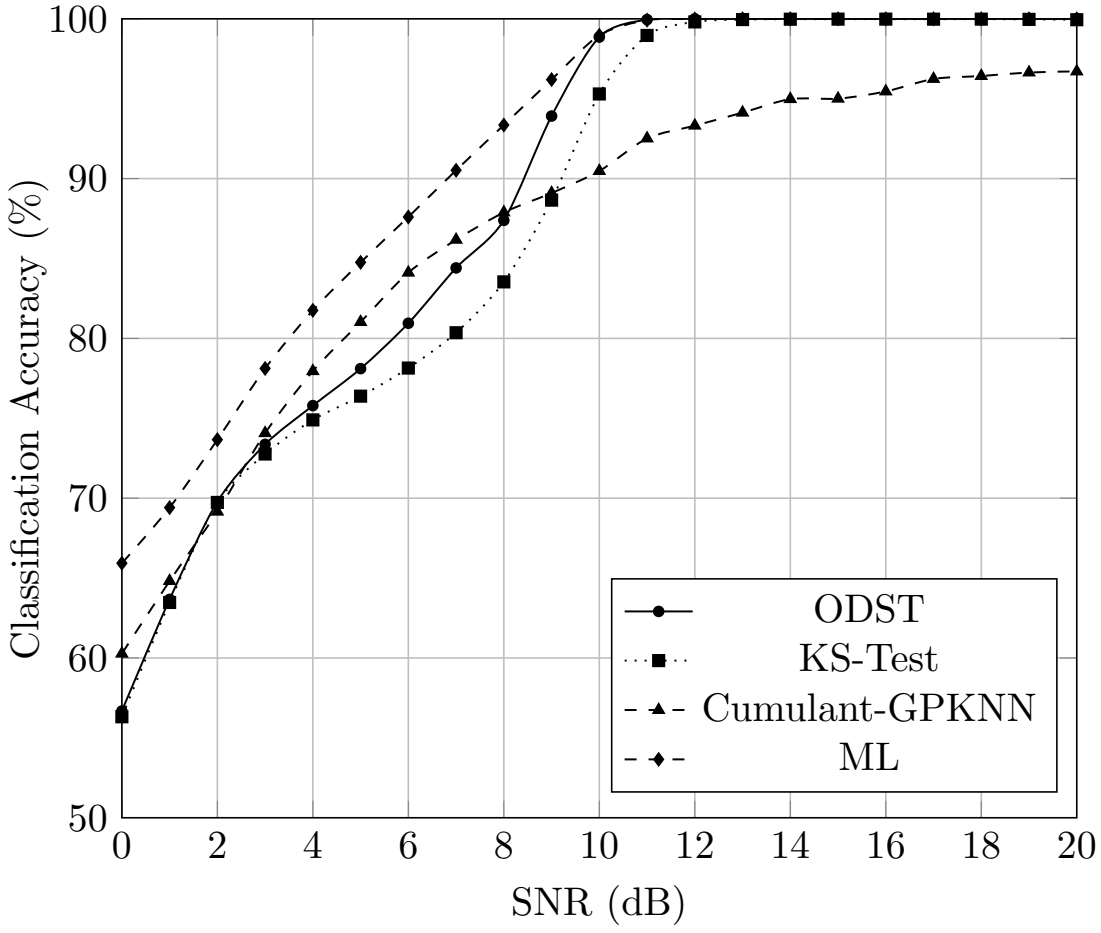

Figure 4.4: Classification accuracy of 4-QAM, 16-QAM and 64-QAM using ODST in AWGN channel.

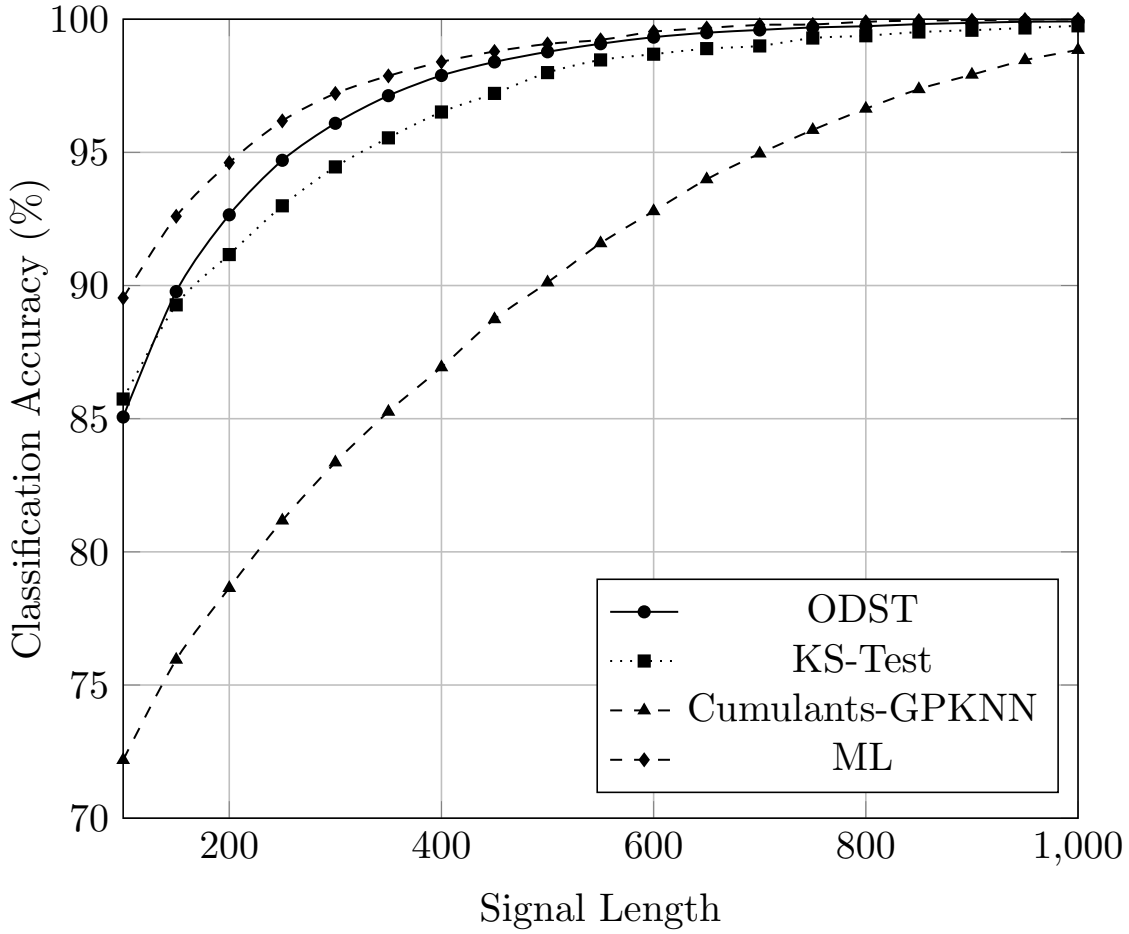

Figure 4.5: Classification accuracy of 4-QAM, 16-QAM and 64-QAM using ODST in AWGN channel with different signal length.

the prime criteria for an AMC solution. In Figure 4.4, four different types of AMC classifiers are included. It is clear that ML provides the most accurate classification throughout the SNR range. Excluding the ML classifier, the results show that the proposed ODST classifier has a clear advantage in mid to high SNRs. At 10 dB, the proposed method achieves almost the same accuracy of 98.9% as the ML classifier and the 100% classification is achieved at 11 dB. At the same SNR settings, KS test provides a successful classification of 95.3% and the perfect classification performance is achieved at 12 dB.

For the cumulant based GP-KNN classifier, it can be seen that its performance is limited by the signal length that is available for analysis. In the mid and lower range of SNRs, the proposed ODST classifier maintains the advantage over KS test. The biggest difference is exhibited at 9 dB where ODST offers an accuracy of 93.9% and KS test offers 88.6%. However, the accuracy advantage is gradually reduced along with the decreasing SNR until the performance become equivalent below 3 dB. On the other hand, this cumulant based GP-KNN classifier shows a robust performance in low SNRs, offering better classification performance from 3 dB to 8 dB against ODST and from 3 dB to 9 dB than KS test. The performance at SNR below 3 dB is generally very similar among all classifiers with only ML classifier having a more than 5% higher accuracy. Complementary results from ODST for different modulations are listed in Table 4.2. Performance means and standard deviations are collected from 100 sets of tests, each includes 30,000 signal realizations (three modulations times 10,000 signal realizations from each modulation).

Table 4.2: Classification accuracy with standard deviation of 4-QAM, 16-QAM, and 64-QAM using ODST in AWGN channel.

Modulations	5 dB	10 dB	15 dB	20 dB
4-QAM	100.0±0.0	100.0±0.0	100.0±0.0	100.0±0.0
16-QAM	68.2±0.4	98.5±0.1	100.0±0.0	100.0±0.0
64-QAM	65.9±0.5	98.1±0.1	100.0±0.0	100.0±0.0

In addition to the benchmarking classifiers, several existing classifiers from other literature have been listed in Table 4.3 for performance comparison with ODST. Results for

ODST come from experiments conducted under the same specific condition as each existing classifiers. It is clear that the proposed classifier outperforms the KS classifier (Wang and Wang, 2010), the reduced complexity version of KS classifier (rcKS) (Urriza et al., 2011), phase based ML classifier (Shi and Karasawa, 2012), as well as cumulant based classifiers (Swami and Sadler, 2000), (Wong et al., 2008). The Minimum Distance (MD) (Wong and Nandi, 2008) classifier, which is a low-complexity version of the ML classifier, presents similar level of performance at or above 14 dB as compared to the proposed ODST classifier. However, with the SNR at or lower than 10 dB, its classification accuracy is significantly degraded. The comparison between MD classifier and ODST classifier at SNR of 10 dB clearly demonstrates the performance advantage of the proposed method.

Having analyzed the performance of ODST against other existing AMC classifier, let us have a look at the effect of GA optimized weighted decision making on the classification performance. The same experimental setup is used only with SNR limited between 0 dB and 10 dB to investigate the effect of GA optimization on low SNR performance. According to the classification performance in Figure 4.6, both GA optimized classifiers follow the performance degradation pattern of the original ODST with an increase in classification accuracy of 1% to 3% sustained over the SNR range. The biggest performance improvement is shown between SNR of 7 dB to 10 dB. At 8 dB, GA optimized ODST with analogue weight achieves a classification accuracy of 90.5% providing the largest performance improvement of 4% as compared to the 86.5% classification accuracy of the original ODST classifier. The reason for such improvement can be explained with the analysis of sampling location quality in Section 3. In Figure 4.3, it is clear that some of the sampling locations start to merge and disappear between 7 dB and 10 dB. The performance improvement provided by GA optimized weights verified these sampling locations need to be given lower weights to achieve better classification performance. Between the binary weights and analogue weights, analogue weights provide better performance at 8 dB, 9 dB and 10 dB while being almost equal to the binary weights from 0 dB to 7 dB. Overall, both types of optimized weights help to improve the classification by a fair amount.

The robustness against a limited signal length is another important quality for a good

Table 4.3: Performance comparison between ODST and existing methods.

Classifier	Modulation	Channel	Setting	Accuracy	ODST
KS 2-D	4-QAM 16-QAM 64-QAM	AWGN	$N = 100$ 10 dB	78.0%	85.2%
KS magnitude	4-QAM 16-QAM 64-QAM	AWGN	$N = 100$ 14 dB	87.0%	99.6%
rcKS	4-QAM 16-QAM 64-QAM	AWGN	$N = 50$ 10 dB	72.5%	77.3%
Phase Based ML	4-QAM, 16-QAM	AWGN	$N = 1000$ 0 dB	73.5%	82.3%
MD	4-QAM, 16-QAM	AWGN	$N = 100$ 10 dB	50.0%	86.5%
MD	4-QAM, 16-QAM	AWGN	$N = 100$ 14 dB	91.5%	97.3%
Cumulants	16-QAM, 64-QAM	Noise Free	$N = 10,512$	90.0%	100.0%
Cumulants Naive Bayes	4-QAM 16-QAM 64-QAM	AWGN	$N = 512$ 10 dB	87.3%	98.5%

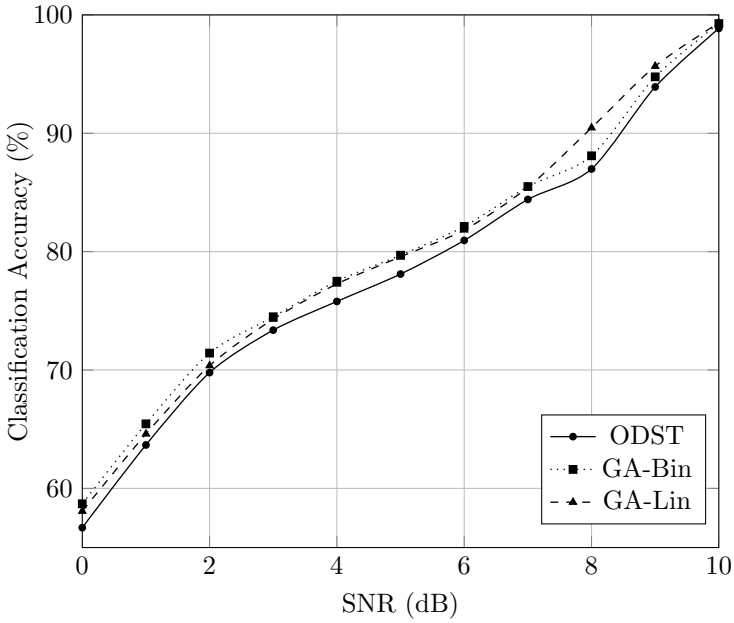

Figure 4.6: Classification accuracy of 4-QAM, 16-QAM and 64-QAM using GA and ODST in AWGN channel.

AMC classification. In the experiments, same four classifiers are tested and compared in Figure 4.5. Again, ML excels in all signal length from $N = 100$ to $N = 1000$. Excluding ML classifier, ODST is the best among the remaining classifiers. The largest performance difference of ODST against ML is about 5% at $N = 100$. As the signal length increases the difference starts to reduce and at $N = 600$ ODST achieves performance similar to ML classifier. When compared with KS test, OSDT shows a superior robustness especially when the signal length is in the range from $N = 150$ to $N = 500$. The biggest advantage of ODST is observed at $N = 250$, where KS test returns a classification accuracy of 93.0%, which is 1.7% below ODST's 94.7%. Unfortunately, culumant based GP-KNN classifier suffers severely with the reduced signal length. However, as its performance is improving consistently with the increasing signal length, it is clear that, with large enough signal length, GP-KNN classifier is still able to achieve equal level of performance.

In fading channel, the signal length was fixed at $N = 512$ samples and the SNR at 10 dB. Again 100,000 signal realizations from each modulation were tested under separate conditions

of phase and frequency offset. In the experiment for phase offset, the range of offset is limited within 10 degrees. This is purely for testing the performance of classifiers when handling conditions with inaccurately estimated phase offset. Also, the combination of the proposed method, EML phase estimation and recovery is tested to evaluate its performance. Results are presented in Figure 4.7. When considering frequency offset, the amount of frequency offset ratio is limited in the range of 1×10^{-4} and 2×10^{-4}.

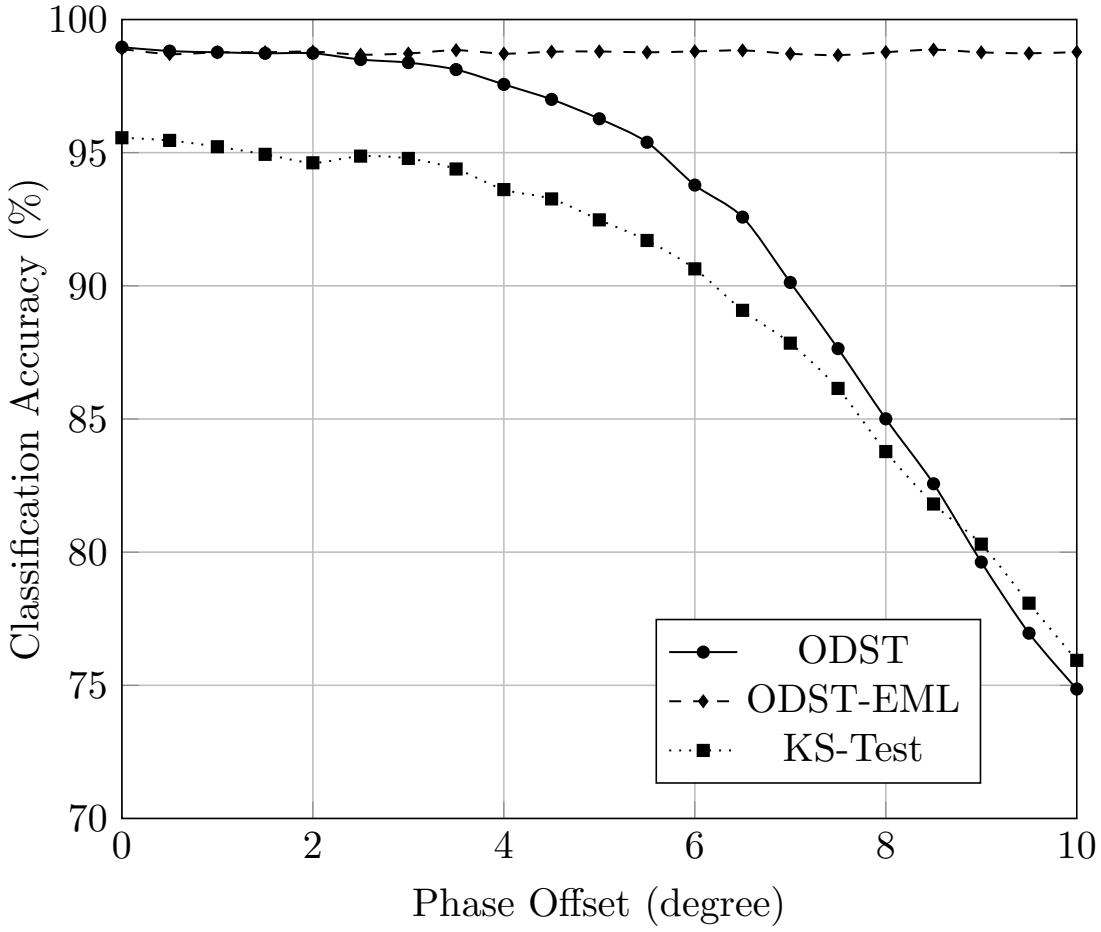

Figure 4.7: Classification accuracy of 4-QAM, 16-QAM and 64-QAM using ODST in fading channels with phase offsets.

In a fading channel with unknown phase offset, we have included the original ODST classifier, the original KS test and ODST classifier with EML phase estimation and recovery.

The results are presented in Figure 4.7. All signals are simulated with a signal length of $N = 512$ and SNR of 10 dB. With no phase error, the classification accuracy difference between the original ODST and KS test coincide the results in pure AWGN channel. The original ODST starts with an advantage of 3.4%. As more phase offset is introduced, both classifiers' performance starts to degrade. Nevertheless, ODST sees less degradation before the phase offset reaches $\theta_o = 6°$. Once again, this illustrates the robustness of ODST when compared with KS test. The degradation of ODST performance accelerates after 6 dB. At $\theta_o = 8.3°$, KS test surpass ODST to have a better performance with more phase offset. It is an understandable phenomenon, as the ODST relies on an accurate signal model more than the KS test, when the signal model mismatching exceeds a certain level, the distribution tests at different locations become barely capable of providing positive contribution towards an accurate classification. Nevertheless, when ODST is teamed up with an accurate phase offset estimation and recovery scheme, this should not be a concern since the mismatching could be limited within a reasonable amount. It is demonstrated with the results from ODST-EML. Regardless of the amount of phase offset experimented with, the classifier delivers a consistent classification accuracy of 98.8%. Under similar conditions, ML classifier and GP-KNN classifier have both exhibited a strong robustness seeing less than 10% degradation in classification accuracy.

As can be seen in Figure 4.8, both ODST and KS test perform poorly when frequency offset is considered. With a frequency offset of 1×10^{-4} to 2×10^{-4}, classification accuracy from both classifier drops significantly. For ODST, its classification accuracy is reduced to 95.5% with a frequency offset of 1×10^{-4}. As the amount of frequency offset increases to 2×10^{-4}, the classification performance decreases almost linearly to 77%. The KS test sees similar performance degradation. However, it starts with lower classification accuracy of 92% with frequency offset at 1×10^{-4} and reduces to 77% with frequency offset of 2×10^{-4}. The ODST classifier provides about 3.5% better classification accuracy between 1×10^{-4} to 1.3×10^{-4}. The performance advantage is gradually reduced beyond 1.3×10^{-4}. One of the causes of this reduced performance comes from the modulations being used, especially 16-QAM and 64-QAM. With their dense signal constellations, there is little room for any frequency offset.

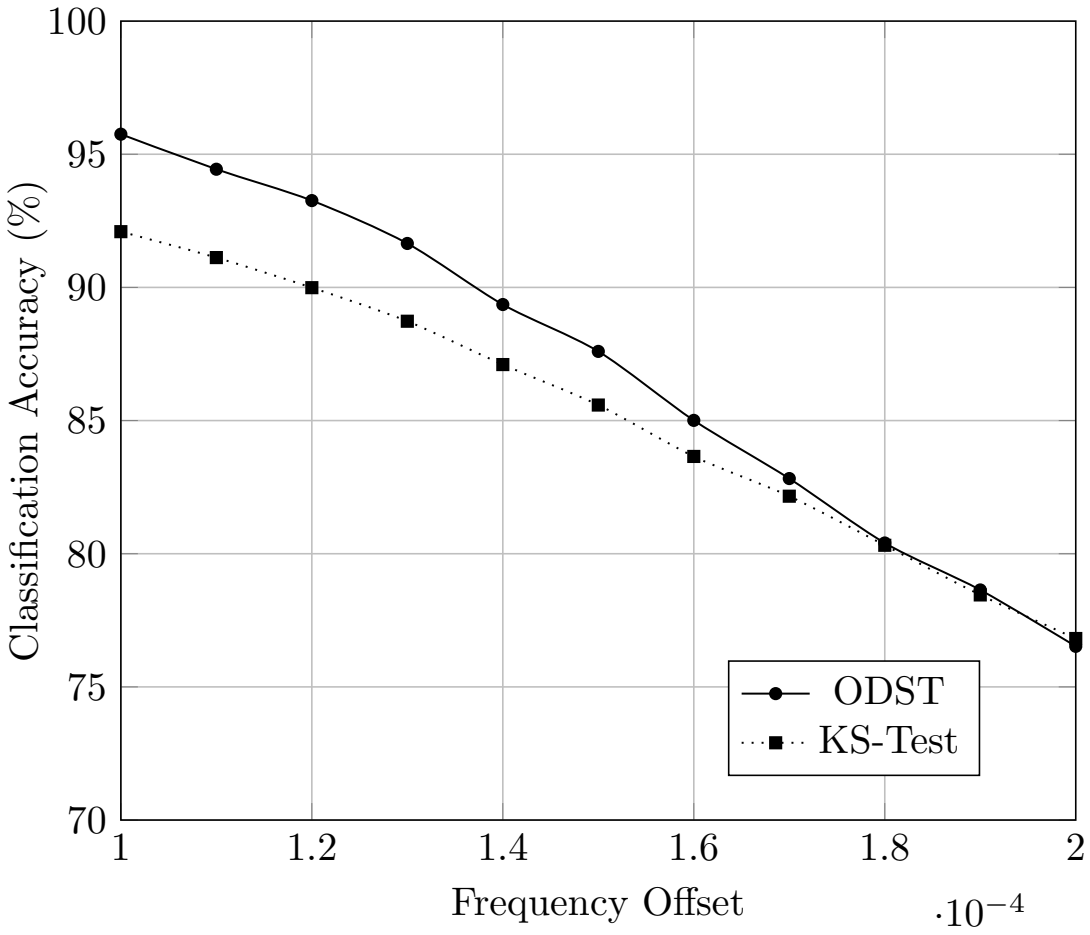

Figure 4.8: Classification accuracy of 4-QAM, 16-QAM and 64-QAM using ODST in fading channels with frequency offsets.

The other reason is to do with the nature of distribution test based classifiers, which rely on a solid signal distribution with little frequency shifting. Even though ODST performs better than KS test, it is difficult to claim its robustness under channels with frequency offsets. Although the frequency offset condition is optimistic, some effective blind frequency offset estimation and compensation approaches for QAM modulated signals have been developed (e.g.(Serpedin et al., 2000)) which would help to achieve the required level of frequency offset.

The numbers of different operations required by different classifiers are listed in Table 4.4. It is obvious that the implementation of ML classifier requires exponential and logarithm operation while others do not. The MD classifier significantly reduced the complexity of ML classifier since no exponential or logarithm operation is needed. However, a considerable amount of multiplication and addition are still needed which is similar to the process of cumulant calculation. When comparing KS test and ODST, given the signal length used and number of different modulation candidates, it is clear that the number of additions used is similar while the memory usage is much lower for ODST. If longer signal length is to be analyzed or more modulations are included, the complexity advantage of ODST will be more evident. Although there is considerable amount of complex computation involved in the training of weights in GA optimized ODST, it is worth clarifying that it is done offline beforehand and will not be repeated for every classification task. Thus only the sampling and decision making should be considered when evaluating the complexity of ODST. With compromised classification performance robustness, the reduced complexity version of KS classifier, which compares the CDFs at single point, requires fewer additions as well as less memory.

Table 4.4: Complexity comparison between ODST and existing methods.

Classifiers	Multiplier	Addition	Exponential	Logarithm	Memory
ML	$5NM \cdot \sum_{m=1}^{M} I_m$	$6NM \cdot \sum_{m=1}^{M} I_m$	$NM \cdot \sum_{m=1}^{M} I_m$	NM	M
MD	$2NM \cdot \sum_{m=1}^{M} I_m$	$NM \cdot (\sum_{m=1}^{M} 3I_m + 1)$	0	0	M
Cumulants	$6N$	$6N$	0	0	M
KS test	0	$2N(2M + log2N)$	0	0	MN
rcKS/rcK	0	$4N \cdot \binom{M}{2}$	0	0	$4M \cdot \binom{M}{2}$
ODST	0	$4N \cdot \binom{M}{2} \cdot K$	0	0	$4M \cdot \binom{M}{2} \cdot K$

4.3 Distribution based features

The distribution based features are inspired by the ODST classifier. By treating the test statistics sampled from different signal distributions as features, many advanced machine learning techniques could be implemented to improve the feature enhancement and decision making. An illustration of the overall process involved in the proposed AMC solution is given in Figure 4.9. Different from cumulants, the proposed features are expected to be simple to collect (low complexity), to require fewer signal samples, and to provide robustness in different channel conditions. The proposed features are optimized for the binary classification of two modulations. To establish a low complexity classifier with reduced feature dimension, we proposed to combine original features into new features each representing a unique binary modulation combination for maximum separation between two modulations using linear binomial logistic regression. The resulting class oriented features are then used to construct a multi-dimensional feature space enabling fast classification using K-nearest neighbour classifier. The extraction of the proposed distribution based binary discriminative features consist of two steps: optimizing sampling locations on signal distributions and extracting the features. The extracted features are subject a further round of enhancement using logistic regression.

In this research, we used the cumulative distribution of signals on I-Q segments (F_M^{XY}), amplitude (F_M^A) and phase (F_M^P) for analysis. Given a set of M-QAM signal $r(\cdot)$ of N samples, its distributions on different signal segments can be collected using the following equations.

$$F_M^{XY}(x) = \frac{1}{2N}\sum_{n=1}^{N}\{\mathbb{I}(r'_X(n) < x) + \mathbb{I}(r'_Y(n) < x)\} \tag{4.18}$$

$$F_M^{A}(x) = \frac{1}{N}\sum_{n=1}^{N}\mathbb{I}(\mid r'(n) \mid < x) \tag{4.19}$$

$$F_M^{P}(x) = \frac{1}{N}\sum_{n=1}^{N}\mathbb{I}(\arg(r'(n)) < x) \tag{4.20}$$

where $\mathbb{I}(\cdot)$ is a logic function which returns 1 if the input is ture and 0 if the input is false, and $arg(\cdot)$ gives the phase of the complex input. An illustration of these CDFs of different

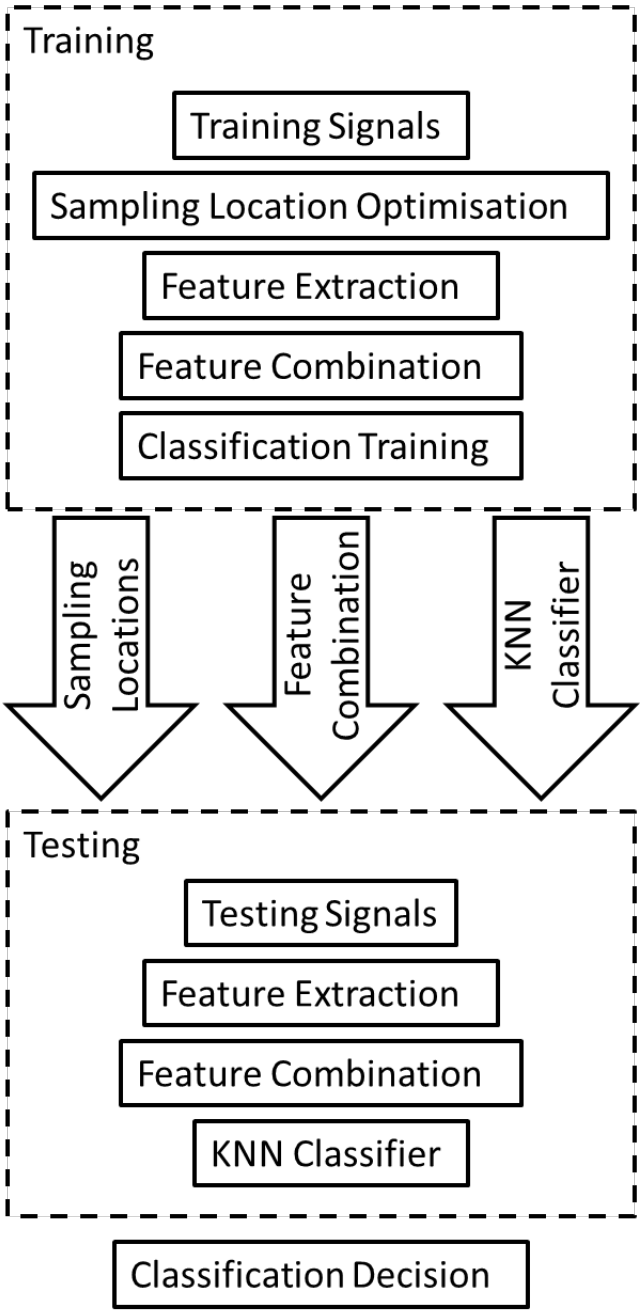

Figure 4.9: Using distribution based features for AMC in two stages.

signal segments are given in Figure 4.10.

4.3.1 Optimization of sampling locations

The optimization of sampling location follows the same procedure as described in Section 4.2.2. However, we extend the distribution considered to signal phase and magnitude. The sampling location on signal distributions for feature extraction is a crucial part of the proposed AMC solution. The optimization of locations should follow these criteria.

Criterion 1: The sampling locations should provide clear discrimination between two modulations.

Criterion 2: The sampling locations should utilize a wider distribution range to provide more comprehensive information of the modulation distribution.

Criterion 3: The locations should be at sufficient distance to avoid collecting repetitive and redundant information.

To satisfy the above criteria, we propose to use the local maximums of the distance between two modulations' cumulative distributions as sampling locations. We denote $D^*_{M_1M_2}$ to be the distance between distributions from modulations M_1 and M_2. "$*$" is used as a uniform representation of different signal segments including I-Q segments, amplitude and phase.

$$D^*_{M_1M_2} =\mid F^*_{M_1} - F^*_{M_2} \mid \tag{4.21}$$

The optimized sampling locations should meet the condition that the distance at location $l^*_{M_1M_2}$ should be the maximum

$$D^*_{M_1M_2}(l^*_{M_1M_2}) = max(D^*_{M_1M_2}(x)) \tag{4.22}$$

within the range of

$$l^*_{M_1M_2} - R^* \leq x \leq l^*_{M_1M_2} + R^* \tag{4.23}$$

where R^* is a range parameter. The manually optimized values of R^* in our simulation can be found in Table 4.5.

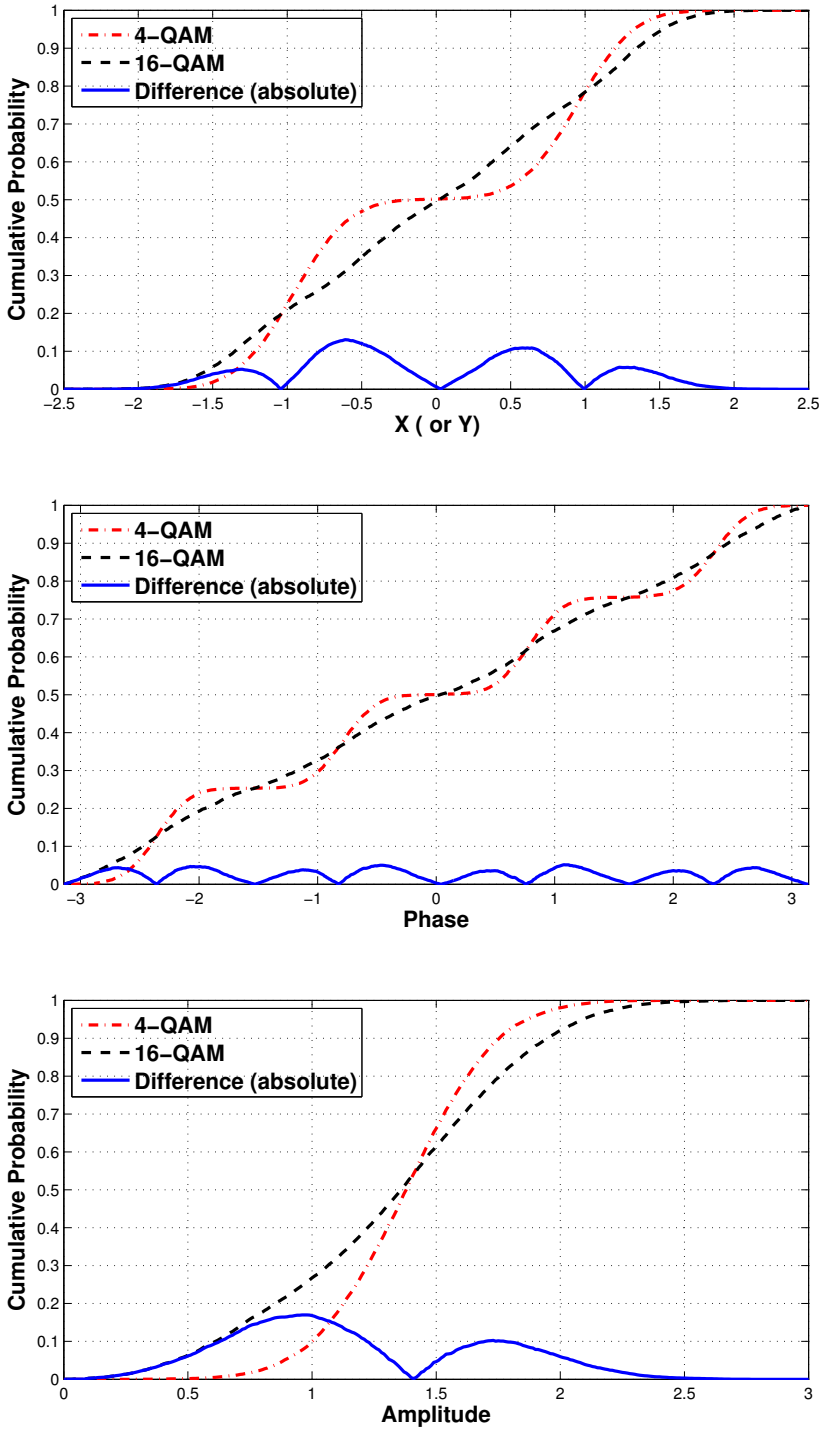

Figure 4.10: Cumulative Distributions of different signal segments from 4-QAM and 16-QAM at SNR of 15 dB.

Table 4.5: Parameters used in the distribution based features classifier.

Parameters	Training	Testing
Modulations	4-QAM, 16-QAM 64-QAM	4-QAM, 16-QAM 64-QAM
# Realization	100x3	10,000x3
Signal Length (N)	512	512
SNR	0-20 dB	0-20 dB
Phase Offset	0-30°	0-30°
R^{XY}	0.2	N/A
R^{A}	0.15	N/A
R^{P}	$\pi/10$	N/A

4.3.2 Feature extraction

With the optimized feature sampling locations, the actual extraction process is very simple. In the case where the underlining modulation is known to the training signals, the reference features can be collected directly using the established cumulative distributions F^*_M.

$$f^*_{M_1M_2}(i) = F^*_M(l^*_{M_1M_2}(i)) \tag{4.24}$$

In the case where the signal being treated has unknown modulation, the features can be extracted using a simple counting measure with the sampling locations as thresholds.

$$f^*_{M_1M_2}(i) = \frac{1}{N}\sum_{n=1}^{N}\mathbb{I}(r^*(n) < l^*_{M_1M_2}(i)) \tag{4.25}$$

Equation (4.25) can be associated with Equation (4.18)-(4.20) to help understand its implementation on different signal segments.

4.3.3 Feature combination

Feature combination is a good way to reduce feature dimension and to better utilize all the available features. The combination processing requires extra computation while the trained

feature combination can vastly reduce the complexity of the classifier. In AMC, feature combination is a frequently used technique to enable fast processing at the classification stage with low computation cost.

In this research, considering the nature of the distribution based features, we employ linear feature combinations for dimension reduction and enhancement. Binomial logistic regression is used to create a linear combination of feature which provides separation between two classes. The implementation of binomial logistic regression is mostly standard. The logistic function is given as

$$p(f^{XY}_{M_1M_2}, f^{A}_{M_1M_2}, f^{P}_{M_1M_2}) = \frac{1}{1+e^{-g(f^{XY}_{M_1M_2}, f^{A}_{M_1M_2}, f^{P}_{M_1M_2})}} \tag{4.26}$$

where $p(\cdot) = 0$ for modulation M_1 and $p(\cdot) = 1$ for modulation M_2. The logit function is linked with the original features in the following format

$$\begin{aligned} g(f^{XY}_{M_1M_2}, f^{A}_{M_1M_2}, f^{P}_{M_1M_2}) = B(0) &+ \sum_{i=1}^{L^{XY}_{M_1M_2}} B(i) f^{XY}_{M_1M_2}(i) \\ &+ \sum_{i=1}^{L^{A}_{M_1M_2}} B(L^{XY}_{M_1M_2}+i) f^{A}_{M_1M_2}(i) \\ &+ \sum_{i=1}^{L^{P}_{M_1M_2}} B(L^{XY}_{M_1M_2}+L^{A}_{M_1M_2}+i) f^{P}_{M_1M_2}(i) \end{aligned} \tag{4.27}$$

where $L^{XY}_{M_1M_2}$, $L^{A}_{M_1M_2}$ and $L^{P}_{M_1M_2}$ are total number of original features collected from each signal segments.

The maximum likelihood estimates of coefficients $B(\cdot)$ are found using Newton-Raphson method after 50 iterations. The coefficients are updated using the following update equation,

$$B^{t+1}(\cdot) = B^{t}(\cdot) + \mathcal{J}^{-1}(B^{t}(\cdot))u(B^{t}(\cdot)) \tag{4.28}$$

where $\mathcal{J}^{-1}(B^{t}(\cdot))$ is the observed information matrix and $u(B^{t}(\cdot))$ is the score function.

The resulting coefficients and original features from I-Q segment $f^{XY}_{M_1M_2}(\cdot)$, amplitude $f^{A}_{M_1M_2}(\cdot)$ and phase $f^{P}_{M_1M_2}(\cdot)$ are combined to create a new feature $F_{M_1M_2}$ specified for the

discrimination of modulation M_1 and M_2.

$$\begin{aligned} F_{M_1M_2} = B(0) &+ \sum_{i=1}^{L^{XY}_{M_1M_2}} B(i) f^{XY}_{M_1M_2}(i) \\ &+ \sum_{i=1}^{L^{A}_{M_1M_2}} B(L^{XY}_{M_1M_2} + i) f^{A}_{M_1M_2}(i) \\ &+ \sum_{i=1}^{L^{P}_{M_1M_2}} B(L^{XY}_{M_1M_2} + L^{A}_{M_1M_2} + i) f^{P}_{M_1M_2}(i) \end{aligned} \tag{4.29}$$

For the case where there are more than two modulation candidates, the enhanced features need normalization to create a properly scaled multi-dimensional feature space for classification. The normalization is implemented by updating the trained coefficients $B(\cdot)$ using training signals. With a number of training signal realizations from each modulation, the enhanced features $F_{M_1M_2}(\cdot)$ for each signal realization can be calculated using Equation (4.29). The coefficients are then updated using following equations.

$$B'(0) = B(0) - \overline{F_{M_1M_2}(\cdot)} \tag{4.30}$$

where $\overline{F_{M_1M_2}(\cdot)}$ is the mean of the training features,

$$B'(i) = \frac{B(i)}{std(F_{M_1M_2}(\cdot))}, \quad i > 0 \tag{4.31}$$

where $std(F_{M_1M_2}(\cdot))$ gives the standard deviation of the training features.

4.3.4 Classification decision making

Once the feature extraction and feature combination are completed, training data is used to establish a reference feature space for the expected testing stage. In this research 100 realizations of training signals from each modulation candidate are used as reference samples for the K-nearest neighbour classifier. Given an unknown testing signal with extracted features F_{416}, F_{464} and F_{1664} and a reference point in the feature space with F'_{416}, F'_{464} and F'_{1664}, the following equation is used for distance calculation between the two,

$$d = \sqrt{(F_{416} - F'_{416})^2 + (F_{464} - F'_{464})^2 + (F_{1664} - F'_{1664})^2} \tag{4.32}$$

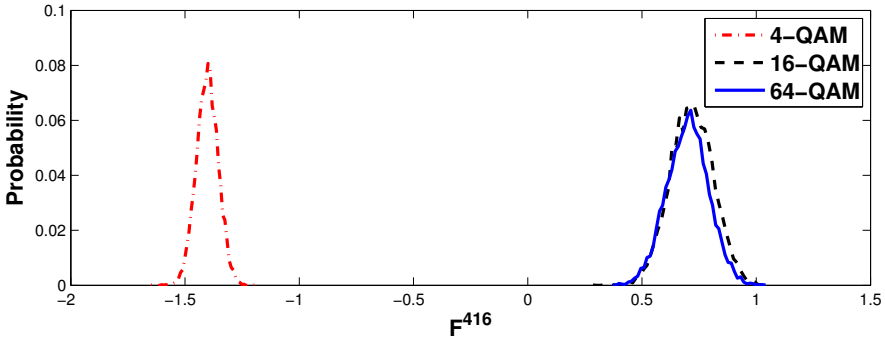

(a) F_{416} for 4-QAM and 16-QAM discrimination

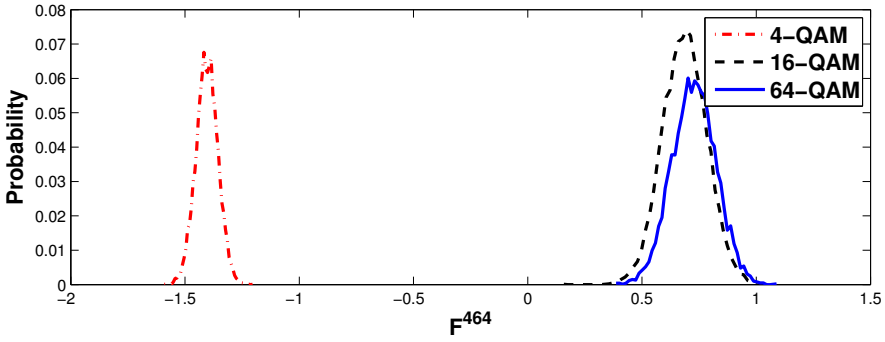

(b) F_{464} for 4-QAM and 64-QAM discrimination

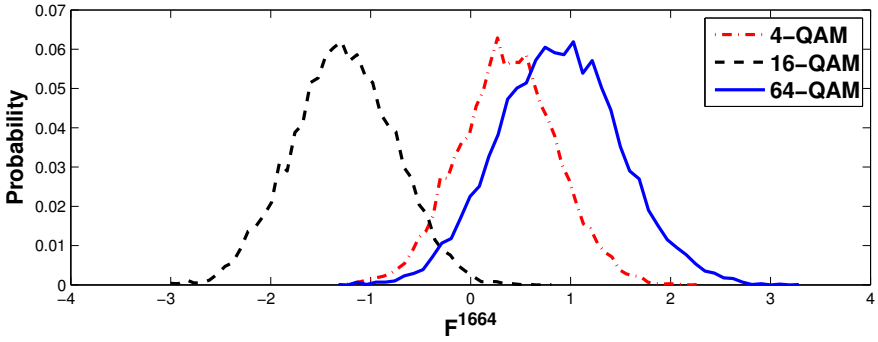

(c) F_{1664} for 16-QAM and 64-QAM discrimination

Figure 4.11: Enhanced distribution based features and their distribution projection on each separate dimension.

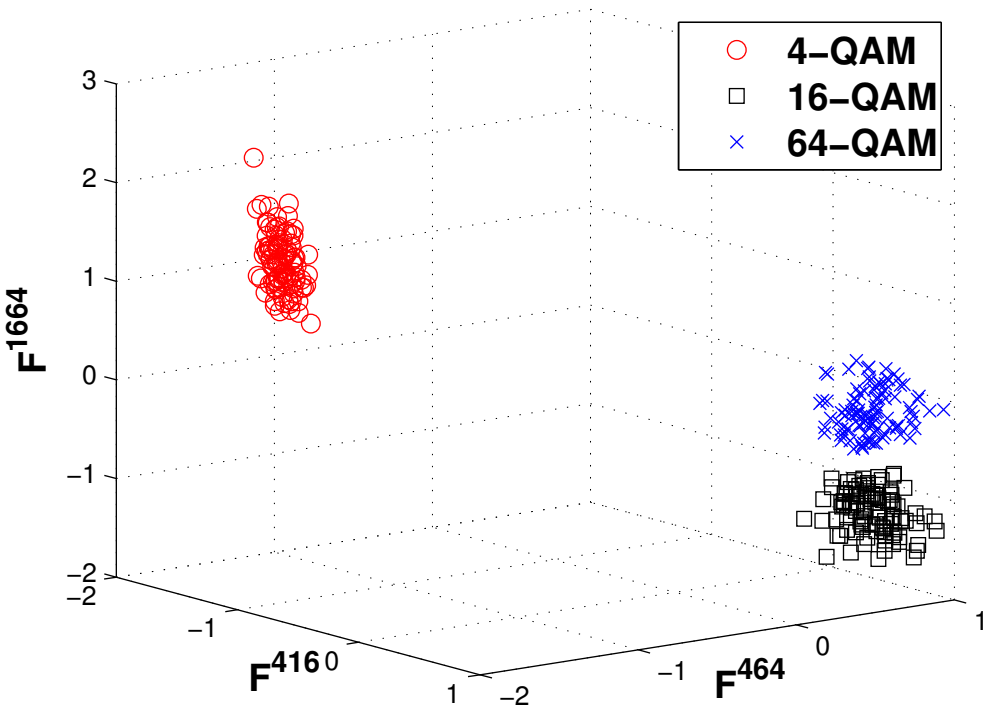

Figure 4.12: Reference samples in new distribution based feature space.

Figure 4.12 gives an example of such feature space. When an incoming signal is to be classified, the 17 nearest signal realizations are found. The signal modulation which has the most instances of appearance in the 17 nearest signal realizations is returned as the classification results.

4.3.5 Simulations and numerical results

To test the performance of the proposed AMC solution, two sets of experiments were conducted in the MATLAB environment. In both experiments, 4-QAM, 16-QAM and 64-QAM signals are generated according to Equation (2.12). For each channel configuration, a total 100 realizations of signals each consisting 512 signal samples from each modulation are generated for training purpose. During testing, the number of realizations is increased to 10,000 for each signal modulation. In sampling location optimization, the 100 signal realizations from the same signal modulation are combined to create a long signal realization of 51,200 samples. The increased number of samples helps to provide a smoother representation of signal distribution for analysis. The classification accuracy is calculated through the correct classification in all signal realizations. The parameters used can be found in Table 4.5.

In the AWGN channel, no phase or frequency offset is considered. SNR from 0 dB to 20 dB are simulated. The signal length N is set to 512. Figure 4.13 shows that 4-QAM is easier to classify and the proposed method is able to achieve 100% accuracy with SNR above 4 dB. For 16-QAM and 64-QAM the classification accuracy is similar throughout the SNR range. Perfect classification is achievable with SNR above 11 dB. The classification results coincide with the resulting feature space through the feature enhancement process. Figure 4.11 also shows that the feature separation between 4-QAM and 16-QAM as well as 4-QAM and 64-QAM are much clearer than the separation between 16-QAM and 64-QAM.

In Figure 4.14, the performance comparison with two existing methods is given. The ML classifier (Wei and Mendel, 2000) gives the best performance at all SNR levels. This is no surprise as the channel condition is ideal and all signal parameters are assumed to have been estimated. However, the proposed method provides a very similar classification accuracy which only shows slight disadvantage at low SNR between 0 and 10 dB. Meanwhile,

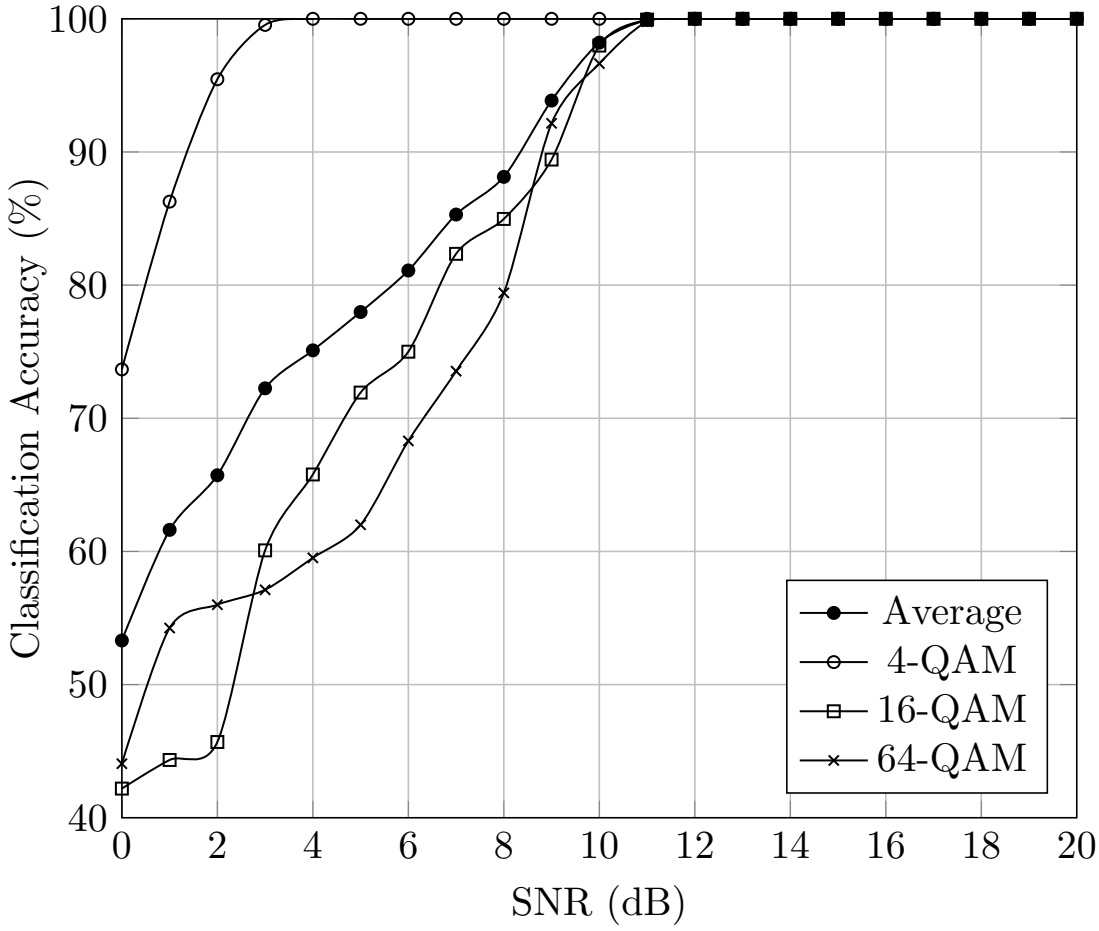

Figure 4.13: Classification accuracy using distribution based features in AWGN channel.

the cumulant based Genetic Programming classifier (Aslam et al., 2012) suffers from the low signal length ($N = 512$) used and gives much low accuracy even with high SNR levels.

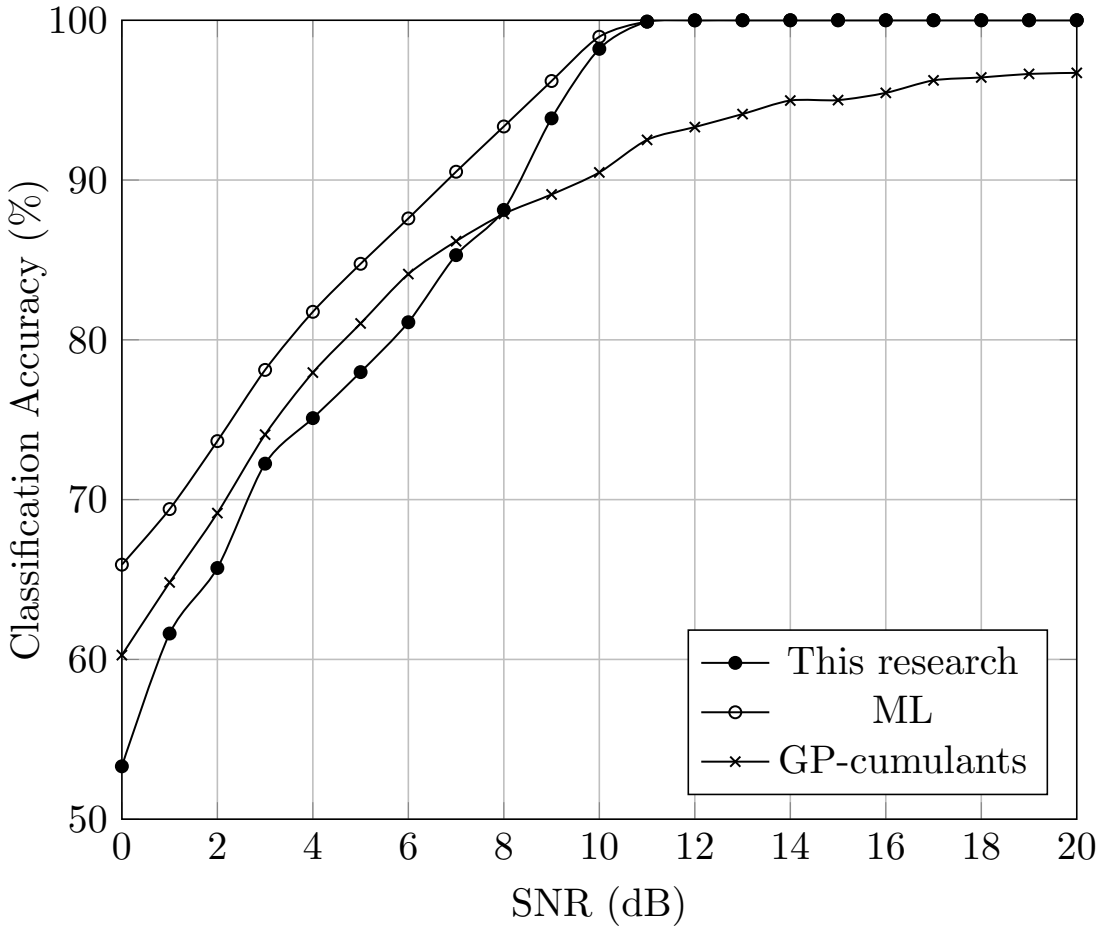

Figure 4.14: Averaged classification accuracy using different classifiers in AWGN channel.

Another common channel condition is carrier phase offset. In this experiment, we simulated the carrier phase offset of 0° to 30°. Other channel conditions are set to the same as the previous experiments with SNR of 10 dB and signal length of 512. Figure 4.15 shows the resulting classification accuracy for three classifiers with different degrees of carrier phase offset. ML classifier achieves the best accuracy with no or little phase offset. Meanwhile, the Kolmogorov Smirnov test classifier (Wang and Wang, 2010) is severely affected by the increasing amount of phase offset. Having similar classification accuracy with little carrier

phase offset, the proposed method is able to maintain an equal level of performance throughout the tested phase offset range. Consequently, it is able to outperform ML with phase offset over 15°, and KS classifier under all conditions.

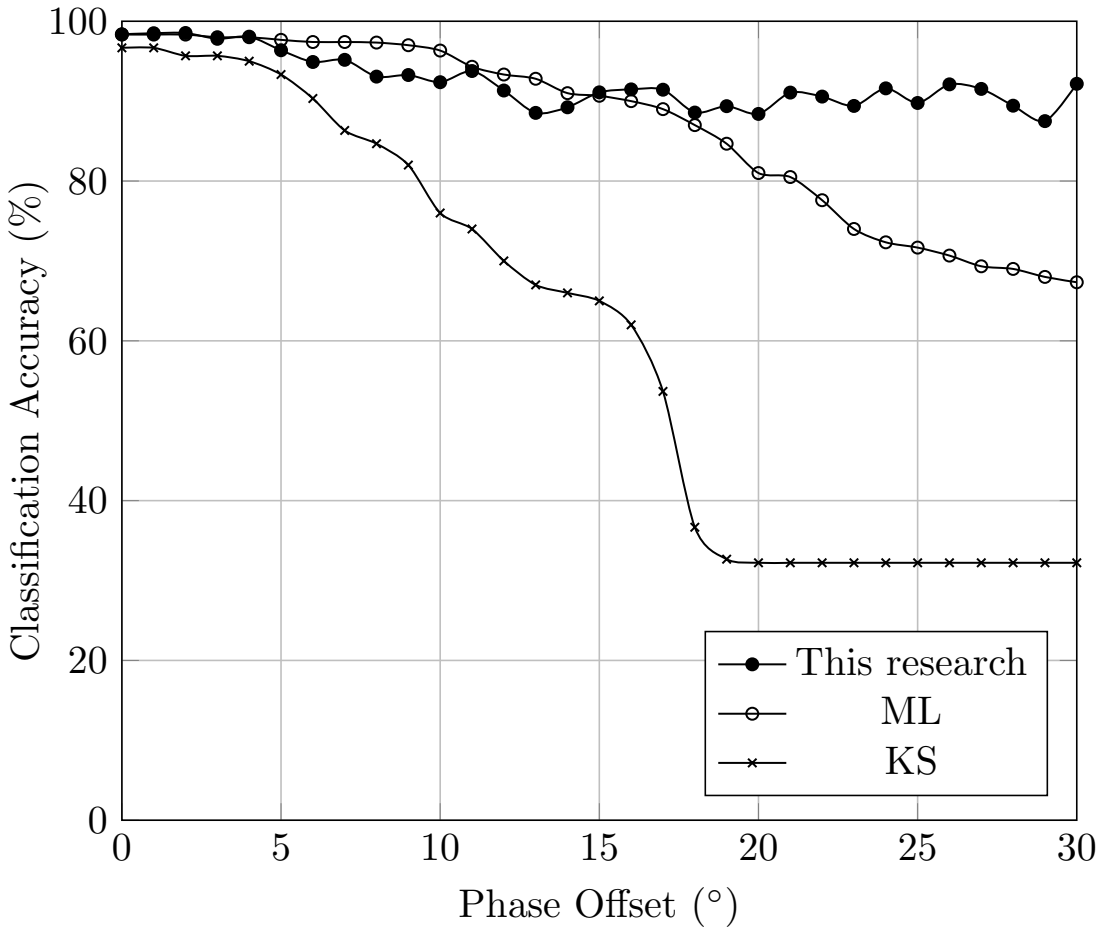

Figure 4.15: Averaged classification accuracy using different classifier in fading channel carrier phase offset .

4.4 Summary

In this chapter, we presented two different approaches to utilize signal distributions for modulation classification. The ODST classifier improves the KS test classifier by optimizing multiple sampling locations for distribution sampling. The ODST goodness of fit is defined by a standard distance metric system and a weight metric system. It is shown that the ODST

classifier is superior to cumulant based classifier who is subject to sever degradation with limited signal length. In addition, the optimization of weights using GA is able to further improve the classification accuracy by a small margin. In another approach, the sampled signal distribution values are treated as features. By extending the signal distributions into phase and magnitude, more features are available for analysis. The dimension reduction problem is solved by a logistic regression process where features combined into smaller new feature sets. The resulting classifier show superior performance in complex channel with phase offset.

Chapter 5

Modulation Classification with Unknown Noise

5.1 Introduction

As discussed in Chapter 2, most of the existing modulation classifiers require the knowledge of noise model and noise power to achieve modulation classifications. Likelihood based classifiers promise optimal classification accuracy (Wei and Mendel, 2000; Gao et al., 2008; Hameed et al., 2009; Xu et al., 2011; Shi and Karasawa, 2011, 2012). Unfortunately, such method requires a matching channel model as well as perfect knowledge of channel parameters to achieve optimality. Efforts have been made to relax some of the rules serving an optimal LB classifier. Wong and Nandi (Wong and Nandi, 2008) suggested a semi-blind LB classifier with carrier phase and noise power estimation in a non-coherent environment. Panagiotou et al. (Panagiotou et al., 2000) employ GLRT and Hybrid likelihood ratio test HLRT to achieve classification with carrier phase as unknown parameters. Huang and Polydoros (Huang and Polydoros, 1995) presented the quasi-Log-Likelihood Ratio Test (qLLRT) with carrier phase as unknown parameter. All these likelihood based semi-blind classifiers mitigate the dependence on one or two channel parameters. None offers the ability of classification in a completely blind environment. Another new branch of decision theoretic methods employs

distribution test for low complexity modulation classification (Wang and Wang, 2010; Urriza et al., 2011; Zhu et al., 2013a). Yet, all channel parameters are assumed to be available.

Feature based methods often provide near-optimal performance with lower complexity. The extraction of most features do not require channel parameters such a channel gain, carrier phase offset, or noise variance. However, they are often acquired for the optimization of decision thresholds and reference values. Nandi and Azzouz (Nandi and Azzouz, 1998) used spectral-based feature sets for effective classification of digital modulations. Cumulant features suggested by Swami and Saddler (Swami and Sadler, 2000) became popular for the classification of digital modulations with different orders (Wu et al., 2008). Cyclic features are another set of features for modulation classification which exploits the cyclostationarity of the signals (Gardner and Spooner, 1992; Punchihewa et al., 2010). Lately, machine learning techniques have become a new trend for feature based methods. Wong and Nandi suggested artificial neural network and genetic algorithm for feature combination and dimension reduction (Wong and Nandi, 2004). Genetic Programming is another advanced machine learning algorithm to provide improved performance (Aslam et al., 2012). Despite their robust performance, all feature based methods require channel parameters to achieve high classification accuracy.

For the purpose of complete blind classification, we propose two centroid estimator for the joint estimation of channel gain and carrier phase. A new non-parametric likelihood function is proposed as a low complexity alternative which aims to serve a wider variety of channel conditions. Figure 5.1 provides an overview of the implementation of the proposed blind modulation classier for M-ary PSK and QAM.

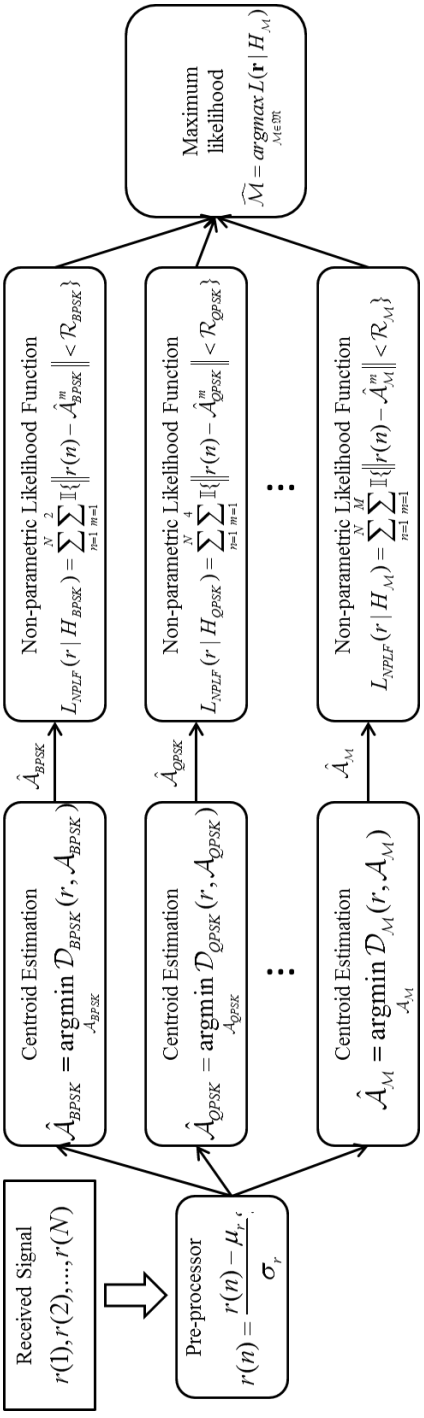

Figure 5.1: Implementation of blind modulation classification with minimum distance centroid estimator and non-parametric likelihood function.

5.2 Classification strategy

Given a set of candidate modulations $\mathfrak{M}$, the classification decision $\hat{\mathcal{M}}$ is drawn from the hypothesis models $H_{\mathcal{M}}$ of modulation $\mathcal{M} \in \mathfrak{M}$ with a maximum likelihood $\mathcal{L}(\mathbf{r}|H_{\mathcal{M}})$

$$\hat{\mathcal{M}} = \underset{\mathcal{M}\in\mathfrak{M}}{argmax}\, \mathcal{L}(\mathbf{r}|H_{\mathcal{M}}) \tag{5.1}$$

Most classifiers require the prior knowledge of the channel gain α, carrier phase θ, modulation symbols $\mathbf{s}_{\mathcal{M}}$, and noise σ variance before the test could be conducted. In addition, in many cases, the parameters are considered identical among different hypothesis models with the exception of modulation symbols.

$$\mathcal{L}(\mathbf{r}|H_{\mathcal{M}}) = \mathcal{L}(\mathbf{r}|\alpha, \theta, \mathbf{s}_{\mathcal{M}}, \sigma) \tag{5.2}$$

In the case of blind modulation classification, parameters have to be estimated. The estimation is likely to differ among different hypothesis models, as it is natural to estimate the parameters with the assumption of modulation type to achieve more accurate likelihood evaluation.

$$\mathcal{L}(\mathbf{r}|H_{\mathcal{M}}) = \mathcal{L}(\mathbf{r}|\hat{\alpha}_{\mathcal{M}}, \hat{\theta}_{\mathcal{M}}, \mathbf{s}_{\mathcal{M}}, \hat{\sigma}_{\mathcal{M}}) \tag{5.3}$$

To reduced complexity of estimating multiple interlinked parameters, we suggest treating noise variance as unknown parameters and employ alternative likelihood functions to mitigate its necessity.

$$\mathcal{L}(\mathbf{r}|H_{\mathcal{M}}) = \mathcal{L}(\mathbf{r}|\hat{\alpha}_{\mathcal{M}}, \hat{\theta}_{\mathcal{M}}, \mathbf{s}_{\mathcal{M}}) \tag{5.4}$$

The estimations of channel gain and carrier phase are combined as the estimation of received signal centroids $\hat{\mathcal{A}}_{\mathcal{M}}$

$$\hat{\mathcal{A}}_{\mathcal{M}} = \alpha_{\mathcal{M}} e^{j\theta_{\mathcal{M}}} \mathbf{s}_{\mathcal{M}} \tag{5.5}$$

reducing the estimation task to a single parameter and the likelihood function to be related to only the signal centroids.

$$\mathcal{L}(\mathbf{r}|H_{\mathcal{M}}) = \mathcal{L}(\mathbf{r}|\hat{\mathcal{A}}_{\mathcal{M}}) \tag{5.6}$$

We will start the discussion with the estimation of signal centroids $\mathcal{A}_{\mathcal{M}}$ and then progress to the likelihood functions in later sections.

5.3 Centroid estimation

Signal centroids are useful tools for analysis in many signal processing problems, although not often fully utilized in modulation classification problems. In the modulation classification context, a signal centroid represents the cluster centre of noisy signal samples that originate from the same transmitted symbol. It carries information of the signal parameters like channel gain and carrier phase, which provides the possibility of joint estimation of such parameters. Though separate blind estimation of channel gain and carrier phase is achievable (Tomasoni and Bellini, 2012; Zarzoso and Nandi, 1999), its high computational complexity makes the joint estimation through centroid estimation an attractive alternative.

Maximum likelihood estimator is an accurate way of estimating signal centroids (Fisher, 1922). However, ML estimation requires a matching distribution and known parameters. It is not achievable in the context of BMC with unknown channel parameters and noise distributions. Blind symbol estimation provides symbol estimation for every signal samples (Liu and Xu, 1995). It is related to the centroid estimation and the results can be directly utilized for the centroid estimation. Considering that the designed classification approach does not require the estimation of each transmitted samples, the extra amount of computation for blind symbol estimation seems wasteful. Mobasseri used fuzzy c-means clustering to created signal partitions on the constellation plot (Mobasseri, 2000). The subsequent means of the signal clusters can be taken as estimated centroids. Unfortunately, it was not designed with centroid estimation in mind and the resulting cluster means are normally not accurate enough to be used in a decision theoretic classifier.

5.3.1 Constellation segmentation estimator

Assuming that the signal modulation is square M-QAM with M centroids and $I = \sqrt{M}$ components on each dimension, we can obtain the cumulative probability of a segment from the signal constellation between $x = 0$ and $x = 2A$

$$P(0 \leq x \leq 2A) = \frac{I}{M} \sum_{i=-I/2}^{I/2} F_i(2A) - F_i(0) \tag{5.7}$$

where $F_i(x)$ is the cumulative distribution from centroid i

$$F_i(x) = \int_{-\infty}^{x} \frac{1}{\sigma\sqrt{2\pi}} e^{-\frac{(x-A_i')^2}{2\sigma^2}} dx \tag{5.8}$$

Equation (5.7) can be rewritten as

$$P(0 \leq x \leq 2A) = \frac{I}{M} \sum_{i=-I/2}^{I/2} \int_{0}^{2A} \frac{1}{\sigma\sqrt{2\pi}} e^{-\frac{(x-A_i')^2}{2\sigma^2}} dx \tag{5.9}$$

Because the centroids are assigned as

$$A_i = (2i+1)A \tag{5.10}$$

By replacing the A_i in Equation (5.9), the cumulative probability can be obtained as

$$P(0 \leq x \leq 2A) = \frac{I}{M} \int_{(-I+1)A}^{(I+1)A} \frac{1}{\sigma\sqrt{2\pi}} e^{-\frac{x^2}{2\sigma^2}} dx \tag{5.11}$$

Assuming the modulation order $M \geq 16$ and $SNR \geq 5dB$, $(I+1)A > 5\sigma$ and $(-I+1)A < -3\sigma$. The cumulative probability is very close to I/M.

$$P(0 \leq x \leq 2A) \approx \frac{I}{M} \tag{5.12}$$

As the signal distribution is symmetrical for square M-QAM modulations, the distribution in the following segments should also exhibit the same property: $-2A \leq x \leq 0$, $0 \leq y \leq 2A$, $-2A \leq y \leq 0$. The resulting joint distribution probability in the 2-D segment $0 \leq x, y \leq 2A$ can be derived to be

$$P(0 \leq x, y \leq 2A) \approx \frac{1}{M} \tag{5.13}$$

Thus the number of samples K falling into the $0 \leq x, y \leq 2A$ range should equal to N/M, which is the total number of samples from each signal symbol when the total number of samples is N. The conclusion can be easily converted as a method for the estimation of A. By finding the a segment of the signal constellation from $0 \leq x, y \leq 2A$ which contains a number of samples equal to the sample number from a single centroid.

$$K = \sum_{n=1}^{N} \mathbb{I}\{0 < r_X(n), r_Y(n) < 2A\} = N/M \tag{5.14}$$

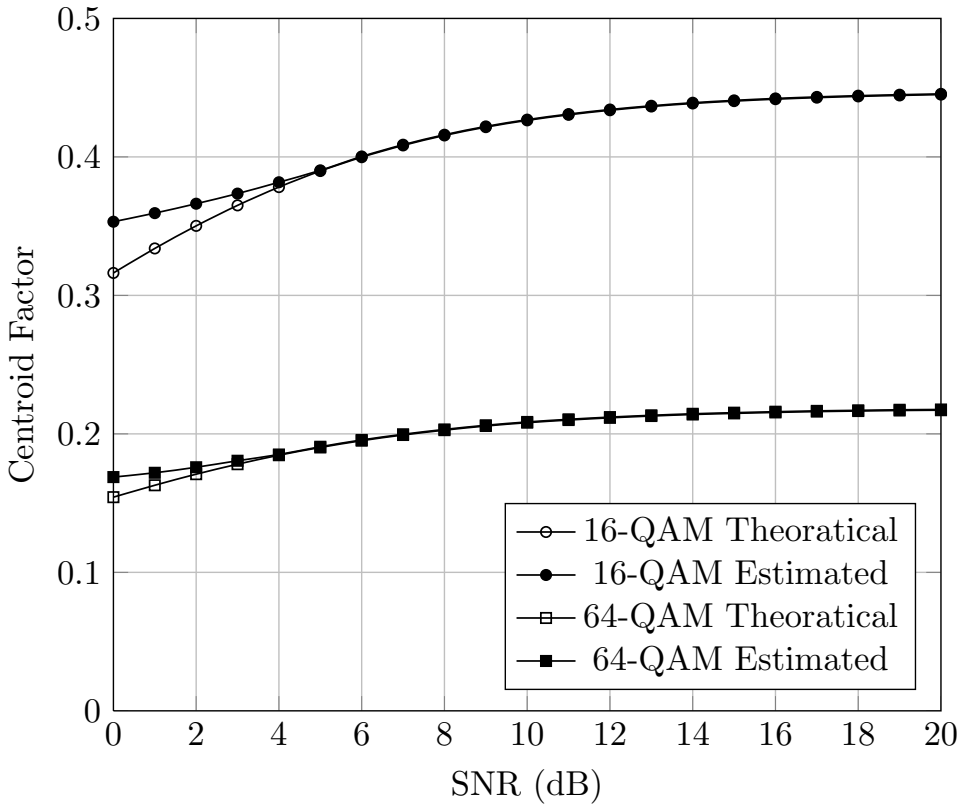

Figure 5.2: Theoretical values of centroid factors A for 16-QAM and 64-QAM with different noise levels and their analytical estimation using proposed blind centroid estimator.

Figure 5.2 shows the exact centroid location and the analytical centroid estimation using the above theory. It is clear that the assumption is practical for the considered blind centroid estimation scenario. Having established the approximate blind centroid estimation theory, we propose the Automatic Constellation Grid Segmentation (ACGS) for the estimation of signal centroids and provide partitioning of samples for future analysis. The process of ACGS is illustrated in Figure 5.3. Details of each step will be given in the following subsections.

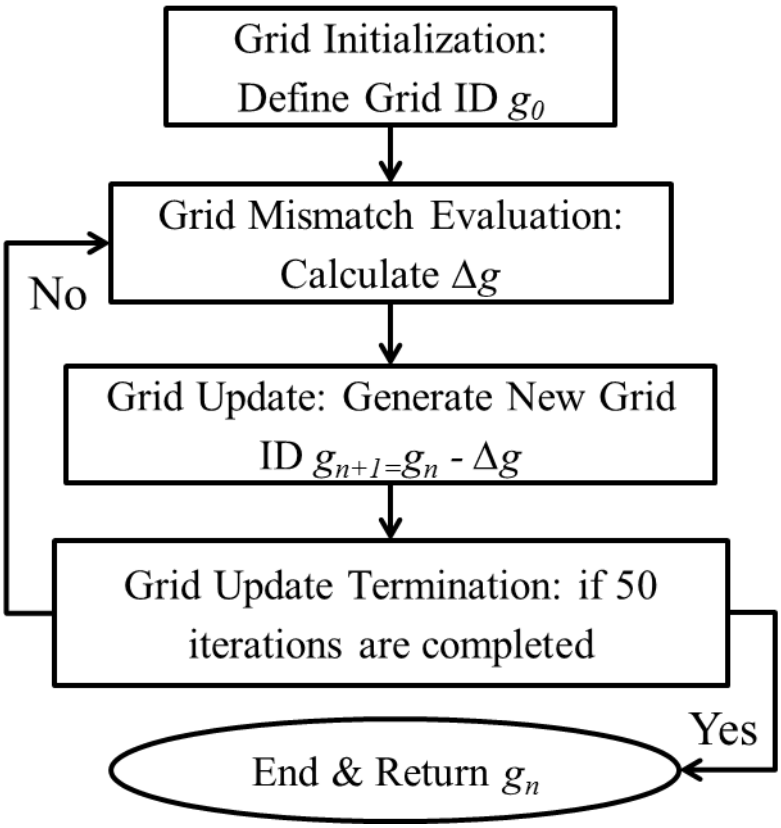

Figure 5.3: Automatic Segmentation for carrier phase offset compensation.

The grid used in ACGS is formed by parallel segmentations with equal distance on two perpendicular directions. The resulting gird consists of a number of identical square compartments, whose total number is equal to the total symbol number of the assumed M-QAM modulation. An example of the grid can be found in Figure 5.4. Grid G_{16} in dashed lines is the initial grid with ID g_0. And the one in solid line is the grid after one iteration of

update with $\triangle g$ and identified by g_1. Crosses indicate the location of actual centroids.

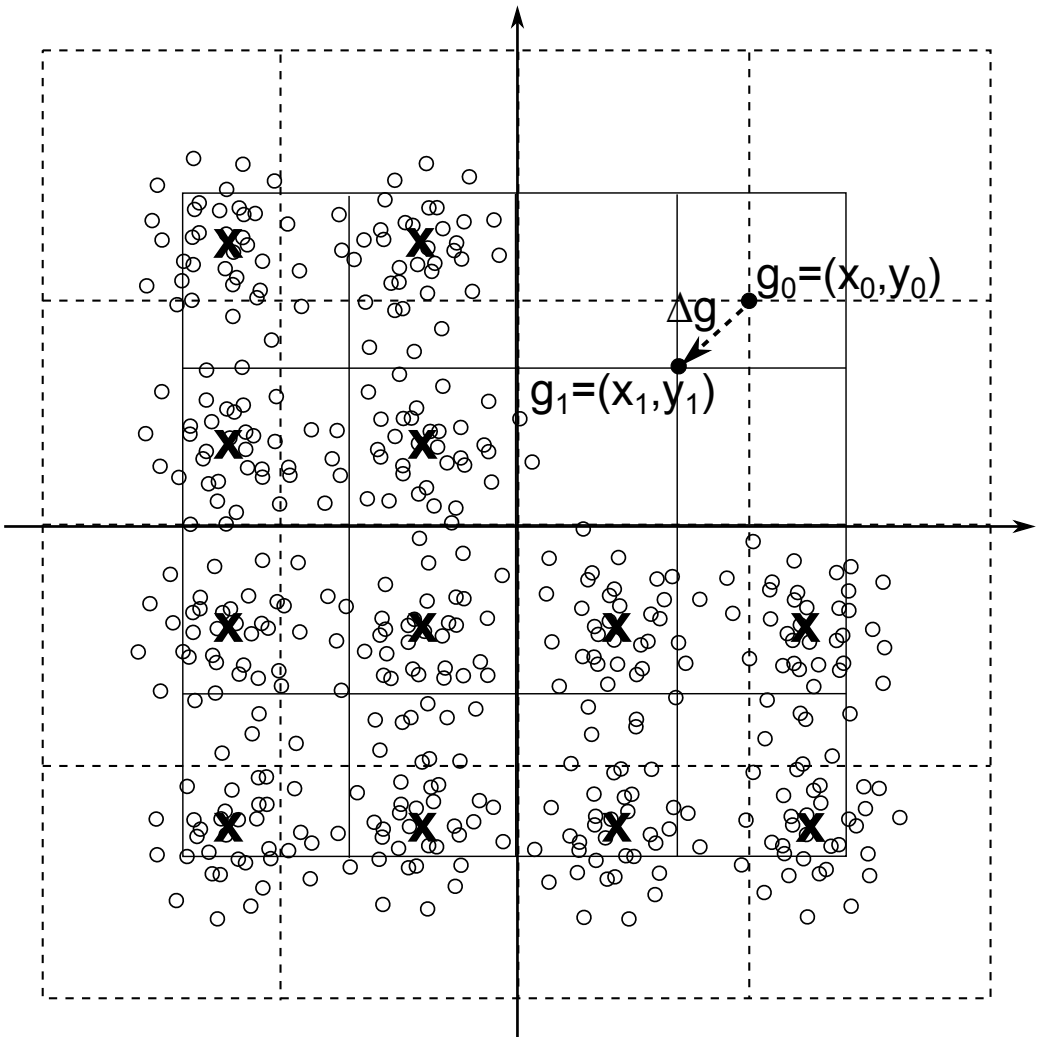

Figure 5.4: Automatic Constellation Grid Segmentation for centroid estimation.

Due to its rigid structure, the whole grid can be defined by the single identification point in the first quadrant which is nearest to the coordinate origin (the grid centre). The initial definition of the grid is given by assigning an initial value for the identification point (grid ID) g_0.

$$g_0 = x_0 + y_0 j \tag{5.15}$$

where x_0 and y_0 are the real and imaginary part of g_0 on I-Q constellation plane. The initial

values of x_0 and y_0 are set to the same. A mathematical expression of grid junctions G_M can be found in Equation (5.16).

$$G_M = \begin{bmatrix} -\frac{I}{2}y + \frac{I}{2}xj & \cdots & -y + \frac{I}{2}xj & x + \frac{I}{2}yj & \cdots & \frac{I}{2}x + \frac{I}{2}yj \\ \vdots & & \vdots & \vdots & & \vdots \\ -\frac{I}{2}y + xj & \cdots & -y + x_0j & x + yj & \cdots & \frac{I}{2}x + yj \\ -\frac{I}{2}x - yj & \cdots & -x - yj & y - xj & \cdots & \frac{I}{2}y - xj \\ \vdots & & \vdots & \vdots & & \vdots \\ -\frac{I}{2}x - \frac{I}{2}yj & \cdots & -x - \frac{I}{2}yj & y - \frac{I}{2}xj & \cdots & \frac{I}{2}y - \frac{I}{2}xj \end{bmatrix} \tag{5.16}$$

By updating the grid, the end results of ACGS should produce a grid which fits the pattern of the centroid distribution. The centre of each partition (square compartment) on the grid should be aligned to the corresponding centroid from the modulated signal. A definition of the grid partition centres S_M for M-QAM modulation is given in Equation (5.17).

$$S_M = \begin{bmatrix} \frac{(1+I/2)(-y+xj)}{2} & \cdots & -\frac{y}{2} + \frac{(1+I/2)x}{2}j & \frac{x}{2} + \frac{(1+I/2)y}{2}j & \cdots & \frac{(1+I/2)(x+yj)}{2} \\ \vdots & & \vdots & \vdots & & \vdots \\ -\frac{(1+I/2)y}{2} + \frac{x}{2}j & \cdots & -\frac{y}{2} + \frac{x}{2}j & \frac{x}{2} + \frac{y}{2}j & \cdots & \frac{(1+I/2)x}{2} + \frac{y}{2}j \\ -\frac{(1+I/2)x}{2} - \frac{y}{2}j & \cdots & -\frac{x}{2} - \frac{y}{2}j & \frac{y}{2} - \frac{x}{2}j & \cdots & \frac{(1+I/2)y}{2} - \frac{x}{2}j \\ \vdots & & \vdots & \vdots & & \vdots \\ \frac{(1+I/2)(-x-yj)}{2} & \cdots & -\frac{x}{2} - \frac{(1+I/2)y}{2}j & \frac{y}{2} - \frac{(1+I/2)x}{2}j & \cdots & \frac{(1+I/2)(y-xj)}{2} \end{bmatrix} \tag{5.17}$$

Having calculated the error, the grid is updated using the following equation.

$$g_{n+1} = (x_n - \triangle g) + (y_n - \triangle g)j \tag{5.18}$$

The grid update process is repeated for 50 iterations. After the last iteration, the final grid and signal partitioning are returned for use in the actual modulation classification. The returned grid ID point $g' = x' + y'j$ will be used to form the complete grid matrix as well as centroid matrix.

In the case where there is carrier phase offset θ_0, the grid is first trained to compensate the phase error. It is accomplished with a phase error function and a grid update function.

$$\triangle\theta = \theta_g - \theta_l \tag{5.19}$$

where θ_g is the phase of the grid defined by the grid ID g_n

$$\theta_g = arg(g_n) \tag{5.20}$$

and θ_l is the average phase of all samples in partition 1 in the 1st quadrant.

$$\theta_l = \overline{arg\{r'(l_n = 1)\}} \tag{5.21}$$

The grid will then be updated using the following equation

$$g_{n+1} =\mid g_n \mid e^{j(\theta_g - \triangle\theta)} \tag{5.22}$$

The training will be repeated for 50 iterations and the the final θ_g will be returned as the estimated carrier phase offset θ'. To compensate the phase offset, Equation (5.15) and (5.18) used in ACGS should be modified to the following two equations

$$g_0 =\mid x_0 + y_0 j \mid e^{j\theta'} \tag{5.23}$$

$$g_{n+1} = \{x_n - cos(\theta') \triangle g\} + \{y_n - sin(\theta') \triangle g\}j \tag{5.24}$$

5.3.2 Minimum distance estimator

Through ACGS, signal centroids can be estimated for square M-QAM modulation signals. However, it is not able to perform centroid estimation for other digital modulations and to assist the classification of these modulations. For this reason, we have developed a different estimation approach named Minimum Distance Centroid Estimator (MDCE). The notion is to define a set of signal centroids that are intended to indicate the modulation symbol after communication channel without the additive noises.

We assume that the estimated centroids $\mathcal{A}_\mathcal{M}$ to possess the original rigid structure after transmission and pre-processing. The mean of centroids $\mu(\mathcal{A}_\mathcal{M})$ should remain at 0, the magnitude of two different centroid elements $\mathcal{A}^p_\mathcal{M}$ and $\mathcal{A}^q_\mathcal{M}$ should follow the original proportion $\left\|\mathcal{A}^p_\mathcal{M}\right\| / \left\|\mathcal{A}^q_\mathcal{M}\right\| = \left\|\mathbf{s}^p_\mathcal{M}\right\| / \left\|\mathbf{s}^q_\mathcal{M}\right\|$, and the phase difference between centroids should remain the same $\phi(\mathcal{A}^p_\mathcal{M}) - \phi(\mathcal{A}^q_\mathcal{M}) = \phi(\mathbf{s}^p_\mathcal{M}) - \phi(\mathbf{s}^q_\mathcal{M})$. The resulting expression for sets of

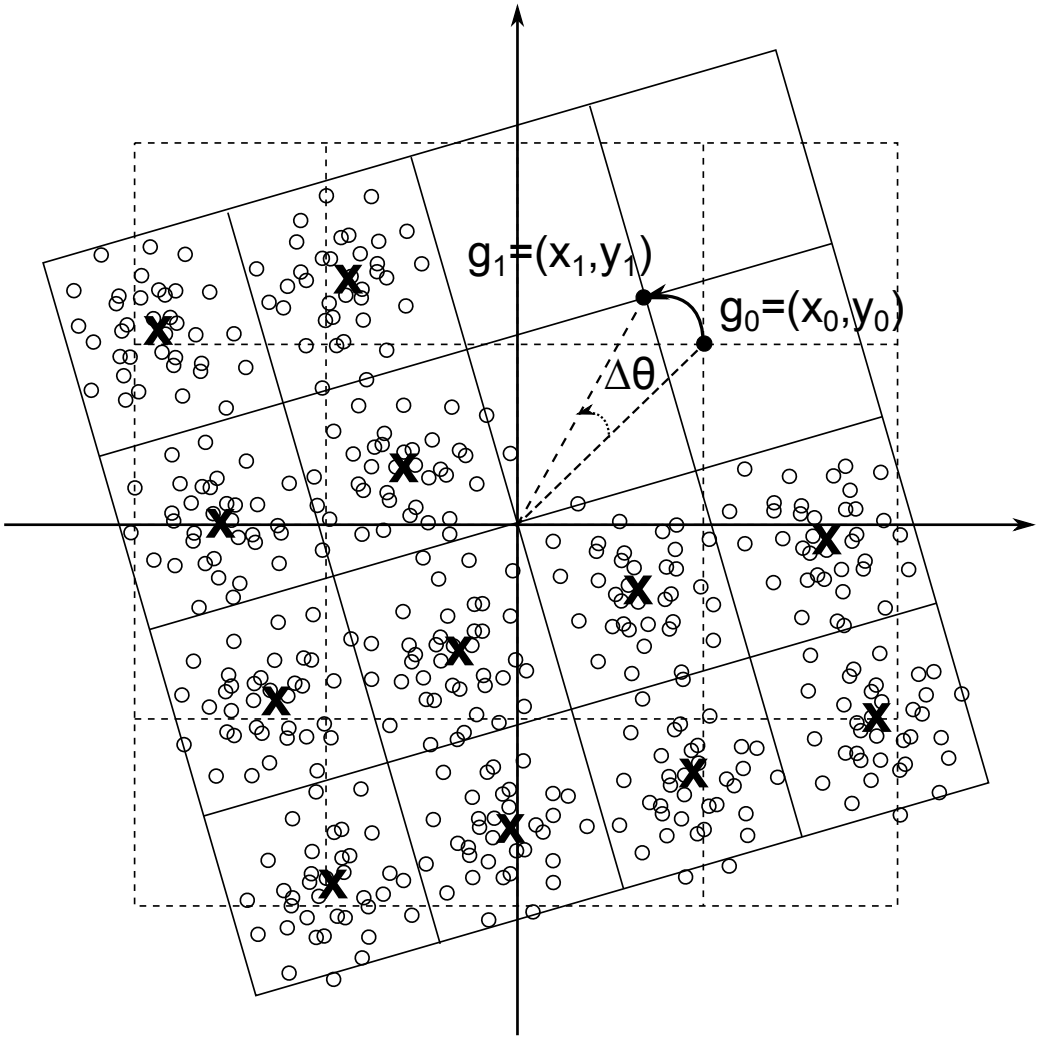

Figure 5.5: Carrier phase offset estimation and compensation for constellation grid segmentation.

centroids for BPSK, QPSK/4-QAM and 8-PSK can be expressed in a simplified form with a single centroid parameter $A = ae^{i\phi}s^0_{\mathcal{M}}$.

$$\mathcal{A}_{BPSK} = \begin{bmatrix} -A & A \end{bmatrix} \tag{5.25}$$

$$\mathcal{A}_{QPSK} = \mathcal{A}_{4-QAM} = \begin{bmatrix} jA & A \\ -A & -jA \end{bmatrix} \tag{5.26}$$

$$\mathcal{A}_{8-PSK} = \begin{bmatrix} & -jA & jA^* & \\ -A^* & & & A \\ A & & & A^* \\ & -jA^* & jA & \end{bmatrix} \tag{5.27}$$

Therefore the estimation of $\mathcal{A}_{\mathcal{M}}$ can be reduced to the estimation of the centroid parameter A. The reference symbol $s^0_{\mathcal{M}}$ is defined as the one which is nearest to the signal mean. The expressions of signal centroid for 16-QAM and 64-QAM modulations are not given here due to their large size and relative ease to derive with the given rules.

To measure the mismatch between the observed signal and the potential centroids estimation, a signal-to-centroid distance is designed to accomplish the task. With no assumption of the noise variance and distribution, we propose the overall distance $\mathcal{D}_{\mathcal{M}}(\mathbf{r}, \mathcal{A}_{\mathcal{M}})$ to be the sum of the Euclidean distance between each signal sample and its nearest centroid

$$\mathcal{D}_{\mathcal{M}}(\boldsymbol{r}, \mathcal{A}_{\mathcal{M}}) = \sum_{n=1}^{N} \min_{m \in [1,..,M]} (\|r(n) - \mathcal{A}^m_{\mathcal{M}}\|) \tag{5.28}$$

where M is the total number of centroids in the centroid collection $\mathcal{A}_{\mathcal{M}}$.

Such distance metric was first proposed by Wong and Nandi in (Wong and Nandi, 2008), where it is used as a model mismatch evaluation for a minimum distance classifier. As a classifier, the distance metric always produce shorter distance for higher order modulations which leads to a bias in classification for higher order modulations. However, such problem does not existence in centroid estimation, as it is conducted within a modulation hypothesis and the mismatch is only caused by the estimated centroids of the same order.

The signal centroids $\mathcal{A}_{\mathcal{M}}$ are estimated by finding the minimum of the distance metrics $\mathcal{D}_{\mathcal{M}}(\boldsymbol{r}, \mathcal{A}_{\mathcal{M}})$.

$$\hat{\mathcal{A}}_{\mathcal{M}} = \arg\min_{\mathcal{A}_{\mathcal{M}}} \mathcal{D}_{\mathcal{M}}(\boldsymbol{r}, \mathcal{A}_{\mathcal{M}}) \tag{5.29}$$

For the estimator to be valid, the expectation of the estimated centroids $E[\hat{\mathcal{A}}_{\mathcal{M}}]$ should equal to $\alpha e^{j\theta}\boldsymbol{s}_{\mathcal{M}}$ with the channel gain α, the carrier phase θ, and the transmitted symbols $\boldsymbol{s}_{\mathcal{M}}$. The estimation of the centroids is a solutions of the derivative of the signal-to-centroid distance expectation $\frac{\partial}{\partial \mathcal{A}_{\mathcal{M}}} E[\mathcal{D}_{\mathcal{M}}(r, \mathcal{A}_{\mathcal{M}})] = 0$. Replace the centroids with the single centroid parameter $A = ae^{i\phi}s^0_{\mathcal{M}}$. The analysis can be divided into $a = \alpha$ when $\frac{\partial}{\partial a} E[\mathcal{D}_{\mathcal{M}}(r, a)] = 0$, and $\phi = \theta$ when $\frac{\partial}{\partial \phi} E[\mathcal{D}_{\mathcal{M}}(r, \phi)] = 0$. The detailed proof is given in Appendix A.

The implementation of MDCE is realized by an iterative sub-gradient optimization process. The details are given in Appendix B.

The estimator is tested in the simulated AWGN channel at different SNR levels from 0 dB to 20 dB. At each noise level, 1,000 signal realizations are tested with each consisting N=1,024 samples. In Figure 5.6, it is clear that the centroid estimator provides a very accurate estimation of the channel gain with a very small amount of deviation at SNR over 10 dB. The accuracy degrades with increased level of noise and a quick acceleration is seen at SNR below 5 dB. Since the estimator of centroid magnitude relies on the approximation of the Rice distribution to a normal distribution as described in Appendix A, the estimation of the 8-PSK centroid magnitude receives a more significant impact than 16-QAM despite having a lower order. I believe the multiple layers of centroids with different magnitudes in 16-QAM help to compensate the biased estimation error caused by the approximation. It is worth noting that the The phase error in Figure 5.7 tells a similar story. The influence of the estimation error in the classification performance will be discussed in Section 5.5.

5.4 Non-parametric likelihood function

To enable likelihood evaluation without known noise model and power, we propose a new low complexity non-parametric likelihood function. Firstly, we relax the assumption of noise distribution to be any symmetrical distribution with higher density at signal mean. Secondly,

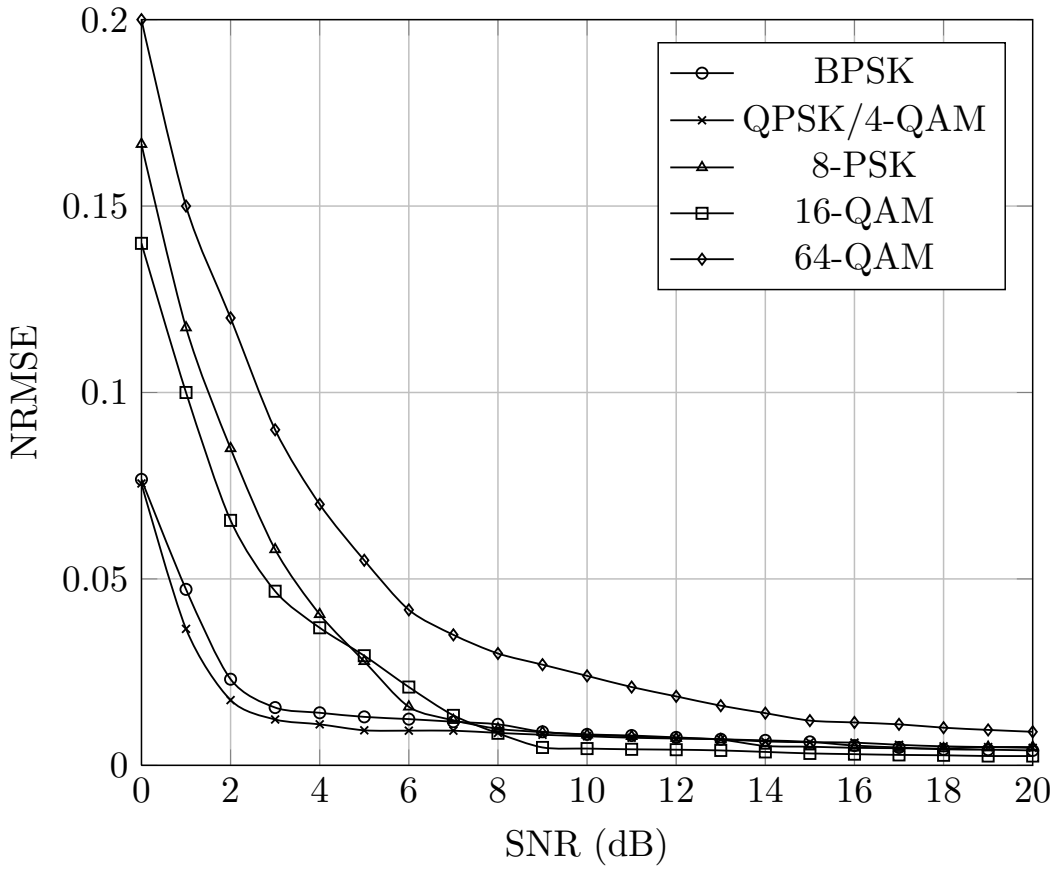

Figure 5.6: Error of channel gain estimation for different modulations using minimum distance centroid estimation.

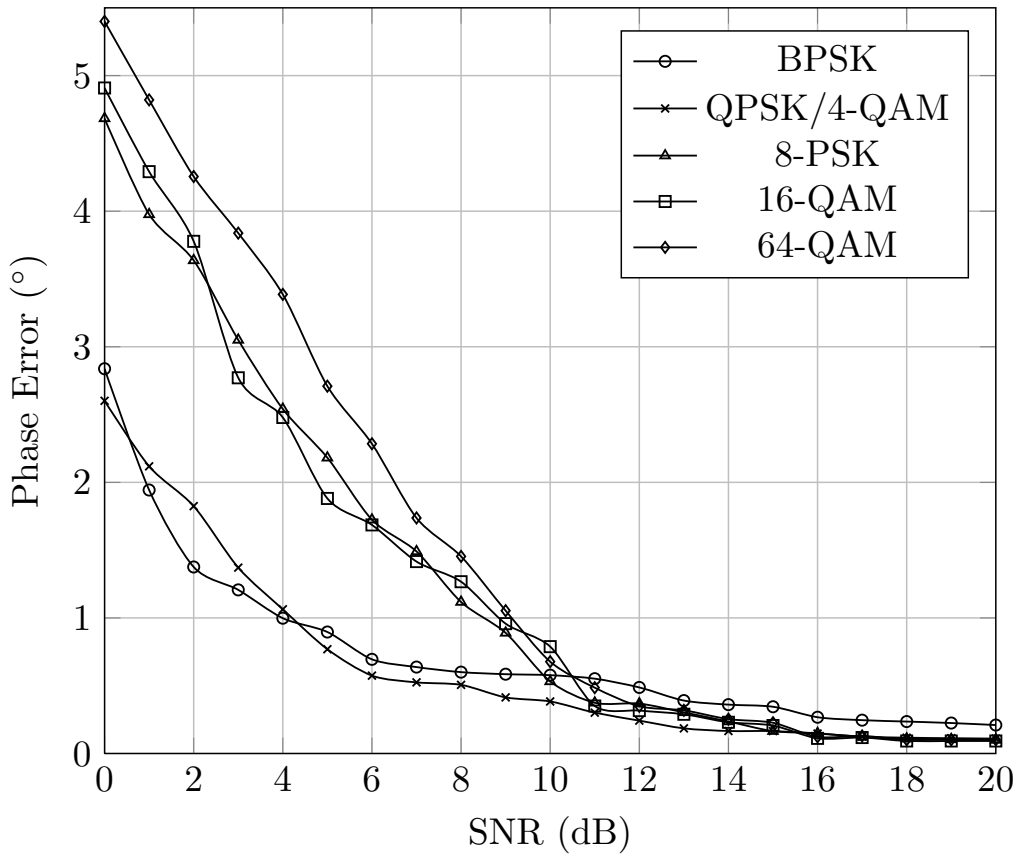

Figure 5.7: Error of carrier phase estimation for different modulations using minimum distance centroid estimation.

we replace the noise variance by an expression of the estimated channel gain and estimated centroids numbers. Thirdly, we reduce logarithm operation of likelihood calculation to simple counting operation. The resulting likelihood function can be found as

$$L_{NP}(r|H_{\mathcal{M}}) = \sum_{n=1}^{N}\sum_{m=1}^{M} \mathbb{I}\{\left\| r(n) - \hat{\mathcal{A}}_{\mathcal{M}}^{(m)} \right\| < \mathcal{R}_{\mathcal{M}}\} \tag{5.30}$$

where $\mathbb{I}(.)$ is a conditional function which returns 1 if the input is true and 0 if input is false, and the radius parameter $\mathcal{R}_{\mathcal{M}}$ is given by

$$\mathcal{R}_{\mathcal{M}} = \mathcal{R}_0/\sqrt{M}. \tag{5.31}$$

The selection of the reference radius $\mathcal{R}_0$ will be discussed in later part of this section.

The non-parametric likelihood function is effectively an estimation of the cumulative probability of the given signal in a set of defined local regions. The expectation of the likelihood can be expressed in the following manner.

$$E[L_{NPLF}(r|H_{\mathcal{M}})] = \int_{S_{\mathcal{M}}} f(x,y)dS \tag{5.32}$$

where $S_{\mathcal{M}}$ is a limit associated with estimated centroids $\hat{\mathcal{A}_{\mathcal{M}}}$ and the test radius $\mathcal{R}_{\mathcal{M}}$, and $f(x,y)$ is the PDF of the testing signal.

$$f(x,y) = \frac{1}{M}\sum_{m=1}^{M} \frac{1}{\sigma\sqrt{2\pi}} e^{-\frac{(x-\Re(\alpha e^{j\theta} s_{\mathcal{M}}^m))^2 + (y-\Im(\alpha e^{j\theta} s_{\mathcal{M}}^m))^2}{2\sigma^2}} \tag{5.33}$$

It is easy to see that, with the given testing radius, the area of $S_{\mathcal{M}} = M \cdot \pi\mathcal{R}_0^2/M = \pi\mathcal{R}_0^2$ is designed to given each hypothesis equal area for the cumulative probability calculation. The decision is based on the assumption that matching model should provide maximum cumulative probability in defined regions of the same total area.

$$\hat{\mathcal{M}} = \underset{\mathcal{M}\in\mathfrak{M}}{argmax} \int_{S_{\mathcal{M}}} f(x,y)dS \tag{5.34}$$

Without examining the centroid estimation for false hypothesis modulations, we evaluate the maximum non-parametric likelihood of different hypothesis in the scenario where each set of estimated centroids have the maximum number of overlaps with the true signal centroids. Such a scenario has been previously examined for the GLRT classifier with unknown channel

gain and carrier phase which results in equal likelihood for nested modulations at high SNR (Panagiotou et al., 2000). Approximating the signal distribution at each transmitted signal symbol to a Rayleigh distribution,

$$f(\mathcal{R}) = \frac{\mathcal{R}}{\sigma^2} e^{-\mathcal{R}^2/2\sigma^2} \tag{5.35}$$

the likelihood function estimation become a function of the testing radius.

$$E[L_{NPLF}(r|H_{\mathcal{M}})] = \mathbb{N}_{\mathcal{M}} \int_0^{\mathcal{R}_{\mathcal{M}}} \frac{x}{\sigma^2} e^{-x^2/2\sigma^2} dx \tag{5.36}$$

where $\mathbb{N}_{\mathcal{M}}$ is the maximum number of matching centroids for the hypothesis $\mathcal{M}$. For example, given a piece of QPSK signal, the value of $\mathbb{N}_{\mathcal{M}}$ for different hypothesises would be: $\mathbb{N}_{BPSK} = 2$, $\mathbb{N}_{QPSK} = 4$ and $\mathbb{N}_{8-PSK} = 4$. To simplify the analysis, we generalize the analysis to three general scenarios: hypothesis of lower order $\mathcal{M}^-$, hypothesis of matching model and order $\mathcal{M}^0$, and hypothesis of higher order $\mathcal{M}^+$. In order to satisfy $E[L_{NPLF}(r|H_{\mathcal{M}^0})] > E[L_{NPLF}(r|H_{\mathcal{M}^-})]$, and $E[L_{NPLF}(r|H_{\mathcal{M}^0})] > E[L_{NPLF}(r|H_{\mathcal{M}^+})]$. The radius factor $\alpha_{\mathcal{R}}$ should satisfy the restriction of

$$\mathcal{R}_0 = \alpha_{\mathcal{R}} \max(\alpha_{\mathcal{M}}), \mathcal{M} \in \mathfrak{M} \tag{5.37}$$

where $\alpha_{\mathcal{R}} > 2.07$ is the radius factor and $\alpha_{\mathcal{M}}$ is the channel gain estimated under hypothesis $\mathcal{M}$. The derivation of the above condition is given in Appendix C. The final value of the radius factor $\alpha_{\mathcal{R}}$ is optimized empirically and the value used in simulation is given in Table 5.1.

5.5 Simulations and numerical results

To validate the proposed method further, experiments are set up in the MATLAB environment to simulate classification problems under various channel conditions. The modulations considered in this research include popular PSK modulations $\mathfrak{M}_{PSK} = \{BPSK, QPSK, 8-PSK\}$ and QAM modulations $\mathfrak{M}_{QAM} = \{4-QAM, 16-QAM, 64-QAM\}$. Under each channel condition, 1,000 signal realizations are generated for each signal modulation. Classification decision is drawn for each signal realization from the modulation candidate pool of

Table 5.1: Experiment settings used to validate MDCE and NPLF classifier.

Parameters	Notation	Values
Modulation Pool	$\mathcal{M} \in \mathfrak{M}$	{BPSK, QPSK, 8-PSK}, {4-QAM, 16-QAM, 64-QAM}
Centroid Number	M	{2, 4, 8}, {4, 16, 64}
Signal length	N	1024 & $50, 100...1000$
SNR	SNR	$0dB, 1dB...20dB$
Phase offset (slow)	θ_o	$0°, 1°...20°$
Phase offset (fast)	σ_θ	$0°, 1°...20°$
Frequency offset (ratio)	f_oT	$1E{-}5, 2E{-}5...2E{-}4$
NPLF radius	$\alpha_{\mathcal{R}}$	2.5
Non-Gaussian noise mixture proportion	ε	0.9
Non-Gaussian noise variance ratio	κ	100

the same type. The resulting classification accuracy is averaged over all 6,000 realizations. Other parameters used in the experiments are given in Talbe 5.1.

The proposed combination of MDCE and NPLF is benchmarked against some of the state-of-the-art non-blind MC classifiers. Without the limitation of blind classification, the Maximum Likelihood classifier is assumed to have perfect knowledge of the channel gain and noise variance (Wei and Mendel, 2000). The cumulant features are combined with K-nearest neighbour classifier which utilizes reference signal samples generated in the same channel condition which known to the classifier (Aslam et al., 2012). A semi-blind alternative of the cumulants based classifier is also used which has noise variance as unknown parameters and the classification is based on theoretical values of the cumulant in noise free channels. Phase offset and frequency offset, however, are not compensated for the aforementioned classifiers. Also utilizing the MDCE, a classifier with the GRLT likelihood function as described in section 5.4 is tested as another blind classifier.

5.5.1 AWGN channel

In channel with additive white Gaussian noise (AWGN) where the noise distribution $\omega(.) \sim \mathcal{N}(0, \sigma_\omega^2)$, two sets of experiments are conducted.

In the first set of experiments, different noise levels are tested to understand how the classifier performs with AWGN noise. Signals are tested at SNR level between 0 dB and 20 dB. For each modulation and each noise level, 1,000 signal realizations are generated each consists of $N = 1,024$ samples. As demonstrated in Figure 5.8, classifiers with perfect channel knowledge outperform semi-blind and blind classifiers with the ML classifier achieving the highest accuracy at all SNR levels. Despite the lack of knowledge of channel gain and carrier phase, both MDCE assisted blind classifiers have good classification accuracy especially at SNR $>$ 12 dB. The semi-blind cumulant based classifier has the worst performance among all the classifiers.

It is worth noting that the GLRT classifier has a much lower accuracy than an ideal ML classifier at SNR below 10 dB. The GLRT classifier is considered as a ML classifier with only the noise variance being an unknown parameter. The likelihood function in GLRT

provides a rough estimation of noise variance by maximizing the resulting likelihood. In a way, the GLRT approach can be seen as a combination of a ML noise variance estimator and a ML classifier. One may question the significant performance difference between the GLRT classifier and the ML classifier. Part of the difference is caused by the inaccurate estimation of signal centroid as suggested in Figure 5.6 and 5.7. The other part of the difference is caused by the noise variance used in GLRT likelihood function being different for different hypothesis models. The maximization of the likelihood reduces the mismatch between the testing signal and a false hypothesis model. Meanwhile, due to the identical variance used in a ML classifier, the mismatch is exaggerated. Therefore, it appears that the results achieved by the GLRT method is a more realistic reflection of the performance of a likelihood based method in a blind classification scenario.

At the same time, the proposed NPLF classifier actually has very similar accuracy compared with the GLRT classifier, despite having much lower complexity. A confusion matrix of the classification results from a NPLF classifier is given in Table 5.2. It is clear that the modulation of higher order is more difficult to be classified. The false classification often comes from the modulation of same type and of similar constellation shape.

Table 5.2: Classification confusion matrix using the NPLF classifier in AWGN channel with SNR=10 dB.

	BPSK	QPSK/4-QAM	8-PSK	16-QAM	64-QAM
BPSK	1000	0	0	0	0
QPSK/4-QAM	0	1000/1000	0	0	0
8-PSK	0	0	1000	0	0
16-QAM	0	0	0	991	9
64-QAM	0	7	0	277	716

In the second set of experiments, the classification accuracy against limited number of observation samples is tested. Keeping majority of the settings in the previous experiment and fixing the SNR at 10 dB, different signal lengths N between 50 and 1000 are used. According to the results shown in Figure 5.9, the proposed method is much limited when the number of samples available for analysis is below 200. However, it is able to achieve a

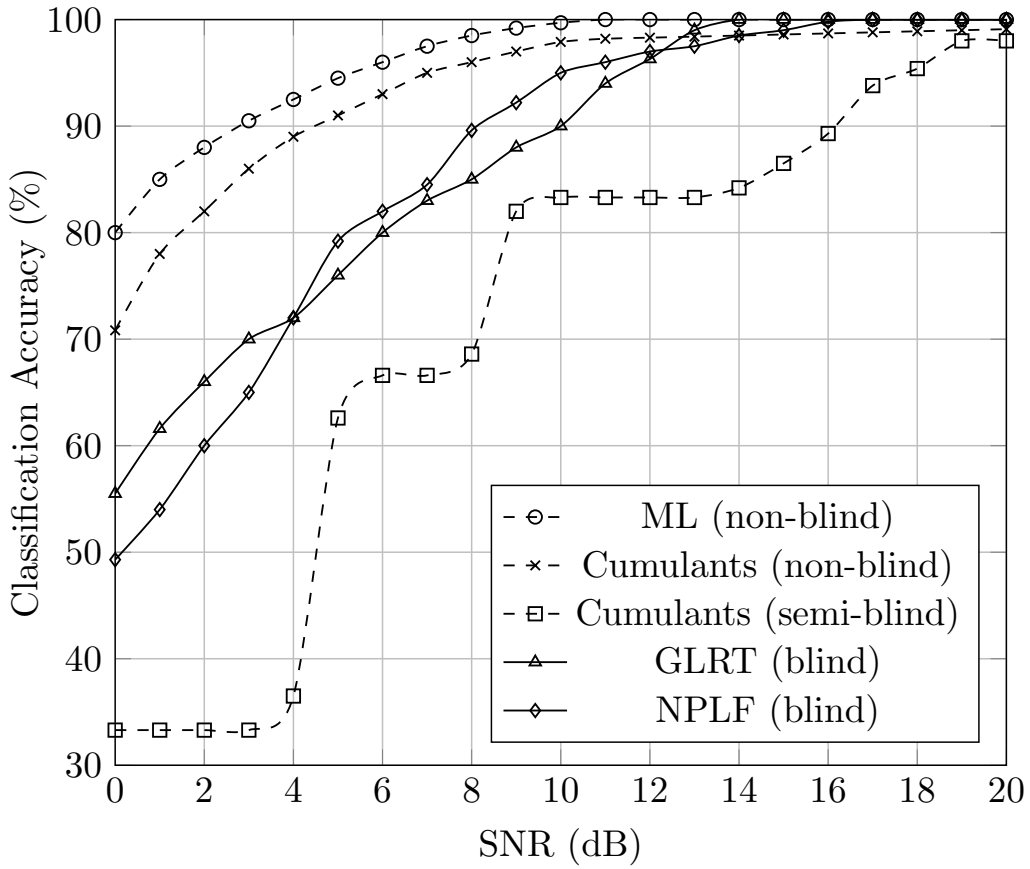

Figure 5.8: Classification accuracy using differen classifiers in AWGN channel.

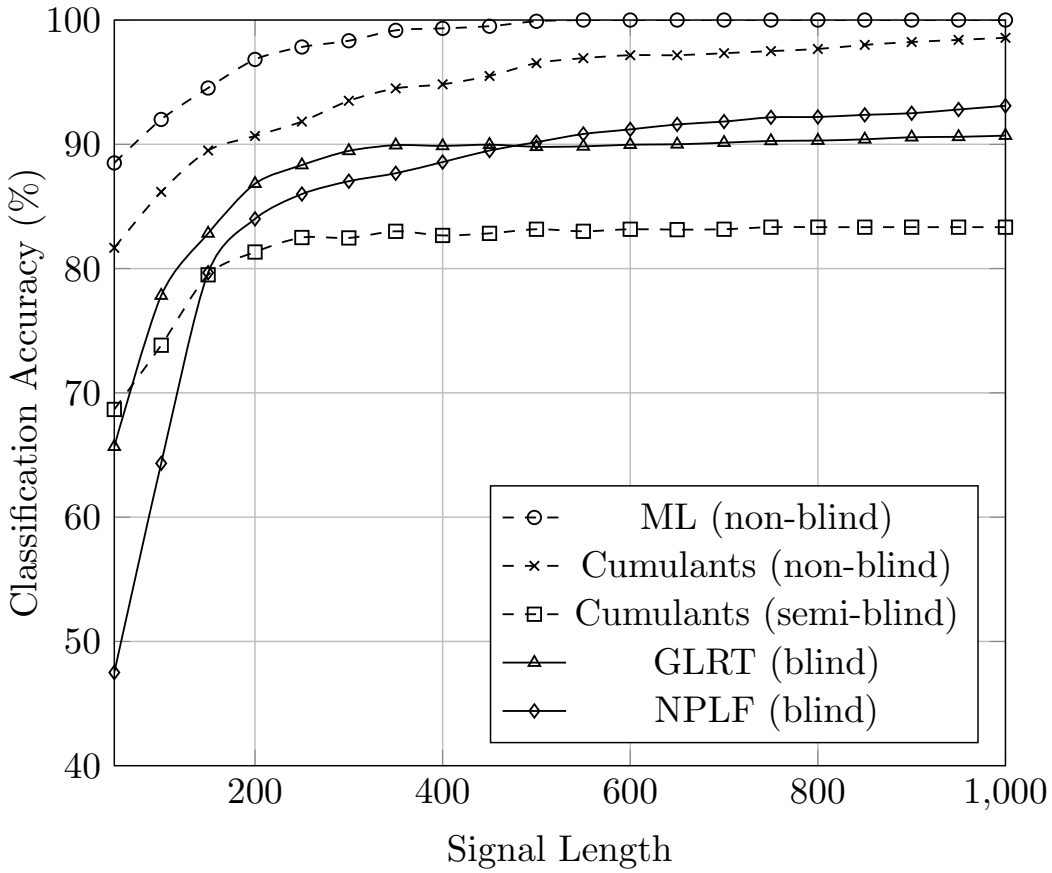

Figure 5.9: Classification accuracy using different classifiers in AWGN channel with different signal length.

Table 5.3: Classification accuracy over 100 runs at every combination of SNR and Signal Length using the NPLF classifiers.

	SNR			
Signal Length	5 dB	10 dB	15 dB	20 dB
N=100	52.2±1.8	66.3±1.6	67.5±1.4	68.9±1.2
N=200	75.9±1.5	90.6±0.9	96.9±0.5	98.8±0.4
N=500	80.2±1.0	92.9±0.7	99.7±0.2	99.9±0.1
N=1000	82.5±0.4	93.7±0.2	100.0±0.0	100.0±0.0

consistent level of accuracy when there is more than 400 samples available for analysis.

Combining the two experiments, the classification task for the proposed MDCE-NPLF classifier is repeated 100 times for the settings of SNR=[5 dB, 10 dB, 15 dB, 20 dB] and sample length N=[100, 200, 500, 1000]. The averaged classification accuracy as well as the standard deviation over the 100 runs are listed in Table 5.3.

5.5.2 Fading channel

In order to understand the effect of different channel conditions, we test phase offset and frequency offset separately but both with certain level of AWGN noise. Phase offset is simulated in two different fading scenarios: slow fading and fast fading. In slow fading, the phase offset θ_0 is assumed to be consistent throughout the signal realization. While in fast fading, we assume the phase offset to have a normal distribution with variance of σ_θ. Using the same set up as in AWGN channel, the SNR is fixed at 10 dB with the signal length N set to 1,024.

In channel with slow phase offset, it is obvious from Figure 5.10 that the proposed method is able to mitigate its effect and provide a consistent classification accuracy of 92% to 94%. It is mostly due to the capability of the proposed MDCE to compensate the slow fading as demonstrated in the analysis given in Appendix A. On the contrary, the ML classifier and cumulant based classifier are rather sensitive to the slow phase offset. From Figure 5.10, it can been seen that, despite being more accurate without phase offset, the ML classifier and

cumulant classifier become less accurate when more than 5° of phase offset is introduced. When there is more than 7° of phase offset, the proposed MDCE-NPLF become the best option among the benchmarked methods.

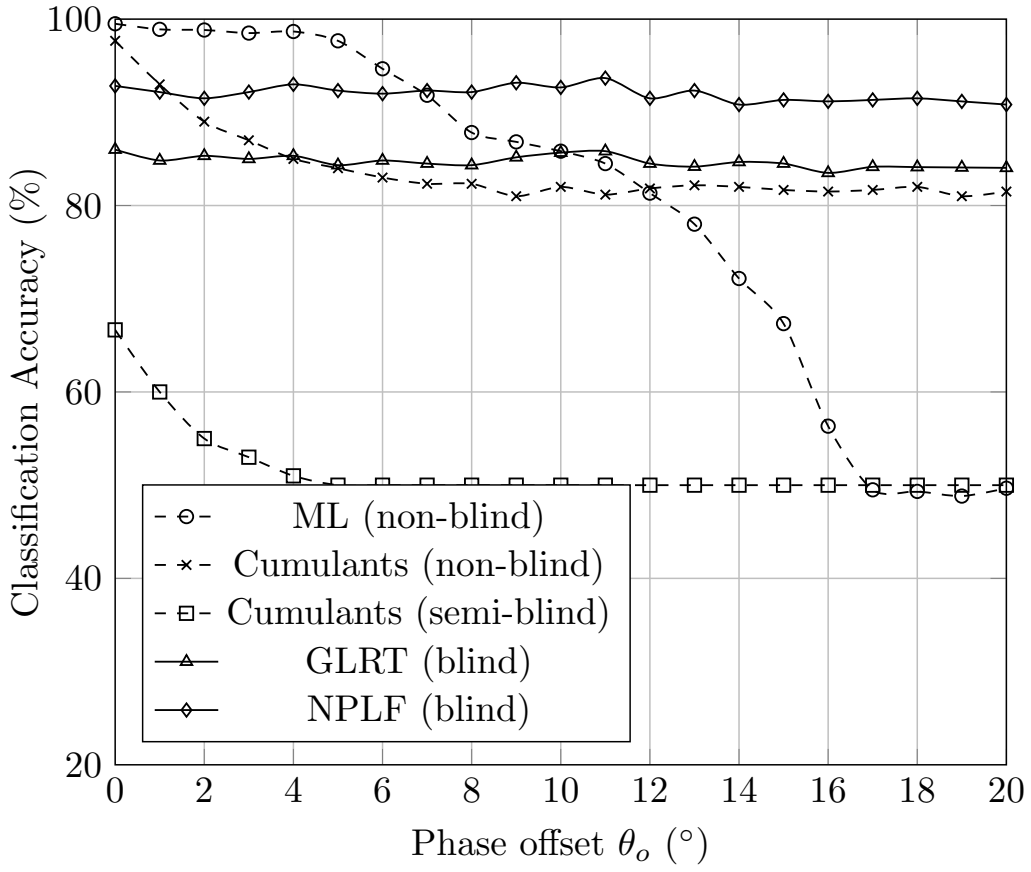

Figure 5.10: Classification accuracy of using different classifiers in fading channel with slow phase offset.

In the fast fading channel with phase offset $\theta_o \sim \mathcal{N}(0, \sigma_\theta^2)$, Figure 5.11 demonstrates that all likelihood based methods show more robust performance as compared to cumulant based methods. While ML classifier outperforms both likelihood based blind classifiers, the difference between ML and NPLF classifier remains marginal for $\sigma_\theta < 14°$. With an increased amount of phase offset, the NPLF classifier is able to achieve superior accuracy at $\sigma_\theta > 14°$. Meanwhile, the cumulant based classifier suffers with the increased amount of fast phase offset. Thus, the proposed classifier is able to surpass the performance of cumulants based

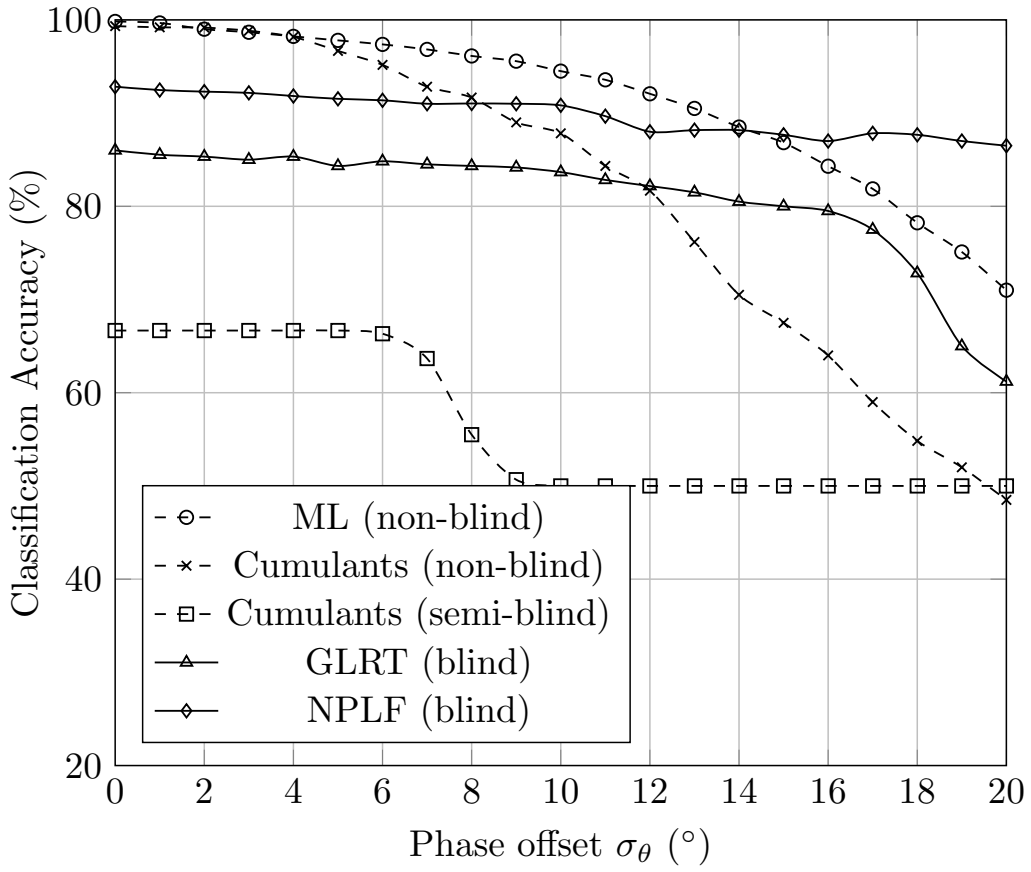

Figure 5.11: Classification accuracy using different classifiers fading channel with fast phase offset.

classifier at $\sigma_\theta > 8°$.

When frequency offset is considered, it can be observed from Figure 5.12 the proposed NPLF classifier excels all other classifiers benchmarked in the tests. The performances of ML and cumulant classifier are significantly affected by the frequency offset due to the sever mismatching between received signals and ideal models. The only classifier, which is able to sustain a consistent level of performance is the proposed NPLF classifier, which sees very little degradation in the given frequency offset range and achieves a classification accuracy of 90% to 94%.

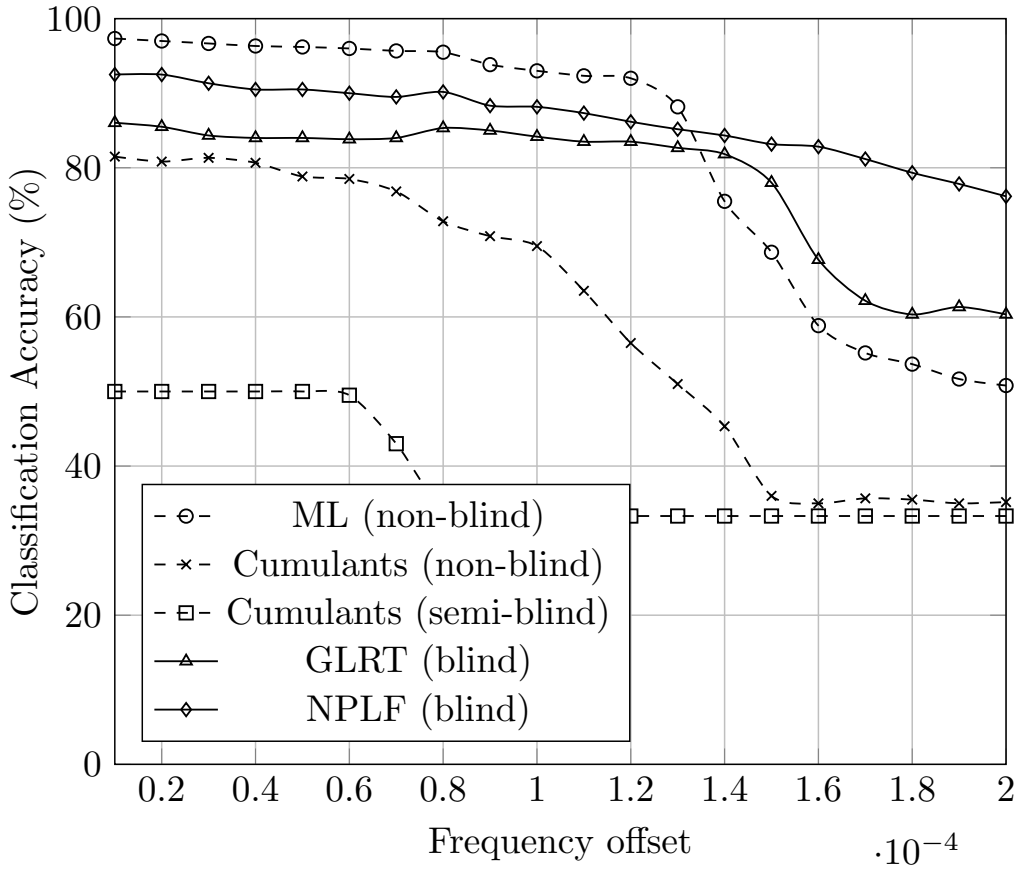

Figure 5.12: Classification accuracy using different classifiers in fading channel with frequency offset.

5.5.3 Non-Gaussian channel

Recent developments in MC pay attention to the understanding of MC with impulsive noise(Chavali and da Silva, 2011, 2013). Here we consider the impulsive noise in the form of a two-term Gaussian mixture. The formation of the non-Gaussian noise is given in section 2.4 with mixture parameters in Table 5.1.

The results shown in Figure 5.13 indicate obvious performance degradation of most methods in their classification accuracies in the AWGN channel with same noise level. It is not difficult to understand the cause of the performance degradation that comes from the mismatching noise model. The only exception in the group is the proposed NPLF which maintains the same level of classification accuracy despite the different noise model used.

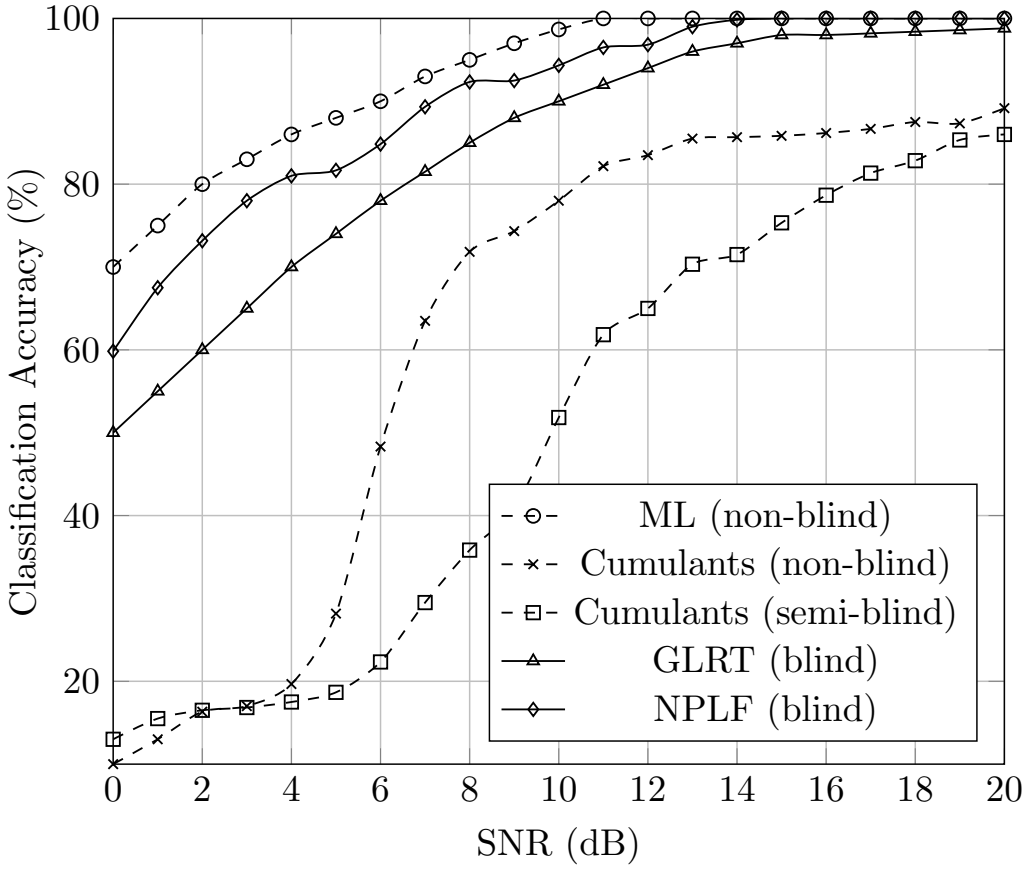

Figure 5.13: Classification accuracy using different classifiers in non-Gaussian channels.

Table 5.4: Number of operators needed for different classifiers.

Classifier	Exponential	Logarithm	Multiplication	Addition	Memory
ML	$NI\sum_{i=1}^{I} M_i$	NI	$5NI\sum_{i=1}^{I} M_i$	$6NI\sum_{i=1}^{I} M_i$	I
Cumulant	0	0	$6KN$	$6KN$	KI
GLRT	$VNI\sum_{i=1}^{I} M_i$	VNI	$5VNI\sum_{i=1}^{I} M_i$	$6VNI\sum_{i=1}^{I} M_i$	$2I$
NPLF (This research)	0	0	0	$4NI\sum_{i=1}^{I} M_i$	I

5.5.4 Complexity

To evaluate the complexity of different classifiers, numbers of operations needed are calculated for each classifier and listed in Table 5.4. The calculation is based on a signal with N number of samples being classified among I potential modulations. M_i denotes the alphabet size of the ith modulation candidate. The number of testing point for noise variance used in GLRT is defined by V. And number of training sample in the cumulant based method is defined by K.

Among all the tested methods, the ML classifier is known to have a very high computational complexity due to the large number of exponential and logarithmic operations needed. For a GLRT classifier, the complexity is dramatically increased because the log-likelihood evaluation is effectively repeated V times. Cumulants based classifiers have lower complexity compared ML and GLRT classifier. However, the reference values needed for KNN classifier impose a high demand for memory. The classifier with lowest complexity is the proposed NPLF classifier which uses only additions and does not require extra memory allocation for reference values.

5.6 Summary

In this chapter, the combination of centroid estimation and non-parametric likelihood function for modulation classification is studied. Two different approach to the centroid estima-

tion are discussed. The constellation segmentation estimator is developed for fast centroid estimation for square M-QAM modulations with the assumption of symbol assignment at the transmitter end being equal probable. The minimum distance centroid estimator, on the other hand, is much more versatile, which is able to both M-PSK and M-QAM modulations. The non-parametric likelihood function is proposed to realize likelihood function without knowing either the noise model or the noise power. The numerical results show that the combination of MDCE and NPLF is able to achieve good classification accuracy in the AWGN channel. Moreover, the classifier shows stronger robustness in fading channel and non-Gaussian channels. Last but not least, the computational complexity of the NPLF is much lower compared with some of the existing methods.

Chapter 6

Blind Modulation Classification for MIMO systems

6.1 Introduction

While majority of modulation classification algorithms have been dedicated to Single-input Single-output (SISO) systems (Azzouz and Nandi, 1996b; Nandi and Azzouz, 1998; Azzouz and Nandi, 1996a; Swami and Sadler, 2000; Dobre et al., 2007; Punchihewa et al., 2010; Amuru and da Silva, 2012; Zhu et al., 2013b), blind modulation classification for multiple-input multiple-output systems has become an attractive novelty. MIMO systems with associated techniques such as Spatial Multiplexing (SM) and Space-time Coding (STC) provides benefits including array gain and spatial gain for improved spectrum efficiency and link reliability. Some recent publications address the issue of BMC for MIMO systems. Choqueuse et al. developed the average likelihood ratio test classifier for MC with perfect channel knowledge (Choqueuse et al., 2009). In the same paper, they proposed to use ICA with phase correction for channel matrix estimation in order to achieve BMC. The ICA estimator is endorsed by the following publications but accompanied with different classifiers (Mühlhaus et al., 2013; Kanterakis and Su, 2013). Mhlhaus et al. proposed high order cumulants based likelihood ratio test classifier for low complexity BMC (Mühlhaus et al., 2013). Kanterakis

and Su suggest complexity reduction to the ALRT classifier by treating ICA recovered signal components at different transmitting antennas as individual processes (Kanterakis and Su, 2013). Most ICA estimation aided classifier achieves very high classification accuracy. However, the aforementioned methods require the perfect knowledge of noise variance. In addition, the ICA estimation imposes the requirement that the number of receiving antennas must exceed the number of transmitting antennas. Hassan et al. proposed a combination of high order statistic and Artificial Neural Network (ANN) for MC. The method is successful in addressing the issue of spatial correlation in MIMO systems (Hassan et al., 2012). However, supervised training required by ANN makes it rather demanding as a blind classifier.

In this research, we propose a more practical BMC solution with both unknown channel matrix and unknown noise variance. There is no existing BMC algorithms for such scenario to our knowledge. Most state-of-the art channel estimation for MIMO systems depend on pilot symbols for data aided estimation which is not suitable for BMC. Therefore, expectation maximization is adopted for non-data aided blind channel estimation. The EM algorithm approaches the channel estimate through an iterative process of maximizing the expected likelihood. Compared to the ICA estimator, the EM estimator provides the additional estimation of noise variance while not needing the phase correction for the channel matrix. The resulting estimate is used for the maximum likelihood classifier for decision making.

6.2 Signal model in MIMO systems

Have defined signal models in different channels, we extend the definition to MIMO systems where multiple transmitters and receivers are considered to formulate multiple propagation paths. The MIMO system is composed of N_t transmitting antennas and N_r receiving antennas. A Rayleigh fading channel with time invariant path gains is considered. The resulting channel matrix H is given by a $N_r \times N_t$ complex matrix with the element $h_{j,i}$ representing the path gain between ith transmitting antenna and jth receiving antenna. Assuming perfect synchronization, the nth received MIMO-SM signal sample vector

$\boldsymbol{r}_n = [r_n(1), r_n(2), ..., r_n(N_r)]^T$ in a total observation of N samples is expressed as

$$\boldsymbol{r}_n = H\boldsymbol{s}_n + \omega_n \tag{6.1}$$

where $\boldsymbol{s}_n = [s_n(1), s_n(2), ..., s_n(N_t)]^T$ is the nth transmitted signal symbol vector and $\omega_n = [\omega_n(1), \omega_n(2), ..., \omega_n(N_r)]^T$ is the additive noise observed at the nth signal sample. The transmitted symbol vector is assumed to be independent and identically distributed with each symbol assigned from the modulation alphabet with equal probability. The additive noise is assumed to be white Gaussian with zero mean and variance σ^2 which gives $\omega_n \in \mathcal{N}(0, \sigma^2 I_{N_r})$, where I_{N_r} is the identity matrix of size $N_r \times N_r$.

6.3 EM channel estimation

To evaluate likelihood for the ML classifier, the complex channel matrix H and noise variance σ^2 must be estimated beforehand. Since the modulation is unknown to the receiver, many data-aided approaches using pilot symbols are not suitable. Expectation maximization has been employed for joint channel estimation through an iterative implementation of maximum likelihood estimation(Wautelet et al., 2007; Das and Rao, 2012). In MIMO systems, we consider the received signal $R = [\boldsymbol{r}_1, \boldsymbol{r}_2 ... \boldsymbol{r}_N]$ as the observed data. Meanwhile, the membership Z of the observed samples is considered as the latent variables. Z is a $M \times N$ matrix with the (m, n)th element being the membership of the nth signal sample $\mathbf{r}_n$, given the transmitted symbol vector S_m. The possible transmitted symbol set $\mathbf{S} = [S_1, S_2 ... S_M]$ gathers all the combinations of transmitted symbols from N_t number of antennas. Given a modulation with L number of states, there exist $M = L^{N_t}$ number of transmitted symbol vectors and a transmitted symbol set of size $N_t \times L^{N_t}$. With $\Theta = \{H, \sigma^2\}$ representing the channel parameters, the complete likelihood is given by

$$q(R, S|\Theta) = \int_S p(S|R, \Theta) \log(p(R|S, \Theta)p(S|\Theta))dS \tag{6.2}$$

where $p(R|S, \Theta)$ is the probability of the received signal been observed given transmitted symbols vector S and channel parameter Θ. Since the additive noise is assume to have a

complex Gaussian distribution. $p(R|S,\Theta)$ can be calculated as

$$p(R|S,\Theta) = \prod_{n=1}^{N} \frac{1}{(\pi\sigma^2)^{N_r}} \exp(-\frac{\|r_n - Hs_n\|_F^2}{2\sigma^2}). \tag{6.3}$$

Meanwhile, $p(S|R,\Theta)$ represents the probability of S being transmitted given the observed signal R and the channel parameter Θ, also know as the posteriori probability of S. In (Wautelet et al., 2007), this probability is acquired by a posteriori probability calculator which is not presented. In this research, we replace the a posteriori probability with a soft membership z_{nm} representing the likelihood of nth transmitted symbol vector being S_m with $\sum_{m=1}^{M} z_{mn} = 1$. Since the assignment of transmitted symbol is independent of the channel parameter, $p(S|\Theta)$ is a constant $1/M$ when equal probability is assumed. The estimation of Θ is achieved by iterative steps of expectation evaluation and maximization.

6.3.1 Evaluation step

The evaluation step (E-step) provides the expected log-likelihood under the current estimate of Θ_t at tth iteration. The expectation is then subsequently maximized for the updated estimation of Θ. From Equation (6.2) the expected value of the complete log-likelihood is derived as

$$\begin{aligned} \mathcal{Q}(R,S|\Theta_t) &= \log \prod_{n=1}^{N} \prod_{m=1}^{M} p(r_n, S_m|H_t, \sigma_t^2)^{z_{mn}} \\ &= -\sum_{n=1}^{N} \sum_{m=1}^{M} z_{mn} \left[N_r \log(\pi\sigma_t^2) + \frac{\|r_n - H_t S_m\|_F^2}{\sigma^2} \right] \end{aligned} \tag{6.4}$$

where $p(r_n, S_m|H^t, \sigma^t)$ is the probability of the nth received signal vector being observed given the current estimation of channel matrix H_t and noise variance σ_t^2. $\|\cdot\|_F^2$ is the Frobenius norm. The soft membership z_{mn} is evaluated using the following equation

$$z_{mn} = \frac{p(r_n|S_m,\Theta^t)}{\sum_{m=1}^{M} p(r_n|S_m,\Theta^t)} = \frac{\exp(-\frac{\|r_n - HS_m\|_F^2}{\sigma^2})}{\sum_{m=1}^{M} \exp(-\frac{\|r_n - HS_m\|_F^2}{\sigma^2})}. \tag{6.5}$$

6.3.2 Maximization step

The update of the parameter estimation is achieved through the maximization of the current expected log-likelihood (M-step). To derive the close form update function for the channel matrix and noise variance, we first find the derivatives of $\mathcal{Q}(R, S|\Theta^t)$ with respect to H and σ^2 separately. Given that

$$\|r_n - HS_m\|_F^2 = \sum_{j=1}^{N_r} \left| r_n(j) - \sum_{i=1}^{N_t} h_{j,i} S_m(i) \right|^2 \tag{6.6}$$

the derivative of $\mathcal{Q}(R, S|\Theta^t)$ with respect to the individual element $h_(j, i)$ of the channel matrix is given by

$$\begin{aligned} &\frac{\partial \mathcal{Q}(R, S|\Theta^t)}{\partial h_{j,i}} \\ &= -\sum_{n=1}^{N} \sum_{m=1}^{M} z_{mn} \frac{\sum_{i=1}^{N_t} h_{j,i}{}^* |S_m(i)|^2 - r_n(j)^* S_m(i)}{\sigma^2} \end{aligned} \tag{6.7}$$

In the same way, the derivative of $\mathcal{Q}(R, S|\Theta^t)$ with respect to the noise variance σ^2 is found as

$$\frac{\partial \mathcal{Q}(R, S|\Theta^t)}{\partial \sigma^2} = -\sum_{n=1}^{N} \sum_{m=1}^{M} z_{mn} \left(-\frac{N_r}{\sigma^2} + \frac{\|r_n - HS_m\|_F^2}{\sigma^4} \right) \tag{6.8}$$

When the derivatives are set to zero, the update functions of $h_{j,i}$ and σ^2 can be derived from Equation (6.7) and (6.8). However, it is obvious that different channel parameters are coupled. To simplify the maximization process, the coupled channel parameters are estimated in turns. The path gain $h_{j,i}$ is estimated with the rest of the channel matrix known and represented with the lasted estimate for each path gain. The path gains are updated in ascending order with respect to j and i. The resulting update function for $h_{j,i}$ is given by

$$\begin{aligned} &h_{j,i}^{t+1} \\ &= \frac{\sum_{n=1}^{N} \sum_{m=1}^{M} z_{mn} \left[r_n(j) S_m(i)^* - S_m(i)^* \sum_{k=1, k\neq i}^{N_t} h'_{k,i} S_m(k) \right]}{\sum_{n=1}^{N} \sum_{m=1}^{M} z_{mn} |S_m(i)|^2} \end{aligned} \tag{6.9}$$

where $h'_{k,i}$ is the lasted estimate of path gain $h_{k,i}$. At tth iteration, $h'_{k,i} = h^t_{k,i}$ if it has not been updated or $h'_{k,i} = h^{t+1}_{k,i}$ if it has been updated. After the channel matrix is completely updated, H_{t+1} is used to acquire the noise variance estimation.

$$\sigma^2_{t+1} = \frac{\sum_{n=1}^{N}\sum_{m=1}^{M} z_{mn} \sum_{j=1}^{N_r} \left| r_n(j) - \sum_{i=1}^{N_t} h^{t+1}_{j,i} S_m(i) \right|^2}{N_r \sum_{n=1}^{N}\sum_{m=1}^{M} z_{mn}} \tag{6.10}$$

The EM algorithm with such maximization process is known as expectation conditional maximization. ECM shares the convergence property of EM (Meng and Rubin, 1993) and can be constructed to converge at similar rate as the EM algorithm (Sexton, 2000). The ECM joint estimation of channel parameters has previously been successfully applied in BMC for SISO systems (Chavali and da Silva, 2011; Soltanmohammadi and Naraghi-Pour, 2013; Chavali and da Silva, 2013).

6.3.3 Termination

The final estimation of channel matrix H and noise variance σ^2 is achieve when the iterative process is terminated by one of two conditions. The first condition terminates the process when the estimation reaches convergence. The condition is represented numerically with the different between the expected likelihoods of the current iteration and the previous iteration along with a predefined threshold. In the second condition, termination is triggered when the predefined number of iterations has been reached.

6.4 Maximum likelihood classifier

For classification likelihood evaluation, the average likelihood ratio test approach is adopted (Choqueuse et al., 2009). The average likelihood function is given by

$$\mathcal{L}(R|\Theta) = \prod_{n=1}^{N} \frac{1}{M} \sum_{m=1}^{M} \frac{1}{(\pi\sigma^2)^{N_r}} \exp\left(-\frac{\|r_n - HS_m\|_F^2}{2\sigma^2}\right) \tag{6.11}$$

with the corresponding log-likelihood function derived as

$$\log \mathcal{L}(R|\Theta) = -NN_t \log(M) - NN_r log(\pi\sigma^2) + \sum_{n=1}^{N} \log \left(\sum_{m=1}^{M} \frac{1}{(\pi\sigma^2)^{N_r}} \exp(-\frac{\|r_n - HS_m\|_F^2}{2\sigma^2}) \right) \tag{6.12}$$

In the case of BMC, the channel matrix and noise variance estimated by EM is used to substitute the known values in the ALRT likelihood evaluation for each modulation hypothesis. The likelihood evaluation of modulation candidate $\mathcal{M}$ is given by

$$\log \mathcal{L}(R|S_{\mathcal{M}}\Theta_{\mathcal{M}}) = -NN_t \log(M) - NN_r log(\pi\sigma_{\mathcal{M}}^2) + \sum_{n=1}^{N} \log \left(\sum_{m=1}^{M} \frac{1}{\left(\pi\sigma_{\mathcal{M}}^2\right)^{N_r}} \exp(-\frac{\left\|r_n - \hat{H}_{\mathcal{M}} S_m^{\mathcal{M}}\right\|_F^2}{2\sigma_{\mathcal{M}}^2}) \right) \tag{6.13}$$

where $S_{\mathcal{M}}$ is the transmitted symbol set defined by modulation $\mathcal{M}$ and $\Theta_{\mathcal{M}}$ is the channel estimation for the same modulation candidate.

The resulting classification decision $\hat{\mathcal{M}}$ is found by comparing the likelihood evaluated from different modulation candidates. The modulation candidate $\mathcal{M}$ in the candidate pool $\mathfrak{M}$ which provides the highest likelihood with the observed data is assigned as the classification decision.

$$\hat{\mathcal{M}} = \underset{\mathcal{M}\in\mathfrak{M}}{\operatorname{argmax}}(\log \mathcal{L}(R|S_{\mathcal{M}}, \Theta_{\mathcal{M}})) \tag{6.14}$$

6.5 Simulation and numerical results

To validate the proposed BMC algorithm, MIMO systems in Rayleigh fading channel with AWGN noise is simulated for BMC. Three popular digital modulations are included in the modulation candidate pool $\mathfrak{M}$={BPSK,QPSK,16-QAM}. Other digital modulations can be classified in the same procedure with very little modification. In the simulation, two sets of experiments are set up to investigate the classifier performance under different noise levels and with different observation length. The specifications of the simulations are summarized in Table 6.1.

Table 6.1: Experiment settings for validating the blind MIMO classifier.

Parameter	Notation	Value
Candidate Modulations	$\mathcal{M} \in \mathfrak{M}$	{BPSK, QPSK, 16-QAM}
Number of Transmitting Antennas	N_t	2
Number of Receiving Antennas	N_r	4
AWGN Noise Level	SNR	-10 dB, -9 dB,..., 10 dB
Observed Signal Length	N	1024; 50, 100,..., 1000
EM Estimation Iterations	T	20

In the first set of experiments, 1,000 testing realizations of modulation signals are generated for each modulation candidate and each SNR varying from -10 dB to 10 dB. Each signal realization consists of 512 observed signal samples at each receiving antenna. In the following figures, classification results averages over 1,000 realizations are listed for each testing modulation at each noise level. The classification accuracy for BPSK signals are rather robust until SNR drops below -5 dB, as shown in Figure 6.1. With high noise level, the classification of BPSK signals has a tendency to be biased towards 16-QAM. The same phenomenon can be observed from classification results of QPSK signals in Figure 6.2. The classification accuracy of QPSK signals are almost perfect with SNR above 0 dB. However, the performance degrades rapidly with increased noise level until majority of the signals being wrongly classified as 16-QAM at SNR between -10 dB and -6 dB. The classification result of 16-QAM in Figure 6.3 concurs the biased behaviour of the classifier. The classification accuracy sees little degradation between -3 dB and 1 dB but returns to 100% accuracy below -3 dB. Compared to ALRT classifier with known channel parameters, the classifier performance of the prosed EM-ML classifier share very similar high classification accuracy at SNR above 0 dB. However, the performance degradation is much steeper with increased noised level. There are two possible explanation to the steeper degradation of EM-ML. First, the mis-

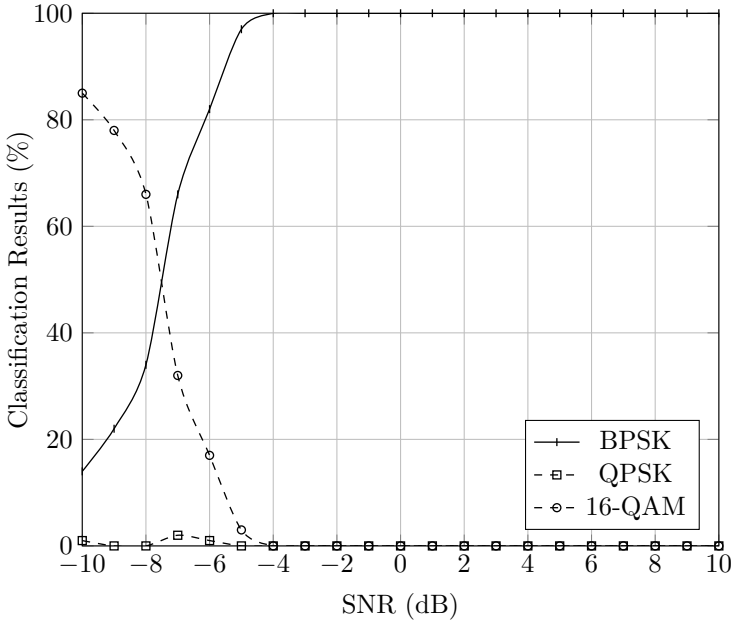

Figure 6.1: Classification accuracy of BPSK signals using the proposed blind MIMO classifier in Rayleigh fading channels.

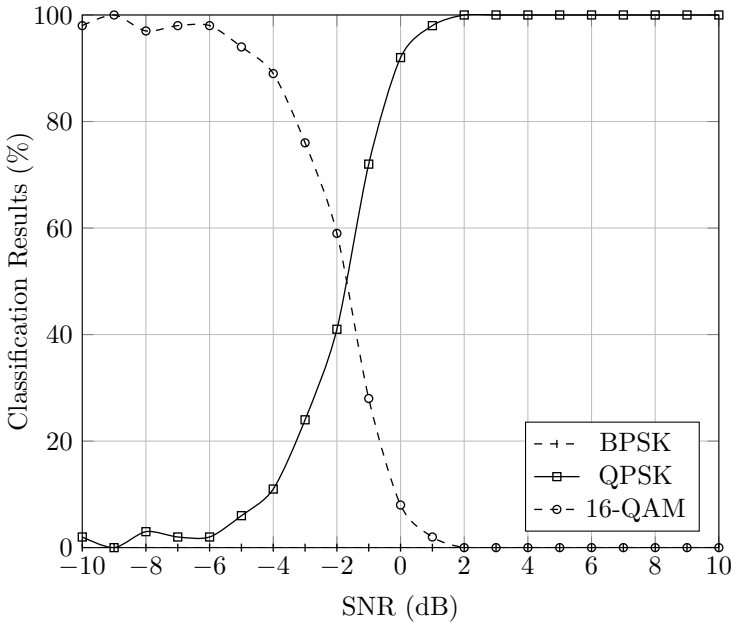

Figure 6.2: Classification accuracy of QPSK signals using the proposed blind MIMO classifier in Rayleigh fading channels.

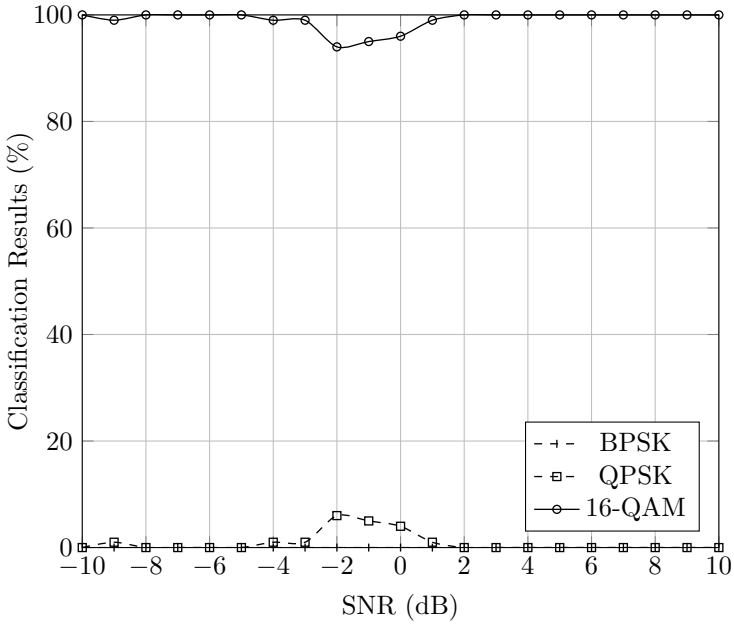

Figure 6.3: Classification accuracy of 16QAM signals using the proposed blind MIMO classifier in Rayleigh fading channels.

match between the estimated channel status and the actual channel status introduced by EM channel estimation may degrade the performance. Second, EM, being a ML estimator, not only provides channel estimate for matching modulation candidate but also maximizes the evaluated likelihood of those mismatched modulation candidates. Compared to the ALRT classifier with known and uniform channel status for all modulation candidates, the EM-ML approach marginalizes the difference between the likelihood evaluation of a matching hypothesis and a mismatching hypothesis. This phenomenon is reported in (Soltanmohammadi and Naraghi-Pour, 2013) where likelihood evaluation with EM estimation some time provides higher likelihood for the mismatched modulation candidate.

In the second set of experiments, the robustness of the proposed classifier against limited number of observed signal samples is investigated. Now, 1,000 testing realizations of modulation signals are generated for each modulation candidate, each signal length varying from 25 to 500. The SNR level is fixed at 0 dB in all experiments. The classification of BPSK is almost independent of the signal length. With only 25 samples from each receiving antenna,

the classification of BPSK signals is able to achieve a 99% accuracy as shown in Figure 6.4. The robust performance for BPSK signal is mostly due to its lower modulation order as well as unique constellation shape compare to QPSK and 16-QAM's similar square constellation shapes. For QPSK, a linear degradation can be observed with reduced signal length in Figure 6.5. Meanwhile, the degradation is rather moderate giving 77% classification accuracy with 25 sample at each receiving antenna compare to 94% accuracy with 500 samples. Due to the similarity between QPSK and 16-QAM signals, up to 20% of QPSK signals are classified as 16-QAM signals. The same behaviour is also observed for the 16-QAM where majority of the false classification goes to QPSK. However, it is obvious that the limited number of observed samples has a more significant impact on the classification performance of 16-QAM signal. Figure 6.6 shows that rate of performance degradation accelerates with reduced signal length. Especially when $N < 100$, the classification accuracy sees a sharp drop where more signals are classified as QPSK with 50 samples and the accuracy reduced to 20% when only 25 samples are available for analysis. However, the performance with more than 200 observed samples is well over 80%.

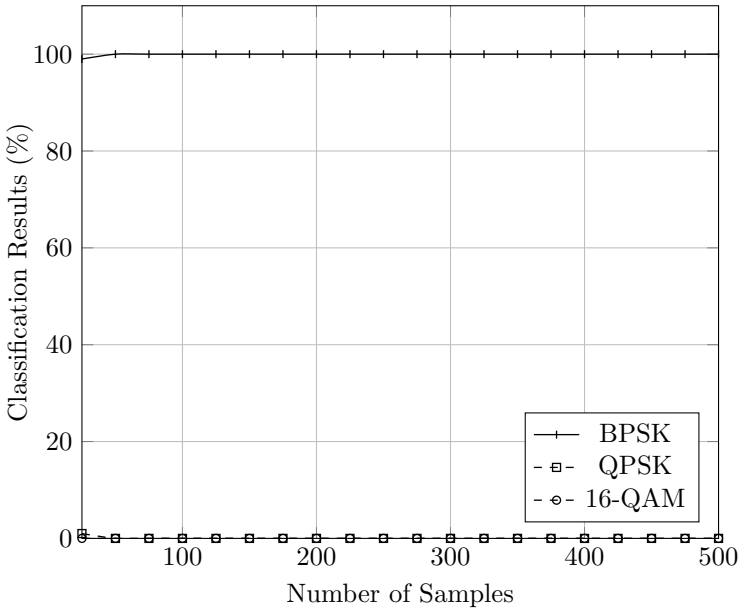

Figure 6.4: Classification accuracy of BPSK signals using the proposed blind MIMO classifier in Rayleigh fading channels with varying signal length.

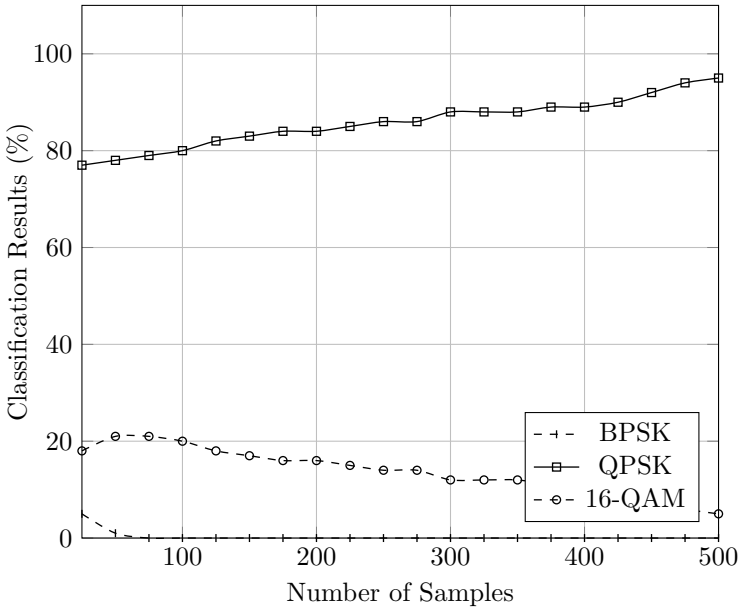

Figure 6.5: Classification accuracy of QPSK signals using the proposed blind MIMO classifier in Rayleigh fading channels with varying signal length.

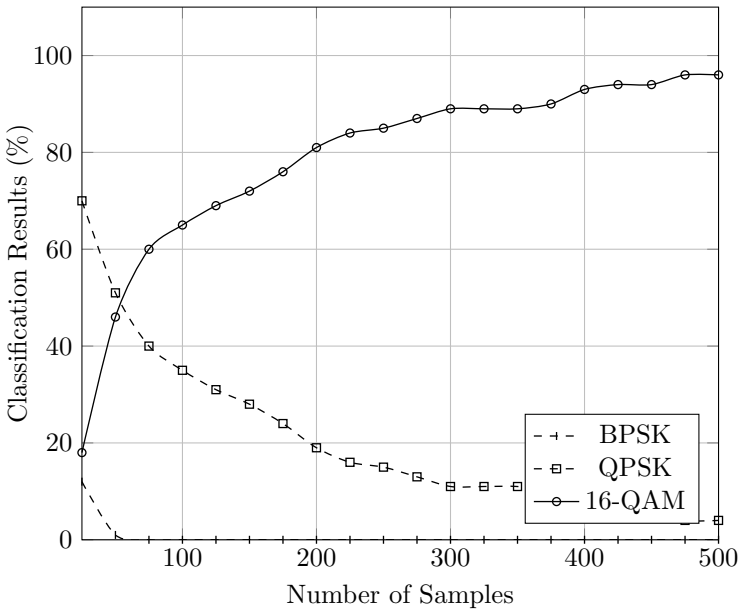

Figure 6.6: Classification accuracy of 16QAM signals using the proposed blind MIMO classifier in Rayleigh fading channels with varying signal length.

6.6 Summary

A blind modulation classifier is proposed for MIMO system with unknown channel state. The assumption of both unknown channel matrix and unknown noise variance has not been previous considered in other BMC classifiers for MIMO systems. The employment of expectation maximization provides estimation of noise variance which is not enjoyed by the popular ICA estimator. The expectation conditional maximization strategy is adopted to deal with coupling of the parameters in the maximization step. With the estimated channel parameters, the maximum likelihood classifier is used for classification decision making. The likelihood of each modulation candidate is evaluated with channel parameters estimated for the specific candidate. The simulation results show robust performance with SNR above 0 dB for BPSK, QPSK, and 16-QAM modulations. Meanwhile, requirement of signal length is rather modest with 200 observed samples being able to provide a reasonable classification accuracy for all modulations.

Chapter 7

Conclusions

In this chapter, we restate the purpose of the research and conclude what has been achieved to further the field. In Chapter 1, it has been demonstrated that automatic modulation classification has an important role to play in both military and civilian applications. Although a good modulation classification is expected to have high accuracy and robustness with low computational complexity, the understanding we have developed through this research is that there is no classifier that excels on all fronts. For example, maximum likelihood classification provide optimal classification accuracy with the limitation of very high computational complexity and high demand for channel knowledge. Moment and cumulant based classifiers provide sub-optimal classification performance with lower complexity but suffers with signals described by fewer samples. Distribution test based classifiers have improved robustness with shorter signal but are more vulnerable against complex channels. With such an understanding we set out to develop AMC algorithms that provide unique performance metrics that excels in certain aspects or replaces certain existing methods with overall improvement.

The introduction of machine learning techniques in feature based AMC methods brings four major benefits. First, the hierarchical decision making process is simplified with a single step approach. Yet multi-stage classification strategy could still be accommodated for performance optimization. Secondly, the determination of decision thresholds is automated through training using a SVM classifier or become unnecessary in a KNN classifier. Thirdly, the classification accuracy is improved over the traditional decision tree approach as demon-

strated in the simulated experiments. Fourthly, the algorithm is simplified because of the dimension reduction realized by feature selection and combination. However, the need for training data is not often feasible. It is a major limitation of these supervised machine learning techniques.

The optimized distribution sampling test classifier is an improvement over the KS test classifier. While KS test is well established for measuring goodness of fit, in the case of modulation classification, much information is underutilized to optimize the classification performance. By establishing a set of optimized sampling location according to hypothesised PDFs from modulation candidates, the ODST classifier is less vulnerable against outliers and more efficient in using more information from the multiple locations on the spectrum. The resulting benefit is higher classification accuracy as well as lower computational complexity. The distribution based features inherent the same attributes from the ODST classifier and extend to a wider set of signal distribution. The corresponding machine learning techniques enables the consolidation of this big array of distribution based features to provide more robust performance with the same level of efficiency. As non-blind classifiers, all of the distribution test based classifiers are based on the assumption of perfection knowledge of the transmission channel as well as the noise type and power. Predictably, these classifiers are prone to performance degradation in the presence of channel estimation error and mismatching channel mode.

The combination of centroid estimation and non-parametric likelihood function is an unique approach to the modulation classification problem. It resembles the mechanism of a likelihood based classifier. However it is not strictly likelihood that the NPLF is measuring. In essence, it is estimating the cumulative probability of the received signal in a region that is defined by the signal centroid and a normalized radius. Both factors jointly create a total region of equal area for different candidate modulations. The resulting classifier does not require a known noise model neither does it need the knowledge of noise power. The performance is inferior compared to some of the non-blind classifiers with perfect channel knowledge. However, when a GMM modelled impulsive noise is considered non-blind classifiers suffers greatly because of mismatching noise model. In the meantime, the NPLF

classifier is able to sustain a consistent level of classification accuracy regardless of the type of noise. That is without mentioning the significantly lower computational complexity. In addition, the centroid estimation process is able to estimate the carrier phase offset and achieves compensation in combination with the NPLF.

The extension of modulation classification to MIMO systems is very timely, considering its wide application in 3G, 4G, and, predictably 5G cellular standards. In this research we build on the likelihood based classifier for MIMO systems and reduce the amount of the channel state information that is needed for the classifier. The EM process is developed for the joint estimations of channel matrix and noise power. The resulting estimation enables the likelihood evaluation based on a likelihood function that is adapted for the MIMO systems. As the assumption of unknown noise power has yet been considered by other research, the conclusion drawn from the simulated experiments is that the EM and ML combination achieve good classification accuracy for BPSK, QPSK and 16-QAM modulations. Perfect classification is observed when the SNR is above 0 dB in most cases. The demanded signal length to achieve this performance is no more than for SISO systems. Due to the complexity of MIMO systems, the likelihood evaluation is computationally much more expensive. In fact, the complexity grows exponentially with the increasing modulation order as well as number of transmitters.

In summary, our work has filled the void in the spectrum of existing methods with low complexity classifiers of little compromise on classification accuracy. Novel classification strategies have also been developed to solve modulation classification problems in more practical scenarios. As of now, much attention of modulation classifier development has shifted towards MIMO systems. As stated above, computational complexity reduction is still a challenging task for MIMO systems, especially for higher order modulations and systems with higher number of transmitter. It would be very interesting to adapt some of the SISO modulation classifiers for the MIMO systems as only likelihood based classier has been considered at the moment. While briefly touched upon in our experiments and discussions, the issues of frequency offset is still not effectively solved by most of the current classifiers. To create a classifier, especially a blind classifier, which is indeed practical in a real world situation,

the ability to compensate frequency offset is extremely valuable and much desired.

Bibliography

Akay, M. F. Support Vector Machines Combined with Feature Selection for Breast Cancer Diagnosis. *Expert Systems with Applications*, 36(2):3240–3247, 2009.

Amuru, S. and da Silva, C. R. C. M. Cumulant-based channel estimation algorithm for modulation classification in frequency-selective fading channels. In *Military Communications Conference*, pages 1 – 6, 2012.

Aslam, M. W., Zhu, Z., and Nandi, A. K. Robust QAM Classification Using Genetic Programming and Fisher Criterion. In *European Signal Processing Conference*, pages 995–999, 2011.

Aslam, M. W., Zhu, Z., and Nandi, A. K. Automatic Modulation Classification Using Combination of Genetic Programming and KNN. *IEEE Transactions on Wireless Communications*, 11(8):2742–2750, 2012.

Azzouz, E. E. and Nandi, A. K. Automatic Identification of Digital Modulation Types. *Signal Processing*, 47(1):55–69, 1995.

Azzouz, E. E. and Nandi, A. K. *Automatic Modulation Recognition of Communication Signals*. Kluwer, Boston, MA, 1996a.

Azzouz, E. E. and Nandi, A. K. Procedure for Automatic Recognition of Analogue and Digital Modulations. *IEE Proceedings - Communications*, 143(5):259–266, 1996b.

Bennett, W. R. Methods of solving noise problems. *Proceedings of the IRE*, 44:609–638, 1956.

Chan, Y. T. and Gadbois, L. G. Identification of the Modulation Type of a Signal. *Signal Processing*, 1(4):838–841, 1989.

Chavali, V. G. and da Silva, C. R. C. M. Maximum-Likelihood Classification of Digital Amplitude-Phase Modulated Signals in Flat Fading Non-Gaussian Channels. *IEEE Transactions on Communications*, 59(8):2051 – 2056, 2011.

Chavali, V. G. and da Silva, C. R. C. M. Classification of Digital Amplitude-Phase Modulated Signals in Time-Correlated Non-Gaussian Channels. *IEEE Transactions on Communications*, 61(6):2408–2419, 2013.

Choqueuse, V., Azou, S., Yao, K., Collin, L., and Burel, G. Blind Modulation Recognition for MIMO Systems. *Military Technical Academy Review*, XIX(2):183–196, 2009.

Conover, W. *Practical Nonparametric Statistics*. Wiley, 1980.

Dan, W., Gu, X., and Qing, G. A New Scheme of Automatic Modulation Classification Using Wavelet and WSVM. In *Asia Pacific Conference on Mobile Technology, Applications and Systems*, pages 1–5. IEEE, 2005.

Das, A. and Rao, B. D. SNR and Noise Variance Estimation for MIMO Systems. *IEEE Transactions on Signal Processing*, 60(8):3929–3941, 2012.

Dobre, O. A., Abdi, A., and Bar-Ness, Y. Survey of automatic modulation classification techniques: classical approaches and new trends. *IET Communications*, 1(2):137–156, 2007.

Espejo, P. G., Ventura, S., and Herrera, F. A Survey on the Application of Genetic Programming to Classification. *IEEE Transactions on Systems, Man, and Cybernetics, Part C (Applications and Reviews)*, 40(2):121–144, 2010.

Fabrizi, P. M., Lopes, L. B., and Lockhart, G. B. Receiver Recognition of Analogue Modulation Types. In *IERE Conference on Radio Receiver and Associated Systems*, pages 135–140, 1986.

Fasano, G. and Franceschini, A. A Multidimensional Version of the Kolmogorov-Smirnov Test. *Monthly Notices of the Royal Astronomical Scoeity*, 225:155–170, 1987.

Fisher, R. A. On the Mathematical Foundations of Theoretical Statistics. *Philosophical Transactions of the Royal Society A: Mathematical, Physical and Engineering Sciences*, 222:309–368, 1922.

Gallager, R. G. *Principles of Digital Communication*. Cambridge University Press, 2008.

Gao, F., Cui, T., Nallanathan, A., and Tellambura, C. Maximum Likelihood Detection for Differential Unitary Space-Time Modulation with Carrier Frequency Offset. *IEEE Transactions on Communications*, 56(11):1881–1891, 2008.

Gardner, W. A. and Spooner, C. M. Signal interception: performance advantages of cyclic-feature detectors. *IEEE Transactions on Communications*, 40(1):149–159, 1992.

Goldsmith, A. *Wireless communications*. Cambridge University Press, 2005.

Goldsmith, A. J. and Chua, S.-G. Adaptive Coded Modulation for Fading Channels. *IEEE Transactions on Communications*, 46(5):595–602, 1998.

Gunn, S. R. Support Vector Machines for Classification and Regression. Technical Report 2, 1998.

Guo, H. and Nandi, A. K. Breast cancer diagnosis using genetic programming generated feature. In *Machine Learning for Signal Processing, IEEE Workshop on (MLSP)*, pages 215–220, 2006.

Hameed, F., Dobre, O. A., and Popescu, D. On the Likelihood-based Approach to Modulation Classification. *IEEE Transactions on Wireless Communications*, 8(12):5884–5892, 2009.

Hassan, K., Dayoub, I., Hamouda, W., Nzeza, C. N., and Berbineau, M. Blind Digital Modulation Identification for Spatially-Correlated MIMO Systems. *IEEE Transactions on Wireless Communications*, 11(2):683–693, 2012.

Hero, A. O. and Hadinejad-Mahram, H. Digital Modulation Classification Using Power Moment Matrices. In *International Conference on Acoustics, Speech, and Signal Processing*, pages 3285–3288, 1998.

Hipp, J. E. Modulation Classification Based on Statistical Moments. In *Military Communications Conference*, pages 20.2.1 – 20.2.6, 1986.

Hong, L. and Ho, K. C. BPSK and QPSK Modulation Classification with Unknown Signal Level. In *Military Communications Conference*, pages 976–980, 2000.

Hosmer, D. W. and Lemeshow, S. *Applied Logistic Regression*. Wiley, 2000.

Huang, C. Y. and Polydoros, A. Likelihood Methods for MPSK Modulation Classification. *IEEE Transactions on Communications*, 43(2):1493–1504, 1995.

Jovanovic, S. D., Doroslovacki, M. I., and Dragosevic, M. V. Recognition of Low Modulation Index AM Signals in Additive Gaussian Noise. In *European Association for Signal Processing V Conference*, pages 1923–1926, 1990.

Kanterakis, E. and Su, W. Modulation Classification in MIMO Systems. In *Military Communications Conference*, pages 35–39, 2013.

Kolmogorov, A. N. Sulla Determinazione Empirica di una Legge di Distribuzione. *Giornale dell' Istituto Italiano degli Attuari*, (4):83–91, 1933.

Koza, J. R. *Genetic Programming: On the Programming of Computers by Means of Natural Selection*. The MIT Press, Cambridge, Massachusetts, 1992.

Leib, H. and Pasupathy, S. The phase of a vector perturbed by Gaussian noise and differentially coherent receivers. *IEEE Transactions on Information Theory*, 34(6):1491–1501, 1988.

Liu, H. and Xu, G. Closed-form blind symbol estimation in digital communications. *IEEE Transactions on Signal Processing*, 43(11), 1995.

Massey, F. The Kolmogorov-Smirnov Test for Goodness of Fit. *Journal of the American Statistical Association*, 46(253):68–78, 1951.

Meng, X.-L. and Rubin, D. B. Maximum Likelihood Estimation via the ECM Algorithm: a General Framework. *Biometrika*, 80(2):267–278, 1993.

Middleton, D. Non-Gaussian Noise Models in Signal Processing for Telecommunications : New Methods and Results for Class A and Class B Noise Models. *IEEE Transactions on Information Theory*, 45(4):1129–1149, 1999.

Mobasseri, B. G. Digital modulation classification using constellation shape. *Signal Processing*, 80(2):251–277, 2000.

Mühlhaus, M. S., Öner, M., Dobre, O. A., and Jondral, F. K. A Low Complexity Modulation Classification Algorithm for MIMO Systems. *IEEE Communications Letters*, 17(10):1881–1884, 2013.

Mustafa, H. and Doroslovacki, M. Digital Modulation Recognition Using Support Vector Machine Classifier. *Asilomar Conference on Signals, Systems and Computers*, pages 2238–2242, 2004.

Nandi, A. K. and Azzouz, E. E. Automatic Analogue Modulation Recognition. *Signal processing*, 46:211–222, 1995.

Nandi, A. K. and Azzouz, E. E. Algorithms for automatic modulation recognition of communication signals. *IEEE Transactions on Communications*, 46(4):431–436, 1998.

Panagiotou, P., Anastasopoulos, A., and Polydoros, A. Likelihood Ratio Tests for Modulation Classification. In *Military Communications Conference*, pages 670–674, 2000.

Peacock, J. A. Two-dimensional Goodness-of-fit Testing Astronomy. *Monthly Notices of the Royal Astronomical Scoeity*, 202:615–627, 1983.

Poisel, A. R. *Introduction to Communication Electronic Warfare Systems.* Artech House, 2008.

Polat, K. and Güne, S. Breast Cancer Diagnosis Using Least Square Support Vector Machine. *Digital Signal Processing*, 17(4):694–701, 2007.

Polydoros, A. and Kim, K. On the Detection and Classification of Quadrature Digital Modulations in Broad-band Noise. *IEEE Transactions on Communications*, 38(8):1199–1211, 1990.

Punchihewa, A., Zhang, Q., Dobre, O. A., Spooner, C. M., Rajan, S., and Inkol, R. On the cyclostationarity of OFDM and single carrier linearly digitally modulated signals in time dispersive channels: theoretical developments and application. *IEEE Transactions on Wireless Communications*, 9(8):2588–2599, 2010.

Roberts, S. J. and Penny, W. D. Variational Bayes for Generalized Autoregressive Models. *IEEE Transactions on Signal Processing*, 50(9):2245–2257, 2002.

Serpedin, E., Chevreuil, A., Giannakis, G., and Loubaton, P. Blind Channel and Carrier Frequency Offset Estimation Using Periodic Modulation Precoders. *IEEE Transactions on Signal Processing*, 48(8):2389–2405, 2000.

Sexton, J. ECM Algorithms That Converge at the Rate of EM. *Biometrika*, 87(3):651–662, 2000.

Shi, Q. and Karasawa, Y. Noncoherent Maximum Likelihood Classification of Quadrature Amplitude Modulation Constellations: Simplification, Analysis, and Extension. *IEEE Transactions on Wireless Communications*, 10(4):1312–1322, 2011.

Shi, Q. and Karasawa, Y. Automatic Modulation Identification Based on the Probability Density Function of Signal Phase. *IEEE Transactions on Communications*, 60(4):1–5, 2012.

Sills, J. A. Maximum-likelihood Modulation Classification for PSK/QAM. In *Military Communications Conference*, pages 217–220, 1999.

Silva, S. GPLAB - A Genetic Programming Toolbox for MATLAB. (http://goo.gl/zk1g2O), 2007.

Smirnov, H. Sur les Ecarts de la Courbe de Distribution Empirique. *Recueil Mathematique (Matematiceskii Sbornik)*, (6):3–26, 1939.

Soliman, S. S. and Hsue, S.-Z. Signal Classification Using Statistical Moments. *IEEE Transactions on Communications*, 40(5):908–916, 1992.

Soltanmohammadi, E. and Naraghi-Pour, M. Blind Modulation Classification over Fading Channels Using Expectation-Maximization. *IEEE Communications Letters*, 17(9):1692–1695, 2013.

Spooner, C. M. Classification of Co-channel Communication Signals Using Cyclic Cumulants. In *Conference Record of the Twenty-Ninth Asilomar Conference on Signals, Systems and Computers*, pages 531–536, 1996.

Swami, A. and Sadler, B. M. Hierarchical Digital Modulation Classification Using Cumulants. *IEEE Transactions on Communications*, 48(3):416–429, 2000.

Theodoridis, S. *Pattern Recognition.* Academic Press, 4th edition, 2008.

Tomasoni, A. and Bellini, S. Efficient OFDM channel estimation via an information criterion. *IEEE Transactions on Wireless Communications*, 12(3):1352–1362, 2012.

Urriza, P., Rebeiz, E., Pawelczak, P., and Cabric, D. Computationally Efficient Modulation Level Classification Based on Probability Distribution Distance Functions. *IEEE Communications Letters*, 15(5):476–478, 2011.

Vastola, K. S. Threshold detection in narrow-band non-Gaussian noise. *IEEE Transactions on Communications*, 32(2):134–139, 1984.

Wang, F. and Wang, X. Fast and Robust Modulation Classification via Kolmogorov-Smirnov Test. *IEEE Transactions on Communications*, 58(8):2324–2332, 2010.

Wautelet, X., Herzet, C., Dejonghe, A., Louveaux, J., and Vandendorpe, L. Comparison of EM-Based Algorithms for MIMO Channel Estimation. *IEEE Transactions on Communications*, 55(1):216–226, 2007.

Wei, W. and Mendel, J. M. Maximum-Likelihood Classification for Digital Amplitude-Phase Modulations. *IEEE Transactions on Communications*, 48(2):189–193, 2000.

Wong, M. L. D. and Nandi, A. K. Automatic Digital Modulation Recognition Using Artificial Neural Network and Genetic Algorithm. *Signal Processing*, 84(2):351–365, 2004.

Wong, M. L. D. and Nandi, A. K. Semi-blind Algorithms for Automatic Classification of Digital Modulation Schemes. *Digital Signal Processing*, 18(2):209–227, 2008.

Wong, M. L. D., Ting, S. K., and Nandi, A. K. Naive Bayes classification of adaptive broadband wireless modulation schemes with higher order cumulants. *International Conference on Signal Processing and Communication Systems*, (Ml):1–5, 2008.

Wu, H., Saquib, M., and Yun, Z. Cumulant Features for Communications via Multipath Channels. *IEEE Transactions on Wireless Communications*, 7(8):3098–3105, 2008.

Wu, Z., Wang, X., Gao, Z., and Ren, G. Automatic Digital Modulation Recognition Based on Support Vector Machines. In *International Conference on Neural Networks and Brain*, volume 2, pages 1025–1028. IEEE, 2005.

Xu, J. L., Su, W., and Zhou, M. Likelihood-Ratio Approaches to Automatic Modulation Classification. *IEEE Transactions on Systems, Man, and Cybernetics, Part C (Applications and Reviews)*, 41(4):455–469, 2011.

Zarzoso, V. and Nandi, A. K. Blind separation of independent sources for virtually any source probability density function. *IEEE Transactions on Signal Processing*, 47(9):2419–2432, 1999.

Zhu, Z. and Nandi, A. K. Blind Digital Modulation Classification using Minimum Distance Centroid Estimator and Non-parametric Likelihood Function. *IEEE Transactions on Wireless Communications*, pages 1–12 (early access), 2014a.

Zhu, Z. and Nandi, A. K. Blind Modulation Classification for MIMO Systems using Expectation Maximization. In *Military Communications Conference*, pages 1–6 (under review). IEEE, 2014b.

Zhu, Z., Aslam, M. W., and Nandi, A. K. Augmented Genetic Programming for Automatic Digital Modulation Classification. In *IEEE International Workshop on Machine Learning for Signal Processing*, pages 391–396, 2010.

Zhu, Z., Aslam, M. W., and Nandi, A. K. Support Vector Machine Assisted Genetic Programming for MQAM Classification. In *International Symposium on Signals, Circuits and Systems*, pages 1–6, 2011.

Zhu, Z., Aslam, M. W., and Nandi, A. K. Adapted Geometric Semantic Genetic Programming for Diabetes and Breast Cancer Classification. In *IEEE International Workshop on Machine Learning for Signal Processing*, pages 1–5, 2013a.

Zhu, Z., Nandi, A. K., and Aslam, M. W. Approximate Centroid Estimation with Constellation Grid Segmentation for Blind M-QAM Classification. In *Military Communications Conference*, number 1, pages 46–51, 2013b.

Zhu, Z., Nandi, A. K., and Aslam, M. W. Robustness Enhancement of Distribution Based Binary Discriminative Features for Modulation Classification. In *IEEE International Workshop on Machine Learning for Signal Processing*, pages 1–6, 2013c.

Zhu, Z., Aslam, M. W., and Nandi, A. K. Genetic Algorithm Optimized Distribution Sampling Test for M-QAM Modulation Classification. *Signal Processing*, 94:264–277, 2014.

Appendix A: Minimum Distance Centroid Estimation

The distance between a signal sample $r(n) = \alpha e^{j\theta} s(n)$ and an estimated centroid $\mathcal{A}_{\mathcal{M}}^m = ae^{j\phi} s_{\mathcal{M}}^m$ can be written as

$$\begin{aligned} D(r(n), \mathcal{A}_{\mathcal{M}}^m) &= \|r(n) - \mathcal{A}_{\mathcal{M}}^m\| \\ &= \sqrt{\alpha^2 \|r(n)\|^2 + a^2 \left\|s_{\mathcal{M}}^m\right\|^2 - 2\alpha \|s(n)\| \, a \left\|s_{\mathcal{M}}^m\right\| \cos(\theta - \phi)} \end{aligned} \tag{7.1}$$

Assuming a signal sample is assigned to its nearest centroid $s(n) = s_{\mathcal{M}}^m$, we replace the expression for $r(n)$ and $\mathcal{A}_{\mathcal{M}}$ with $r(n) = \alpha e^{j\theta}$ and $\mathcal{A}_{\mathcal{M}}^m = ae^{j\phi}$, where $\alpha = \alpha s(n)$ and $a = as_{\mathcal{M}}^m$, for a more concise presentation.

Given that all signal symbol assignments are equiprobable, the expectation of signal-to-centroid distance is given in equation (29).

$$E[\mathcal{D}_{\mathcal{M}}(r, a, \phi)] = \tag{7.2}$$
$$\frac{N}{M} \int_0^{\infty} \int_{\phi - \pi/M}^{\phi + \pi/M} \sqrt{x^2 + a^2 - 2ax\cos(y - \phi)} f_{mag}(x|\alpha, \sigma) \sum_{m=1}^{M} f_{phase}(y|\theta + m\pi/M, \sigma) dy dx$$

$$\frac{\partial}{\partial \phi} E[\mathcal{D}_{\mathcal{M}}(r, \phi)] = \tag{7.3}$$
$$\frac{N}{M} \int_0^{\infty} \int_{-\pi/M}^{\pi/M} \sqrt{x^2 + a^2 - 2ax\cos(y)} f_{mag}(x|\alpha, \sigma) \sum_{m=1}^{M} \frac{\partial}{\partial (y + \phi)} f_{phase}(y + \phi|\theta + m\pi/M, \sigma) dy dx$$

$$\frac{\partial}{\partial a}E[\mathcal{D}_{\mathcal{M}}(r,a)] =$$
$$\frac{N}{M}\int_0^{\infty}\int_{-\pi/M}^{\pi/M}\frac{2a-2x\cos(y)}{2\sqrt{x^2+a^2-2xa\cos(y)}}f_{mag}(x|\alpha,\sigma)\sum_{m=1}^{M}f_{phase}(y+\pi/M|\theta+m\pi/M,\sigma)dydx \tag{7.4}$$

We take the derivative of $E[\mathcal{D}_{\mathcal{M}}(r,a,\phi)]$ with respect of the centroid parameter phase ϕ as in equation (30).

Given the signal phase distribution from a single symbol in AWGN channel (Bennett, 1956)

$$f_{phase}(\phi)$$
$$= \frac{e^{-\alpha^2/2\sigma^2}}{2\pi}+\frac{\alpha\cos(\phi)}{2\sigma\sqrt{2\pi}}\cdot[1+erf(\frac{\alpha\cos(\phi)}{\sqrt{2\sigma}})]e^{-\frac{\alpha^2}{2\sigma^2}sin^2(\theta)}, \tag{7.5}$$

we simplify the distribution to its von Mises distribution approximation which converges to equation (32) at high SNR (Leib and Pasupathy, 1988).

$$f_{phase}(\phi)=\frac{e^{(\alpha^2/\sigma^2)cos(\phi-\mu)}}{2\pi I_0(\alpha^2/\sigma^2)}. \tag{7.6}$$

The derivative of the distribution with respect to ϕ can be found as

$$\frac{\partial}{\partial\phi}f_{phase}(\phi)=-\frac{\alpha^2\sin(\phi-\mu)}{\sigma^2 2\pi I_0(\alpha^2/\sigma^2)}e^{(\alpha^2/\sigma^2)\cos(\phi-\mu)} \tag{7.7}$$

which has the property that ${f_{phase}}'(\alpha+\phi|\alpha,\sigma)=-f'(\alpha-\phi|\alpha,\sigma)$ and ${f_{phase}}'(\alpha|\alpha,\sigma)=0$. The two possible solutions for $\frac{\partial}{\partial\phi}E[\mathcal{D}_{\mathcal{M}}(r,a,\phi)]$ can be found as $\phi=\theta+m\pi/M$ and $\phi=\theta+(2m-1)\pi/2M$. It is not difficult to see that $\phi=\theta+m\pi/M$ provides the maximum for $E[\mathcal{D}_{\mathcal{M}}(r,a,\phi)]$ while $\phi=\theta+(2m-1)\pi/2M$ delivers the minimum. The term $m\pi/M$ equals the phase difference between received signal centroids which introduces a relative shift of carrier phase to the estimated carrier phase estimation. However, in modulation classification, as long as the resulting centroids have a matching pattern with the true signal means, the relative phase is of no concern. Therefore, the estimated centroid phase is accurate.

Moreover, in a channel with phase offset, it is not difficult to see that the slow fading, which adds a constant phase offset θ_o, results in a compensated of the shifted carrier phase $\phi = \theta + m\pi/M + \theta_o$. In fast fading channel with $\theta_o \sim \mathcal{N}(0, \sigma_\theta^2)$, the single signal phase distribution is modified to

$$f_{phase}(\phi) = \int_{\mu-\pi}^{\mu+\pi} \frac{e^{(\alpha^2/\sigma^2)cos(x-\mu)}}{2\pi I_0(\alpha^2/\sigma^2)} \cdot \frac{1}{\sigma_\theta\sqrt{2\pi}} e^{-\frac{(x-\phi)^2}{2\sigma_\theta^2}} dx \tag{7.8}$$

with the derivative of the distribution with respect to ϕ

$$\begin{aligned} &\frac{\partial}{\partial\phi} f_{phase}(\phi) \\ &= \int_{\mu-\pi}^{\mu+\pi} \frac{(x-\phi)}{2\sqrt{2}\sigma_\theta^3 \pi^{3/2} I_0(\alpha^2/\sigma^2)} \cdot e^{-\frac{(x-\phi)}{2\sigma_\theta^2} + (\alpha^2/\sigma^2)cos(x-\mu)} dx \end{aligned} \tag{7.9}$$

which leads to the same conclusion of $\phi = \theta + m\pi/M$.

Now, let us consider the estimation of channel gain. The derivative of the distance expectation with respect to centroid parameter magnitude is given in equation (31). The magnitude PDF of a PSK modulated signal in AWGN channe is a Rice distribution

$$f_{mag}(x) = \frac{x}{\sigma^2} e^{(\frac{-(x^2+\alpha^2)}{2\sigma^2})} I_0(\frac{x\alpha}{\sigma^2}) \tag{7.10}$$

where $I_0(\cdot)$ is the modified Bessel function of the first kind of order zero. This distribution is often approximated as a normal distribution when α/σ is big enough.

$$f_{mag}(x) = \frac{1}{\sigma\sqrt{2\pi}} e^{-\frac{(x-\alpha)^2}{2\sigma^2}} \tag{7.11}$$

If the condition for the approximation can be met, $a = \alpha$ would be a solution of $\frac{\partial}{\partial a} E[\mathcal{D}_\mathcal{M}(r, a)] = 0$. A more accurate approximation would be

$$f_{mag}(x) = \frac{1}{\sigma\sqrt{2\pi}} e^{-\frac{(x-\mu)^2}{2\sigma^2}} \tag{7.12}$$

where $\mu = \sigma\sqrt{2/\pi} L_{1/2}(-\alpha^2/2\sigma^2)$ is the mean of the Rice distribution. The resulting error of channel gain estimation can be found as $\sigma\sqrt{2/\pi} L_{1/2}(-\alpha^2/2\sigma^2) - \alpha$, which converges to zero when SNR$\rightarrow \infty$.

The analysis for QAM modulation is not given in this research. However, it can be easily derived by considering it as a combination of components with the same magnitude which can be treated similarly as PSK signals.

Appendix B: Iterative Minimum Distance Estimator

With A represented in a complex form $x + jy$, the sub-gradient at $A = x + jy$ is obtained as

$$\nabla\mathcal{D}(x, y) = \frac{D(x + \Delta x, y)}{\Delta x} + j\frac{D(x, y + \Delta y)}{\Delta y}. \tag{7.13}$$

The update function for $A_n = x_n + jy_n$ is expressed as

$$x_{n+1} + jy_{n+1} = x_n + jy_n - \alpha_{\mathcal{M}}\,\nabla\mathcal{D}(x_n, y_n) \tag{7.14}$$

The iterative process starts with $A_0 = x_0 + jy_0$ and should update the estimation for 20 iterations unless the termination condition is met that the sub-gradient is lower than the defined threshold.

$$\nabla\mathcal{D}(x, y) < \eta_{\mathcal{D}} \tag{7.15}$$

The values of parameter used in the centroid estimation is given in Table 7.1.

Table 7.1: Parameters used in the minimum distance estimator

Parameters	Notation	Simulation Values
Staring point	$A_0 = x_0 + jy_0$	$0.1 + 0.1j$,
Update step	$\alpha_{\mathcal{M}}$	$\{2E-4,\ 2E-4,\ 5E-5\}$ $\{2E-4,\ 5E-5,\ 1E-5\}$
Sub-gradient step	Δx, Δy	0.01
Update iterations		20
Termination threshold	$\eta_{\mathcal{D}}$	10

Appendix C: Non-parametric Likelihood Function

For both PSK and QAM modulation, it is not difficult to derive that $\mathbb{N}_{\mathcal{M}^-} = M_{\mathcal{M}^-}$ and $\mathbb{N}_{\mathcal{M}^0} = \mathbb{N}_{\mathcal{M}^+} = M_{\mathcal{M}^0}$. In order to satisfy $E[L_{NPLF}(r|H_{\mathcal{M}^0})] > E[L_{NPLF}(r|H_{\mathcal{M}^-})]$, the following inequality needs to be satisfied.

$$M_{\mathcal{M}^0} \int_0^{\mathcal{R}_{\mathcal{M}^0}} \frac{x}{\sigma^2} e^{-x^2/2\sigma^2} dx > M_{\mathcal{M}^-} \int_0^{\mathcal{R}_{\mathcal{M}^-}} \frac{x}{\sigma^2} e^{-x^2/2\sigma^2} dx \tag{7.16}$$

Simplify the above inequality with cumulative probability function of a Rayleigh distribution $F(x) = 1 - e^{-x^2/2\sigma^2}$.

$$M_{\mathcal{M}^0}(1 - e^{-\mathcal{R}^2_{\mathcal{M}^0}/2\sigma^2}) > M_{\mathcal{M}^-}(1 - e^{-\mathcal{R}^2_{\mathcal{M}^-}/2\sigma^2}) \tag{7.17}$$

Replacing both test radius with equation (21) and considering all modulation cases, the restriction for the reference radius can be written as

$$\mathcal{R}_0 > 2\sqrt{2\log(\frac{1}{2-\sqrt{2}})}\sigma \approx 2.07\sigma. \tag{7.18}$$

Limiting the SNR in the range between 0 dB to 20 dB, taking the maximum of σ equals to α when SNR is 0 dB. The limit for reference radius can be given by $\mathcal{R}_0 > 2.07\alpha$.

In the case when false hypothesis is a modulation of higher order, the likelihood function needs to satisfy $E[L_{NPLF}(r|H_{\mathcal{M}^0})] > E[L_{NPLF}(r|H_{\mathcal{M}^+})]$ and

$$M_{\mathcal{M}^0}(1 - e^{-\mathcal{R}^2_{\mathcal{M}^0}/2\sigma^2}) > M_{\mathcal{M}^0}(1 - e^{-\mathcal{R}^2_{\mathcal{M}^+}/2\sigma^2}). \tag{7.19}$$

It is not difficult to see that with $\mathcal{R}_{\mathcal{M}^0} > \mathcal{R}_{\mathcal{M}^+}$, according to equation (21), the condition is always met and imposes no restriction on the test radius.